



Title	Structure-function relationship of GH13_31 -glucosidase from <i>Bacillus</i> sp. AHU2216
Author(s)	Auiewiryanukul, Waraporn
Citation	北海道大学. 博士(農学) 甲第13326号
Issue Date	2018-09-25
DOI	10.14943/doctoral.k13326
Doc URL	<a href="http://hdl.handle.net/2115/75500">http://hdl.handle.net/2115/75500</a> ; <a href="http://hdl.handle.net/2115/71864">http://hdl.handle.net/2115/71864</a>
Type	theses (doctoral)
File Information	Waraporn_Auiewiryanukul.pdf



[Instructions for use](#)

Structure-function relationship of GH13\_31  $\alpha$ -glucosidase  
from *Bacillus* sp. AHU2216

(*Bacillus* sp. AHU2216 株由来 GH13\_31 $\alpha$ -グルコシダーゼの  
構造と機能に関する研究)

Hokkaido University Graduate School of Agriculture  
Division of Applied Bioscience Doctor course

Waraporn Auiewiriyankul

# CONTENTS

<b>ABBREVIATIONS</b>			<b>I-II</b>
<b>CHAPTER</b>	<b>I</b>	<b>Introduction</b>	
	<b>I.1</b>	<b><math>\alpha</math>-Glucosidase</b>	<b>1</b>
	<b>I.2</b>	<b>Reaction mechanism of AGase</b>	<b>1</b>
	<b>I.3</b>	<b>Transglucosylation of AGases</b>	<b>1-2</b>
	<b>I.4</b>	<b>Classification of AGases</b>	<b>2</b>
	<b>I.5</b>	<b>GH13 AGases</b>	<b>2-4</b>
 <b>CHAPTER</b>	 <b>II</b>	 <b>Characterization and structural analysis of AGase GH13_31</b>	
	<b>II.1</b>	<b>Introduction</b>	
	<b>II.2</b>	<b>Materials and methods</b>	<b>9</b>
	II.2.1	Isolation and identification of <i>Bacillus</i> sp. AHU2216	9-10
	II.2.2	Preparation of the genomic DNA of <i>Bacillus</i> sp. AHU2216	10
	II.2.3	Preparation of the expression plasmid of <i>BspAG13_31A</i>	10
	II.2.4	Preparation of the expression plasmid of <i>BspAG13_31A</i> E256Q mutant	11
	II.2.5	Production and purification of <i>BspAG13_31A</i> wild type and E256Q	11
	II.2.6	Measurement of protein concentration	11
	II.2.7	SDS-PAGE	12
	II.2.8	Standard enzyme activity assay	12
	II.2.9	Analysis of reaction products by thin layer chromatography (TLC)	12
	II.2.10	Optimal pH and temperature	12-13
	II.2.11	pH and thermal stability	13
	II.2.12	Kinetic analysis of reactions with various substrates	13-14

	II.2.13	Transglucosylation with maltooligosaccharides	14
	II.2.14	Structural analysis of transglucosylation product from <i>p</i> NPG	14
	II.2.15	Crystallization and data collection	14-15
	II.2.16	Structure solution and refinement	15
	<b>II.3</b>	<b>Results</b>	
	II.3.1	Identification of AGase in <i>Bacillus</i> sp. AHU2216	15-16
	II.3.2	Purification of the recombinant <i>Bsp</i> AG13_31A	16
	II.3.3	Reaction products from maltooligosaccharides by purified <i>Bsp</i> AG13_31A	16
	II.3.4	Effects of pH and temperature on enzyme activity and stability	16
	II.3.5	Screening of substrates	16-17
	II.3.6	Structural analysis of transglucosylation product from <i>p</i> NPG	17
	II.3.7	Kinetic analysis of reactions with <i>p</i> NPG and G2	17
	II.3.8	Substrate chain-length specificity	17-18
	II.3.9	Overall structures of <i>Bsp</i> AG13_31A	18
	II.3.10	Orientation of maltooligosaccharides bound to <i>Bsp</i> AG13_31A and interaction with the enzyme	18-19
	<b>II.4</b>	<b>Discussions</b>	<b>19-20</b>
<b>CHAPTER</b>	<b>III.</b>	<b>Alternation of substrate specificity and transglucosylation activity of <i>Bsp</i>AG13_31A through site-directed mutagenesis at Asn258</b>	
	<b>III.1</b>	<b>Introduction</b>	<b>43</b>
	<b>III.2</b>	<b>Materials and methods</b>	
	III.2.1	Preparation of Asn258 mutated <i>Bsp</i> AG1_31A	43
	III.2.2	Preparation of the double-mutation enzymes of E256Q/N258G and E256Q/N258P	44

III.2.3	Production and purification of <i>Bsp</i> AG13_31A mutants	44
III.2.4	Measurement of protein concentration	44
III.2.5	Kinetic analysis of reaction with various substrates	44-45
III.2.6	Analysis of the reaction products from sucrose by TLC	45
III.2.7	Determination of transglucosylation products from G2 and sucrose	45
III.2.8	Crystallization and data collection	45
III.2.9	Structure solution and refinement	46
<b>III.3</b>	<b>Results</b>	
III.3.1	Production and purification of <i>Bsp</i> AG13_31A mutants	46
III.3.2	Kinetic analysis of reactions with <i>p</i> NPG and G2	46-47
III.3.3	Substrate specificities for <i>Bsp</i> AG13_31A mutants	47
III.3.4	Reaction products from sucrose	47-48
III.3.5	Protein structures of <i>Bsp</i> AG13_31A E256Q/N258G and E256Q/N258P	48
<b>III.4</b>	<b>Discussions</b>	48-50
<b>CHAPTER IV</b>	<b>General discussions</b>	<b>68-69</b>
<b>REFERENCES</b>		71-79
<b>ACKNOWLEDGMENTS</b>		80

## LISTS OF TABLES

<b>CHAPTER</b>	<b>II</b>	<b>Characterization and structural analysis of AGase GH13_31</b>	
	II.1	Summary of crystallization conditions, data collection and refinement statistics	21
	II.2	Summary of purification of recombinant <i>BspAG13_31A</i>	22
	II.3	Glucose-releasing velocities to various substrates	23
	II.4	Chemical shifts of <i>pNP</i> $\alpha$ -maltoside in the $^1\text{H}$ - and $^{13}\text{C}$ -NMR spectra	24
	II.5	Kinetic parameters for G2 and <i>pNPG</i>	25
	II.6	Hydrolysis and transglucosylation velocities for the reaction with 10 mM maltooligosaccharides	26
	II.7	Kinetic parameters for maltooligosaccharides	27
<b>CHAPTER</b>	<b>III</b>	<b>Alternation of substrate specificity and transglucosylation activity of <i>BspAG13_31A</i> through site-directed mutagenesis at Asn258</b>	
	III.1	Summary of crystallization conditions, data collection, and refinement statistics	51
	III.2	Kinetic parameters of <i>BspAG13_31A</i> Asn258 variants for G2 and <i>pNPG</i>	52
	III.3	Transglucosylation ratio of <i>BspAG_31A</i> Asn258 variants for 10 mM G2	53
	III.4	Reaction velocities of <i>BspAG13_31A</i> Asn258 variants for various substrates	54
	III.5	Kinetic parameters of <i>BspAG13_31A</i> Asn258 variants for MOS and sucrose	55
	III.6	Comparison of torsion angles of G3 bound to <i>BspAG13_31A</i> variants	56

## LISTS OF FIGURES

<b>CHAPTER</b>	<b>I</b>	<b>Introduction</b>	
	I.1	Catalytic mechanism of retaining glycoside hydrolases	5
	I.2	Overall structure of the GH13 enzyme	6
	I.3	The comparison of the active sites between endo-type and exo-type Enzymes belonging to GH13 family	7
	I.4	Multiple alignment of GH13 AGases	8
<b>CHAPTER</b>	<b>II</b>	<b>Characterization and structural analysis of AGase GH13_31</b>	
	II.1	TLC analysis of reaction products by <i>BspAG13_31A</i>	28
	II.2	Phylogenetic tree of GH13_31A AGases and related glycosidases	29
	II.3	Nickel-immobilized Chelating Sepharose Fast Flow column chromatography of <i>BspAG13_31A</i>	30
	II.4	SDS-PAGE analysis of adsorbed proteins containing <i>BspAG13_31A</i> in Nickel-immobilized chelating Sepharose Fast Flow column chromatography	31
	II.5	Effects of pH on enzyme activity and stability	32
	II.6	Effects of temperature on enzyme activity and stability	33
	II.7	Time course of the reactions of purified recombinant <i>BspAG13_31A</i> towards <i>pNPG</i> substrate	34
	II.8	ESI-MS spectra of the transglucosylation product from <i>pNPG</i> of <i>BspAG13_31A</i>	35
	II.9	Structural analysis of transglucosylation from <i>pNPG</i> by HMBC	36
	II.10	Kinetic analysis of reaction of <i>BspAG13_31A</i> with <i>pNPG</i> and G2	37
	II.11	Structure of <i>BspAG13_31A</i>	38
	II.12	A calcium ion located in $\beta \rightarrow \alpha$ loop1	39

		in the ( $\beta/\alpha$ ) <sub>8</sub> barrel structure of <i>BspAG13_31A</i>	
	II.13	Close-up of the active site of the E256Q- substrate complexes	40
	II.14	Schematic drawing of the E256Q-G4 complex	41
	II.15	Comparison of amino acid sequences of <i>BspAG13_31A</i> and related enzymes	42
<b>CHAPTER</b>	<b>III</b>	<b>Alternation of substrate specificity and transglucosylation activity of <i>BspAG13_31A</i> through site-directed mutagenesis at Asn258</b>	
	III.1	Sequence comparison of amino acid residues of exo- $\alpha$ -glucosidases around Asn258 of <i>BspAG13_31A</i>	57
	III.2	SDS-PAGE analysis of Asn258 <i>BspAG13_31A</i> mutants	58
	III.3	Kinetic analysis of reaction of N258D with <i>p</i> NPG and G2	59
	III.4	Kinetic analysis of reaction of N258G with <i>p</i> NPG and G2	60
	III.5	Kinetic analysis of reaction of N258L with <i>p</i> NPG and G2	61
	III.6	Kinetic analysis of reaction of N258P with <i>p</i> NPG and G2	62
	III.7	Kinetic analysis of reaction of N258W with <i>p</i> NPG and G2	63
	III.8	Kinetic analysis of reaction of N258Y with <i>p</i> NPG and G2	64
	III.9	Analysis of reaction products from sucrose	65
	III.10	Close-up of the active sites of E256Q/N258G and E256Q/N258P in complex with G3	66
	III.11	Sucrose binding model of E256Q and E256Q/N258P on E328Q amylosucrase (PDB entry, JGI)	67
<b>CHAPTER</b>	<b>III</b>	<b>General discussion</b>	
	IV.1	Close-up view in active site of <i>BspAG13_31</i> with G2 complex and <i>GsjAGase</i>	70



## ABBREVIATIONS

16S rDNA,	16S ribosomal DNA
Å,	angstrom
AGases,	$\alpha$ -Glucosidase enzymes
<i>BcO16G</i> ,	oligo-1,6-glucosidase from <i>Bacillus cereus</i> ATCC 7064
BSA,	bovine serum albumin
<i>BSAMAG</i> ,	$\alpha$ -glucosidase from <i>Bacillus</i> sp. SAM1606
<i>BsO16G</i> ,	sucrase-maltase-isomaltase MalL from <i>Bacillus subtilis</i> subsp. <i>subtilis</i> strain 168
<i>BspAG13_31A</i> ,	$\alpha$ -glucosidase from <i>Bacillus</i> sp. AHU2216 belonging to glycoside hydrolase family 13 subfamily 31
CaCl <sub>2</sub> ,	calcium chloride
CBB,	coomassie brilliant blue
DEAE,	diethylaminoethyl
DGases,	dextran glucosidases
<i>E. Coli</i> ,	<i>Escherichia coli</i>
EDTA,	ethylenediamine tetra-acetic acid
ESI-MS,	electrospray ionization mass spectrometry
Fru,	fructose
G2,	maltose
G3,	maltotriose
G4,	maltotetraose
G5,	maltopentaose
G6,	maltohexaose
G7,	maltoheptaose
GH,	glycoside hydrolases
GH13_23,	glycoside hydrolases family 13 subfamily 23
GH13_31,	glycoside hydrolases family 13 subfamily 31
GH13,	glycoside hydrolases family 13
Glc-A,	internal D-glucosyl residue
Glc-B,	non-reducing end D-glucosyl residue
Glc,	glucose
<i>GsAG</i> ,	$\alpha$ -glucosidase from <i>Geobacillus Stearothermophilus</i>
<i>GsjAG</i> ,	$\alpha$ -glucosidase from <i>Geobacillus</i> sp. HTA462
<i>HaG</i> ,	$\alpha$ -glucosidase from <i>Halomonas</i> sp. H11

HMBC,	heteronuclear multiple bond correlation
HPAEC-PAD,	high performance anion-exchange chromatography with pulsed amperometric detection
HSQC,	heteronuclear single quantum coherence
IG2,	isomaltose
IG3,	isomaltotriose
IPTG,	isopropyl $\beta$ -D-thiogalactoside
<i>La</i> DG,	dextran glucosidase from <i>Lactobacillus acidophilus</i> NCFM
LB medium,	Luria-Bertani medium
MES-NaOH,	2-( <i>N</i> -morpholino) ethansulfonic acid-NaOH
MOS,	maltooligosaccharides
MR,	molecular replacement
Na <sub>2</sub> CO <sub>3</sub> ,	sodium carbonate
NaCl,	sodium chloride
NaOH,	sodium hydroxide
NMR,	nuclear magnetic resonance
O16Gases,	oligo-1,6-glucosidases
PCR,	polymerase chain reaction
PEG,	polyethylene glycol
<i>p</i> NP,	<i>p</i> -nitrophenyl
<i>p</i> NPG,	<i>p</i> -nitrophenyl $\alpha$ -D-glucoside
RMSD,	root-mean-square deviation
RNase,	ribonuclease
$r_{TG}$ ,	transglucosylation ratio
ScO16G,	oligo-1,6-glucosidase from <i>Saccharomyces cerevisiae</i>
SDS-PAGE,	sodium dodecyl sulfate polyacrylamide gel electrophoresis
SDS,	sodium dodecyl sulfate
<i>Sm</i> DG,	dextran glucosidase from <i>Streptococcus mutans</i>
Suc,	sucrose
TLC,	thin layer chromatography
Tris-HCl,	tris hydrochloride
$v_{ag}$ ,	aglycone- releasing velocity
$v_{glc}$ ,	D-Glucose-releasing velocity
$v_h$ ,	hydrolysis velocity
$v_{tg}$ ,	transglucosylation velocity

## CHAPTER I. General introduction

### I.1 $\alpha$ -Glucosidase

$\alpha$ -Glucosidase (AGase; EC 3.2.1.20) catalyzes the hydrolysis of the non-reducing end  $\alpha$ -glucosidic linkage of the substrates to produce  $\alpha$ -glucose (Chiba, 1998; Chiba, 1997). AGase is involved in the amylolytic pathway of various organisms including microorganisms, plants, and animals (Konishi *et al.*, 1994; Kimura, 2000). The reduction of AGase activity, caused by inhibition, deletion, or mutation, largely influences plant starch metabolism and animal glycogen metabolism. Inhibition of AGases prevents the germination of seeds through an accumulation of maltose (G2) in wheat (Konishi *et al.*, 1994). Deficiency of a tissue acid AGase causes a glycogen-storage disease (Pompe disease type II) in human (Hers 1963). In *Bacillus subtilis*, G2 inducible AGase (MalL) provides D-glucose from  $\alpha$ -D-glucosyl oligosaccharides in the intracellular metabolism (Schönert *et al.*, 1998).

### I.2 Reaction mechanism of AGases

Throughout the AGases, the enzymes are believed to catalyze the reaction by a double displacement mechanism as known 'retaining enzymes' (Figure I.I). This reaction involves the formation of oxocarbenium ion-like transition state (Davies and Henrissat, 1995; Utidehaag *et al.*, 1999; Chiba, 2012). The reaction involves the formation of covalent bond intermediate in the glycosylation step and degradation of the intermediate in the deglycosylation step. Firstly, the catalytic nucleophile attacks the carbon at the anomeric center of sugar to form the covalent bond  $\beta$ -glycosyl-enzyme intermediate while a proton donor protonates the glycosidic oxygen in the glycosylation step as general acid catalyst. The aglycone of the substrate leaves from the active sites. Deprotonated general acid/base catalyst deprotonates water as general base catalyst to assist nucleophilic attack of water to the anomeric carbon of the intermediate in hydrolysis reaction. Moreover, free hydroxy group of a sugar molecule can attack the intermediate in the deglycosylation step in transglycosylation (Wang and Hung, 2009).

### I.3 Transglucosylation of AGases

In addition to hydrolytic activity, AGase possesses transglucosylation activity (McCleary and Gibson, 1989; Nakao *et al.*, 1994; Konishi and Shindo, 1997; Kato *et al.*, 2002). This activity is utilized in the industrial productions of oligosaccharides and glucosides (Patel and Goyal, 2011; Bali *et al.*, 2015). The industrial interests are focused on the AGase-catalyzed production of

oligosaccharides (Chiba *et al.*, 1985; Yamamoto *et al.*, 2004). For example, isomaltooligosaccharides and panose ( $\alpha$ -D-glucopyranosyl-(1 $\rightarrow$ 6)- $\alpha$ -D-glucopyranosyl-(1 $\rightarrow$ 4)-D-glucose), which have prebiotic property and are utilized as food ingredients (Kohmoto T *et al.*, 1988; Kohmoto T *et al.*, 1991), are synthesized from maltooligosaccharides through  $\alpha$ -(1 $\rightarrow$ 6)-glucosyl transfer catalyzed by a fungal AGase (Takaku H 1988). To facilitate the transglycosylation, several approaches have been proposed: 1) optimization of reaction conditions including setting high substrate concentration, adding organic solvent to a reaction mixture, and using activated substrates with good leaving groups such as dinitrophenol and fluorine; 2) enhancing transglycosylation activity by site-directed mutagenesis [e.g. glycosynthase, which is a mutant enzyme of the catalytic nucleophile and transfers glycosyl residue from glycosyl fluoride with the opposite anomeric configuration of original substrates for parent enzymes (Hancock *et al.*, 2006); and substitution of catalytic nucleophile with cysteine sulfinate (Saburi *et al.*, 2013)]. It is generally preferable to avoid using organic solvents and synthetic substrates in industrial production of glycosides. Thus, finding glycoside hydrolases with high transglycosylation activity to native substrates is important to establish an efficient enzymatic synthesis of glycosides.

#### **I.4 Classification of AGases**

AGase shows a wide variety of substrate specificity depending on the enzyme origins, and divided into three groups based on substrate specificity (Chiba S and Minamiura N 1988). Group I enzymes prefer to hydrolyze heterogeneous substrates, (e.g., sucrose and aryl  $\alpha$ -glucosides) to the homogeneous substrates (e.g.,  $\alpha$ -glucobioses, maltooligosaccharides), but show low or no activity towards the polymer substrates (e.g.,  $\alpha$ -glucans). Group II and III enzymes are specific to homogeneous substrates rather than heterogeneous substrates. Group III enzymes hydrolyze polysaccharides. On the basis of amino acid sequence similarity, AGases are classified into four glycoside hydrolase families, glycoside hydrolase family 4 (GH4), GH13, GH31, and GH122 (Henrissat, 1991; Henrissat and Bairoch, 1993; Lombard *et al.*, 2014). Most AGases belong to GH13 and GH31 (Kimura *et al.*, 1992). Roughly, GH13 includes group-I AGases, and GH31 includes group-II and -III AGases (Chiba, 1997; Okuyama *et al.*, 2016). GH13 AGases are predominantly found in bacteria, yeast (*Saccharomyces cerevisiae*), and insects. On the other hand, AGases of plants, animals, fungi, yeast (*Schizosaccharomyces pombe*), and some species of bacteria are the members of GH31.

#### **I.5 GH13 AGases**

GH13, is one of the largest GH families, contains various amylolytic enzymes such as  $\alpha$ -amylase (EC 3.2.1.1), cyclodextrin glucanotransferase (EC 2.4.1.19), pullulanase (EC 3.2.1.41), oligo-1,6-glucosidase (EC 3.2.1.10), AGase, maltotetraohydrolase (EC 3.2.1.60), isoamylase (EC 3.2.1.68), neopullulanase (EC 3.2.1.135), maltogenic amylase (EC 3.2.1.133), amylosucrase (EC 2.4.1.4),  $\alpha$ -

maltosyltransferase (EC 2.4.99.16), 4- $\alpha$ -glucanotransferase (EC 2.4.1.25), cyclomaltodextrinase (EC 3.2.1.54), branching enzyme (EC 2.2.18), and so on. GH13 comprises of not only hydrolases, but also transferases and isomerases. This huge family is subdivided into subfamilies and AGases fall into subfamily 17 (GH13\_17), GH13\_23, GH13\_30, GH13\_31, GH13\_40 (Stam *et al.*, 2006). GH13 enzymes form the clan GH-H together with GH70 and GH77 (Coutinho and Henrissat, 1999; Bourne and Henrissat, 2001).

GH13\_31 AGases have high amino acid sequence similarities to oligo-1,6-glucosidase (EC 3.2.1.10) and dextran glucosidase (3.2.1.70), sucrose isomerase, and isomaltulose synthase. Their overall structures are similar to those of GH13 enzymes, containing domain A, B, and C (Figure I.2, Matsuura *et al.*, 1984; Ramasubbu *et al.*, 1996). Domain A is a catalytic domain formed by a  $(\beta/\alpha)_8$ -barrel fold that is a barrel structure of eight parallel  $\beta$ -strands surrounded by eight helices (Brayer *et al.*, 1995; Brzozowski and Davies, 1997; Knai *et al.*, 2001). Domain B is the variable length of a large loop inserted between the third  $\beta$ -strand and third helix ( $\beta \rightarrow \alpha$  loop 3; Janeček, 1997). Domain C at the C-terminal end folds into eight antiparallel  $\beta$ -strands of the Greek key structure connecting to the domain A (Ramasubbu *et al.*, 1996; Janeček, 1997). Domain C is suggested to stabilize the catalytic domain, and may help substrate binding (Lawson *et al.*, 1994; Dauter *et al.*, 1999). Moreover, GH13 AGases have two extra  $\alpha$ -helices on  $\beta \rightarrow \alpha$  loop 8 of domain A, which form domain B' (Møller *et al.*, 2012). Because of the presence of domain B', the enzymes have the pocket-shaped substrate-binding sites (Hondoh *et al.*, 2008; Møller *et al.*, 2012) unlike endo-type enzymes that have cleft-shaped substrate-binding sites (Figure I.3.A and C) (Kadziola *et al.*, 1994; Qian *et al.*, 1994).

GH13 AGases share four highly conserved regions I, II, III, and IV on  $\beta$ -strand 3, 4, 5, and 7 of the catalytic domain A, respectively, as in other GH13 enzymes (Nakajima *et al.*, 1986; Janeček, 1994; Janeček, 2002; Janeček *et al.*, 2014). The catalytic triad residues corresponding to Asp206 (nucleophile), Glu230 (proton donor), and Asp297 (transition state stabilizer) in Taka-amylase A, are situated on the  $\beta$ -strand 4, 5, and 7 of domain A (Figure I.3B and D, Matsuura *et al.*, 1984). Moreover, well conserved Arg in region II and two His residues (region I and IV) form hydrogen bonds with the glucosyl residue at non-reducing end of the substrate in subsite -1 (Horvathova *et al.*, 2000; Janeček *et al.*, 2014). Tyr on  $\beta \rightarrow \alpha$  loop 2 of domain A stacks on this glucosyl residue (Hondoh *et al.*, 2008)]. Asp and Arg on  $\beta \rightarrow \alpha$  loop 2 of domain A and domain B', respectively, form salt-bridge and recognize the non-reducing end of the substrates through interactions with the 4-OH of the glucosyl residue. The conserved regions of GH13 AGases were shown in Figure I.4.

GH13 AGases show similar substrate binding mode at subsite -1, but they show different substrate binding mode at subsites +1 depending on glucosidic linkage specificity:  $\alpha$ -(1 $\rightarrow$ 4)-glucosidic linkage-specificity and  $\alpha$ -(1 $\rightarrow$ 6)-glucosidic specificity. The amino acid residue next to the catalytic nucleophile is differently conserved depending on the glucosidic linkage specificity. For  $\alpha$ -(1 $\rightarrow$ 4)-

glucosidic linkage specific enzymes, Ala or Thr is found, whereas Val is conserved in the  $\alpha$ -(1 $\rightarrow$ 6)-glucosidic linkage specific enzymes. Val195 next to the catalytic nucleophile in *Streptococcus mutans* dextran glucosidase (*SmDG*) makes hydrophobic contact with  $\alpha$ -(1 $\rightarrow$ 6)-linked substrate at subsite +1 (Hondoh *et al.*, 2008). This Val residue causes steric hindrance upon binding to the  $\alpha$ -(1 $\rightarrow$ 4)-linked substrate. Lys275 and Glu371 of *SmDG* located on the  $\beta$  $\rightarrow$  $\alpha$  loop 6 and domain B', respectively, form hydrogen bonds with the 2-OH and 3-OH of the glucosyl residue of  $\alpha$ -(1 $\rightarrow$ 6)-linked substrate at subsite +1 (Hondoh *et al.*, 2008). Compared with  $\alpha$ -(1 $\rightarrow$ 6)-glucosidic linkage-specific glucosidases, molecular basis for the specificity to  $\alpha$ -(1 $\rightarrow$ 4)-glucosidic linkage is still less understood. Only the crystal structure of *Halomonas* sp. AGase (*HaG*) belonging to GH13\_23 in complex with maltose has been determined (Shen *et al.*, 2015). In addition to the  $\alpha$ -(1 $\rightarrow$ 4)- and  $\alpha$ -(1 $\rightarrow$ 6)-glucosidic bonds, some AGases have hydrolytic activities to sucrose (Glc $\alpha$ 1-2 $\beta$ Fru) and/or trehalose (Glc $\alpha$ 1-1 $\alpha$ Glc) (Nakao *et al.*, 1994; Nishimoto *et al.*, 2001). GH13 AGases and related enzymes generally most prefer trisaccharides as substrate (Suzuki *et al.*, 1982; Suzuki *et al.*, 1984; Saburi *et al.*, 2015). *SmDG* and *Lactobacillus acidophilus* dextran glucosidase (*LaDG*) show higher preference toward long-chain substrates (Saburi *et al.*, 2006; Møller *et al.*, 2012) unlike oligo-1,6-glucosidases (O16Gases). Length of  $\beta$  $\rightarrow$  $\alpha$  loop 4 of domain A in GH13 AGases (Figure I.4) is thought to be the important structure for substrate-chain length specificity. Short  $\beta$  $\rightarrow$  $\alpha$  loop 4 provides the space for long-chain substrates in *SmDG* and *LaDG* (Saburi *et al.*, 2006; Møller *et al.*, 2012). In *HaG*, this loop covers a major part of the active site entrance and obstructs the formation of +2 subsite for disaccharide specificity (Shen *et al.*, 2015).

### **Purpose of the study**

The GH13 is the large family containing several exo-type enzymes acting on  $\alpha$ -glucosidic linkage. The GH13 enzymes share the similar catalytic mechanism, but the activities and substrate specificities are diverse. In this study, AGase *BspAG13\_31A* from a soil isolate, *Bacillus* sp. AHU2216, is focused as the model to understand of the relationship between the structure and function of GH13\_31 AGases. Structural basis for the specificity to  $\alpha$ -(1 $\rightarrow$ 4)-glucosidic linkage and substrate chain-length, and high transglucosylation activity of *BspAG13\_31A* was analyzed through biochemical and structural analyses.

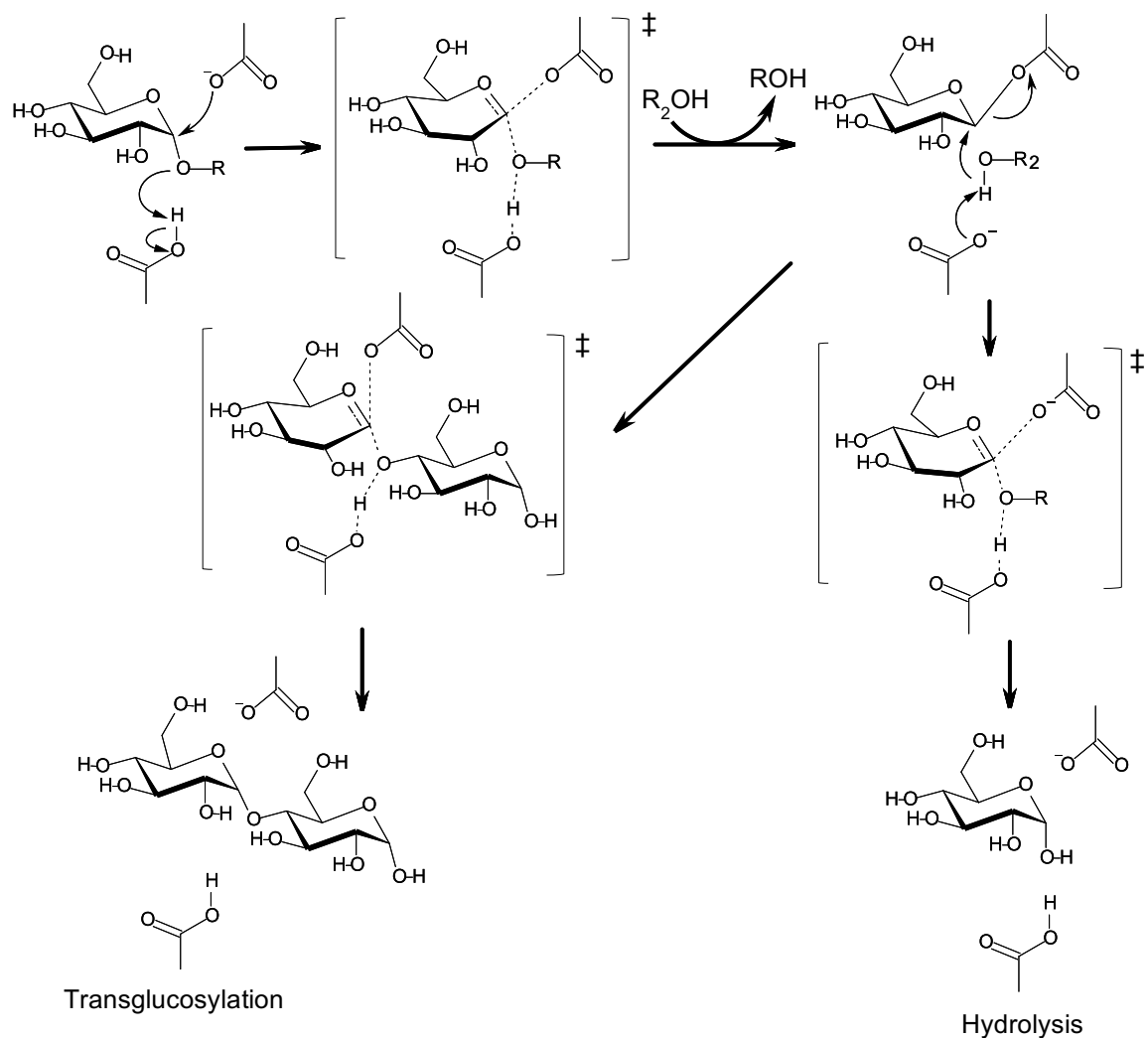


**Figure I.1 Catalytic mechanism of retaining glycoside hydrolases.**

Two potential reaction schemes of hydrolysis and transglucosylation are shown. R<sub>2</sub> refers H and sugar for hydrolysis and transglucosylation, respectively. In the glycosylation step, nucleophile attacks anomeric carbon and forms glycosyl-enzyme intermediate, while general acid protonates to cleave glycosidic linkage. In the deglycosylation step, the water or sugar molecule activated by general base attacks the anomeric carbon in hydrolysis or transglucosylation reaction.

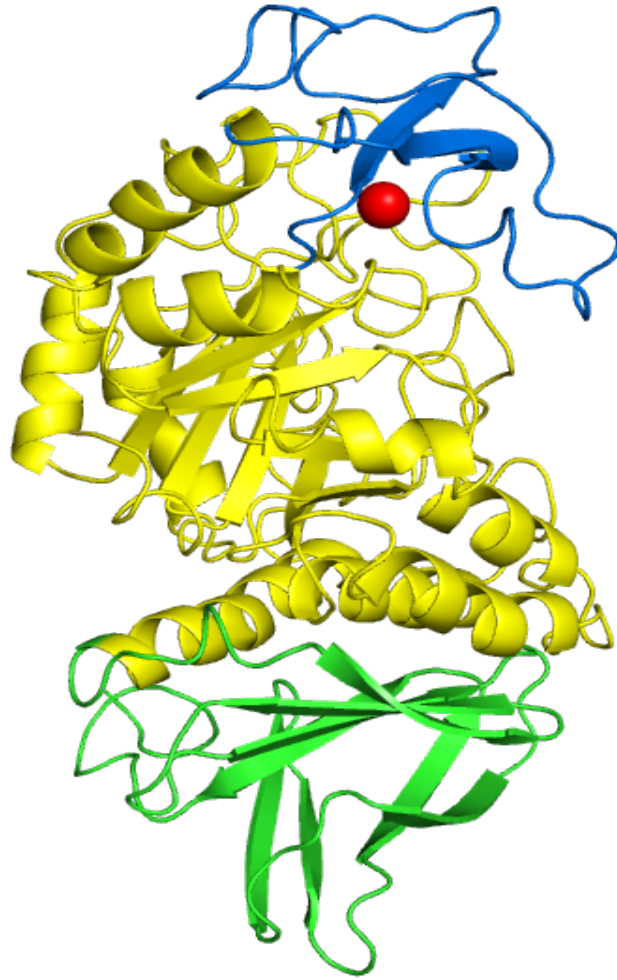


**Figure I.2 Overall structure of the GH13 enzyme.**

The three-dimensional structure of the GH13 enzyme, Taka-amylase A (PDB: 2TAA; Matsuura et al, 1984) was used as the model. Domain A, B, and C are colored in yellow, marine, and green, respectively. The calcium ion is shown by red sphere.



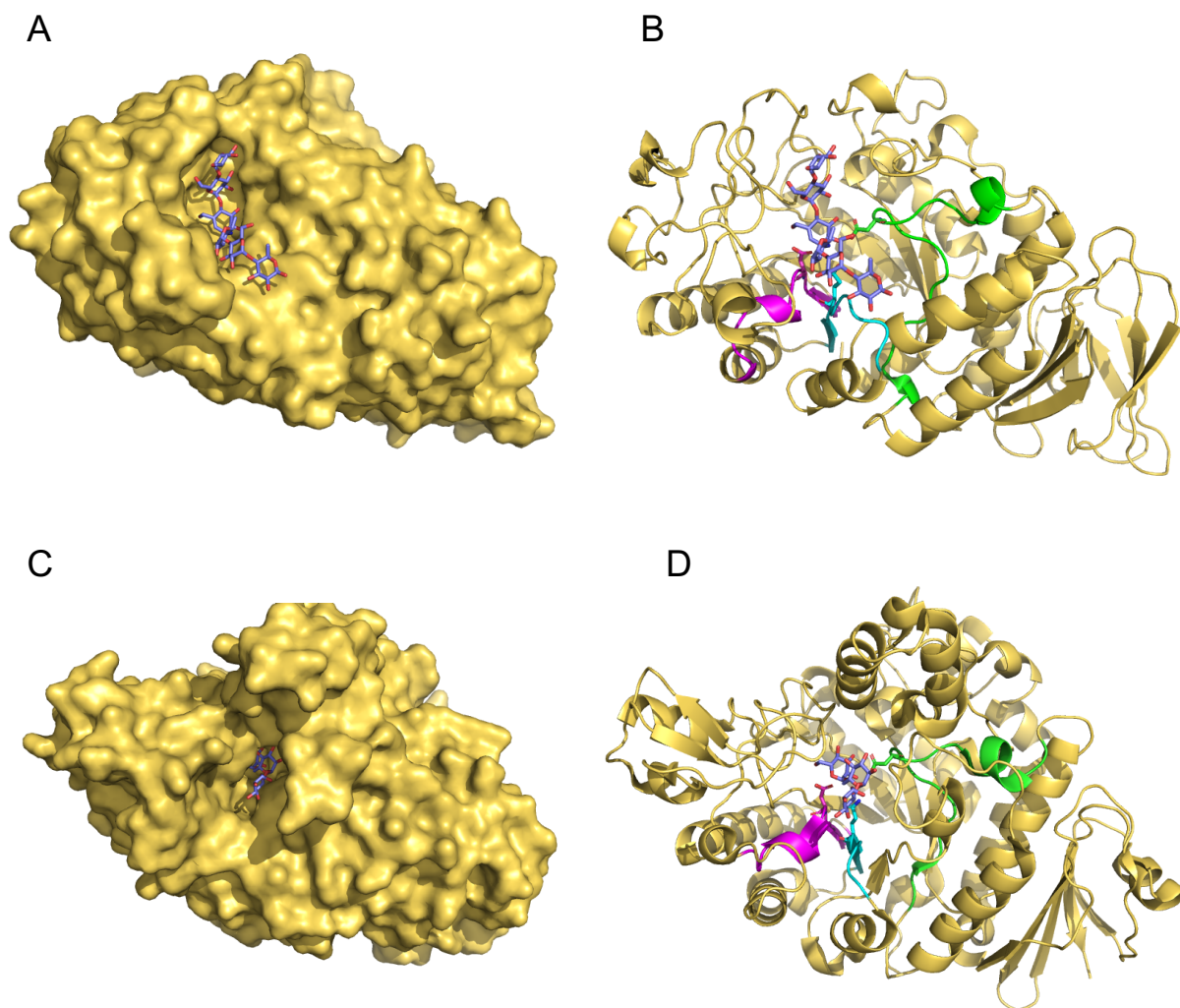


**Figure I.3** The comparison of the active sites between endo-type (A) and exo-type enzymes (B) belonging to GH13 family.

A, and C; The molecular surface of the *Aspergillus oryzae*  $\alpha$ -amylase with acarbose complex (PDB: 7TAA) and E237Q *SmDG* mutant with isomaltotriose (IG3) (PDB: 2ZID), respectively. B, and D; The cartoon model of *A. oryzae*  $\alpha$ -amylase and *SmDG*, respectively. The catalytic triad residues on  $\beta \rightarrow \alpha$  loops 4, 5 and 7 are colored with magenta, cyan, and green, respectively. The substrate-bound enzyme and the catalytic residues are shown by sticks model.

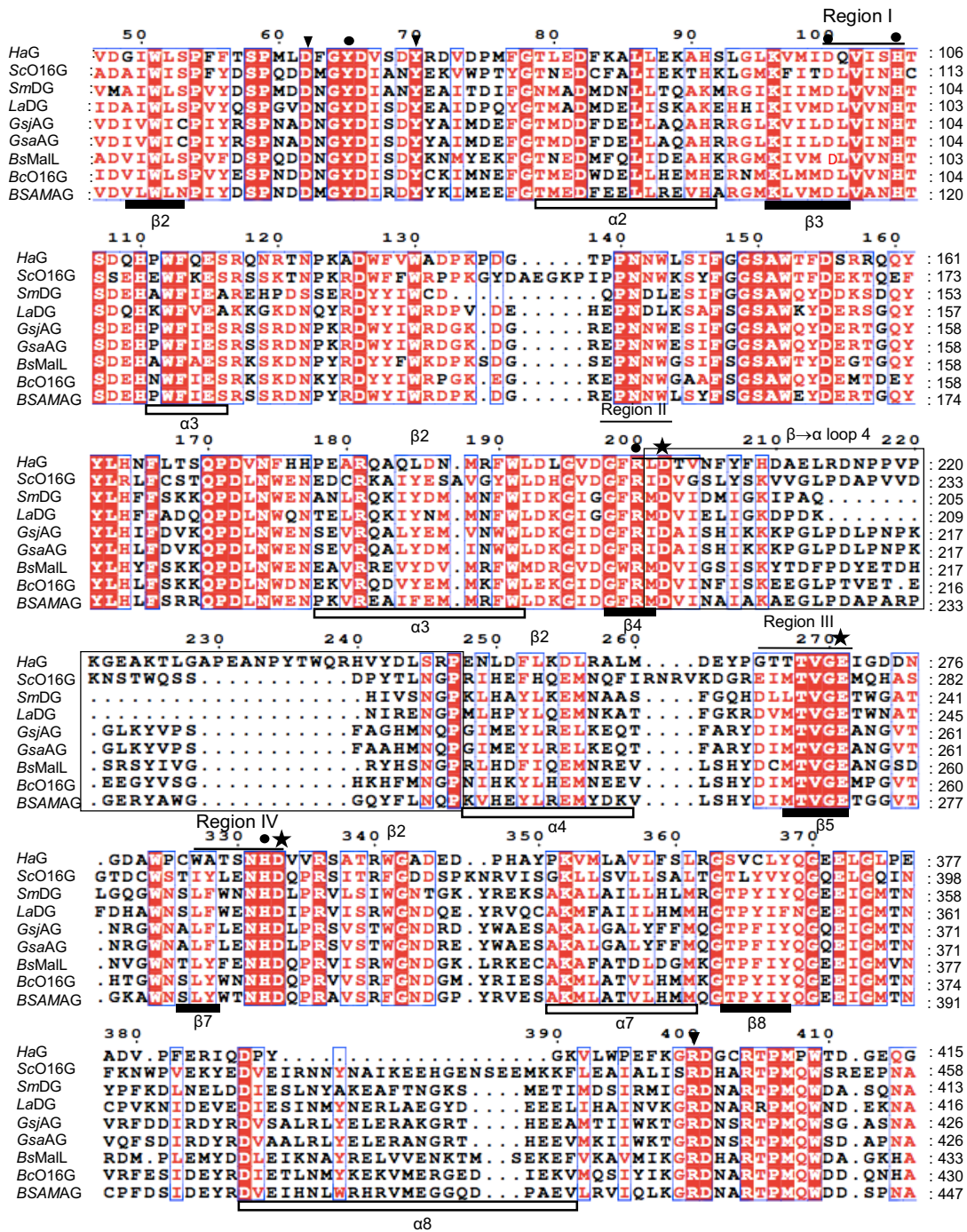


**Figure I.4 Multiple alignment of GH13 AGases.**

Amino acid sequences of GH13 AGases were aligned using the Clustal Omega (<https://www.ebi.ac.uk/Tools/msa/clustalo/>). Then, the sequences were submitted to Esprint ([esprint.ibcp.fr/](https://esprint.ibcp.fr/)). The enzymes used for alignment are: *HaG* (BAL49684.1); *Saccharomyces cerevisiae* isomaltase, *ScO16AG* (BAA07818.1); *SmDG* (BAE79634.1); *LaDG* (AAV42157.1); *Geobacillus* sp. HTA426 AGase, *GsjAG* (BAE48285.1); *Geobacillus stearothermophilus* AGase, *GsaAG* (BAA12704.1); *Bacillus subtilis* strain 168 sucrase-maltase-isomaltase *Mall*, *BsO16AG* (CAB15461.1); *Bacillus cereus* oligo1,6-glucosidase, *BcO16AG* (CAA37583.1); *Bacillus* sp. SAM1606 AGase, *BSAMAG* (CAA54266.1). The conserved regions are indicated, and the conserved residues for GH13 enzymes and GH13 AGases are shown with circles and reverse triangles, respectively.

## **CHAPTER II. Characterization and structural analysis of AGase GH13\_31 from *Bacillus* sp. AHU2216**

### **II.1 Introduction**

AGases catalyze transglucosylation transferring a glycosyl residue to an acceptor molecule under high substrate concentrations. This activity is useful for enzymatic synthesis of oligosaccharides and glucosides (Takaku 1988; Yamamoto *et al.*, 1999; Ojima *et al.*, 2012). The productions of oligosaccharides through transglucosylation catalyzed by several GH13 AGases are published. Hung *et al.* reported that a thermo- and alkaline-stable AGase of *GsjAG*, belonging to GH13\_31, shows transglucosylation activity to G2 to generate G3 (Hung *et al.*, 2005). This enzyme also glucosylates various non-sugar molecules such as alkyl alcohols and phenolphthalein using G2 as a donor. Some AGases, *HaG* and AGase from *Xanthomonas campestris*, belonging to GH13\_23, efficiently glucosylates non-sugar molecules such as 6-gingerol and L-menthol (Nakagawa *et al.*, 2000; Sato *et al.*, 2000; Kurosu *et al.*, 2002; Ojima *et al.*, 2012).

To facilitate the transglucosylation, several approaches have been published (Hancock *et al.*, 2006; Saburi *et al.*, 2013). However, the efficient enzymatic synthetic reactions of glycosides with low cost and high safety are desirable. Thus, finding glycoside hydrolases with high transglucosylation activity to natural substrates is still required for enzymatic synthesis of various carbohydrates and related compounds. Screening enzymes from environment bacteria is still a powerful strategy to find out desired enzymes. In this study, GH13\_31 AGase (*BspAG13\_31A*) with the  $\alpha$ -(1 $\rightarrow$ 4)-linkage specificity and high transglucosylation activity was found in a soil bacterium of *Bacillus* sp. AHU2216. Its functions and structure were described in this chapter.

### **II.2 Materials and methods**

#### **II.2.1 Isolation and identification of *Bacillus* sp. AHU2216**

*Bacillus* sp. AHU2216 was isolated from soil sampled in Hiratanai, Hokkaido, Japan, and grown on starch culture plates (Saburi *et al.*, 2015). Partial 16S rDNA was amplified by PCR from genomic DNA prepared as described previously (Ojima *et al.*, 2011) with primers 9F and 1510R (Nakagawa *et al.*, 2001). Primestar HS DNA polymerase (Takara Bio, Kusatsu, Japan) was used. The reaction mixture (50  $\mu$ L) containing 100 ng of DNA template, 0.2  $\mu$ M primers, Primestar HS DNA polymerase buffer, 0.16 mM dNTP mix, and 1.25 U of Primestar HS DNA polymerase. Thirty cycles of 98°C, 10 sec, 55°C, 15 sec, and 72°C, 2 min were performed. DNA sequence was analyzed using an Applied Biosystems 3130 Genetic Analyzer (Foster City, CA, USA). Sequence identity search was

carried out using the Basic Local Alignment Search Tool (Altschul *et al.*, 1990). This strain is deposited at the Laboratory of Culture Collection of Microorganisms, Research Faculty of Agriculture, Hokkaido University (Sapporo, Japan) as AHU2216.

### **II.2.2 Preparation of the genomic DNA of *Bacillus* sp. AHU2216**

*Bacillus* sp. AHU2216 was grown in 100 mL of the starch medium at 37 °C for 18 h. The cells, harvested by centrifugation (1,680 ×g, 4°C, 10 min), were suspended in 10 mL of 10 mM Tris-HCl buffer (pH 8.0) containing 1 mM EDTA (Nacalai Tesque, Kyoto, Japan), 0.2 mg/mL proteinase K (Takara Bio), and 4 mg/mL lysozyme (Wako Pure Chemical industries, Osaka, Japan), and incubated at 37°C for 30 min. The cells were solubilized by adding 0.5 mL of 100 mg/mL sodium dodecyl sulfate (SDS, Nacalai Tesque) and incubated at 50°C for 30 min. After two times of phenol/chloroform extraction, nucleic acid was recovered by ethanol precipitation, and dissolved in 3 mL of 10 mM Tris-HCl buffer (pH 8.0) containing 1 mM EDTA and 20 µg/mL of RNase (Calbiochem, U.S.A). The sample was incubated at 37°C for 30 min, and the DNA was purified by phenol/chloroform extraction and ethanol precipitation. Finally, the DNA recovered was dissolved in 1 mL of 10 mM Tris-HCl buffer (pH 8.0) containing 1 mM EDTA.

### **II.2.3 Preparation of the expression plasmid of *BspAG13\_31A***

GH13\_31 AGase (*BspAG13\_31A*) gene was amplified from the genomic DNA described above by PCR using primers, 5'-GCGTAAATGCGAACGCTTACGTAAA-3' (sense) and 5'-TACAATTGCGCAATCGGTTGCTCAA-3' (antisense), which were designed based on the sequences of *Bacillus megaterium* WSH\_002 *BMWSH\_3792*. Primestar HS DNA polymerase was used. The reaction mixture and conditions for PCR were as described in II.2.1. For the production of recombinant enzyme with C-terminal His-tag, the *BspAG13\_31A* gene was cloned (Novagen, Darmstadt, Germany). The *NheI* and *XhoI* sites were introduced by PCR using primers, 5'-GAGCACATGGCTAGCAAATGGTGGAAAGAA-3' (sense; the restriction enzyme site underlined) and 5'-TGCTCAACTCTCGAGTGAAAGTAAGTATAC-3' (antisense), and DNA fragment described above was used as template. The reaction mixture and conditions for PCR were as described in II.2.1. Amplified DNA fragment with *NheI* and *XhoI* sites was ligated into pET-23a (+) vector (Novagen, Darmstadt, Germany) using DNA Ligation Kit Mighty Mix (Takara Bio). The entire sequence of inserted DNA and flanking regions was analyzed using Applied Biosystems 3130 Genetic Analyzer (Life Technologies, Carlsbad, CA, USA). The recombinant protein had Ala and Ser, replacing for Glu2 and Lys3, respectively, and extra eight residues, Leu-Glu-His-His-His-His-His-His, at the C-terminal. The DNA cloned was sequenced, and deposited in the DDBJ database under accession number LC342731.

#### **II.2.4 Preparation of the expression plasmid of *BspAG13\_31A* E256Q mutant**

*BspAG13\_31A* E256Q, in which Glu256 was substituted by Gln, was prepared as an inactive mutant enzyme. The expression plasmid for E256Q was constructed using a Primestar Mutagenesis Basal Kit (Takara Bio). The whole DNA of expression plasmid of *BspAG13\_31A* was amplified by PCR using 5′GTTGGACCAGGCAAATGGTGTAACATCG-3′ (sense; mutation site underlined) and 5′-ATTTGCCTGTCCAACCGTCATAATATC-3′ (antisense) as primers. The reaction mixture (10 μL) contained 10 ng DNA, 0.2 μM primers, and Prime STAR Max premix. Thirty cycles of PCR (98°C, 10 sec, 55°C, 15 sec, and 72°C, 30 sec) was performed. The sequence of the gene was analyzed as described above.

#### **II.2.5 Production and purification of *BspAG13\_31A* wild type and E256Q**

The *E. coli* BL21(DE3) transformant harboring the expression plasmid was cultured in 1 L of LB medium containing 100 μg/mL ampicillin. The induction culture was carried out in the presence of 0.1 mM IPTG at 18°C for 20 h (the induction culture was started when  $A_{600}$  reached 0.5). Bacterial cells, harvested by centrifugation (7,300 ×g, 4°C, 10 min), were suspended in 10 mM sodium phosphate buffer (pH 7.0; buffer A) containing 0.5 M NaCl, and disrupted by sonication (output 4, constant duty 50%). Cell-free extract obtained by centrifugation (12,600 ×g, 4°C, 10 min) was applied onto a Ni-immobilized Chelating Sepharose Fast Flow column (φ2.7×2.5 cm, GE Healthcare). After thorough washing with buffer A containing 0.5 M NaCl and 30 mM imidazole, adsorbed protein was eluted by buffer A containing 0.5 M NaCl and 300 mM imidazole. The fractions containing highly purified protein, purity of which was evaluated by SDS-PAGE, were collected and dialyzed against buffer A. The sample was concentrated to several mg/mL by ultrafiltration (Vivaspin 20, 30 kDa cutoff, Sartorius, Göttingen, Germany).

#### **II.2.6 Measurement of protein concentration**

Protein concentration of cell-free extract was measured by the Bradford method (Bradford, 1976), in which bovine serum albumin (BSA) was used as standard. In the column chromatography, protein concentration was determined by the UV method ( $A_{280}$ ) (Dayhoff *et al.*, 1952). The concentration of purified enzyme was calculated, based on the theoretical amino acid concentrations of the protein, from the amino acid concentrations after complete acid hydrolysis in 6 M HCl (Moore and Stein, 1948). From the concentration of purified enzyme, the extinction coefficient ( $A_{280}$  for 1 mg/mL solution) of purified *BspAG13\_31A* was determined to be 1.78.

### **II.2.7 SDS-PAGE**

SDS-PAGE was carried out according to the method of Laemmli (1970). Protein sample (1–2 µg of) or 10 µL of cell-free extract of *E. coli* transformant was mixed with the equal volume of 2× sample loading buffer, containing 0.1 M Tris-HCl (pH 6.8), 4% β-mercaptoethanol, 20% glycerol, and heated at 100°C for 5 min. The sample was applied onto the 10% polyacrylamide separation gel. Electrophoresis was done at a constant voltage, 200 V. The gel was visualized with Rapid CBB Kanto (Kanto Chemical, Tokyo, Japan). Low molecular weight protein size marker (Bio-Rad, U.S.A.) were used

### **II.2.8 Standard enzyme activity assay**

A reaction mixture (50 µL), containing appropriate concentration of enzyme, 4 mM maltose (G2), 42 mM sodium phosphate buffer (pH 7.0), and 0.02 mg/mL BSA, was incubated at 37°C for 10 min. Enzyme was diluted with buffer A containing 0.02 mg/mL of BSA. The reaction was stopped by adding 100 µL of 2 M Tris-HCl (pH 7.0), and liberated D-glucose was determined by the glucose oxidase-peroxidase method (Miwa *et al.*, 1972; Kunst *et al.*, 1984) using Glucose CII Test Wako (Wako Pure Chemical Industries). As standard, 0–0.5 mM D-glucose was used in place of the enzyme reaction mixture. One unit of enzyme activity was defined as the amount of enzyme that hydrolyzes 1 µmol of G2 in 1 min under these conditions.

### **II.2.9 Analysis of reaction products by thin layer chromatography (TLC)**

A Reaction mixture (1 mL), containing the cell-free extract of *E. coli* transformant, 15 or 440 mM G2 (Nihon Shokuhin Kako, Tokyo, Japan), and 10 mM MES-NaOH buffer (pH 6.0), was incubated at 37°C. An aliquot (50 µL) taken from the reaction mixture was heated at 100°C for 5 min. For purified *BspAG13\_31A*, the enzyme (6 nM) was reacted under the same conditions as the cell-free extract. Reactions with 15 mM G3 (Nacalai Tesque) and maltotetraose (G4; Nihon Shokuhin Kako) were also analyzed. Ten µg of carbohydrates were spotted on silica gel TLC plate. For development, solvent [2-propanol: 1-butanol: H<sub>2</sub>O = 12: 3: 4 (v/v/v)] was used. Carbohydrates were visualized with the detection reagent, anisaldehyde: H<sub>2</sub>SO<sub>4</sub>: acetic acid = 1: 2: 100 (v/v/v), followed by heating in an oven.

### **II.2.10 Optimal pH and temperature**

Activity was measured at various pH values to determine optimum pH of *BspAG13\_31A*. As the reaction buffer, 80 mM Britton-Robinson buffer (pH 2.0–11.3; 80 mM sodium acetate, 80 mM sodium phosphate, and 80 mM sodium glycine that was tritrated with 0.2 M NaOH) was used. Optimum

temperature was examined by measuring enzyme activity (section II.2.8) at various temperatures (20–60°C).

### II.2.11 pH and thermal stability

The pH and temperature stability were investigated by measuring residual activity of the enzyme after treatment. For pH stability, a mixture (40 µL) containing enzyme (2.28 nM-0.52 µM) and 100 mM Britton-Robinson buffer (pH 2.0–11.3) was incubated at 37°C for 20 min or 4°C for 24 h. For temperature stability, a mixture (40 µL) containing enzyme (0.13-5.2 nM) and 50 mM sodium phosphate buffer (pH 7.0) was kept at 30–60°C for 20 min. After treatment, the enzyme activity was determined (see, II.2.8), and the residual activity was investigated. The pH and temperature ranges, in which the enzyme showed residual activity higher than 95%, were regarded as stable ranges.

### II.2.12 Kinetic analysis of reactions with various substrates

Enzyme activities for following substrates were measured as the standard assay (section II.2.8): G2, G3, G4, maltopentaose (G5, Wako Pure Chemical Industries, Osaka, Japan), maltohexaose (G6, Wako Pure Chemical Industries), maltoheptaose (G7, Wako Pure Chemical Industries), trehalose (Hayashibara, Okayama, Japan), nigerose (Hayashibara, Okayama, Japan), kojibiose (Wako Pure Chemical Industries), isomaltose (Tokyo Chemical Industry, Tokyo, Japan), sucrose (Kanto Chemical), and *p*-nitrophenyl α-D-glucoside (*p*NPG, Wako Pure Chemical Industries). A reaction mixture (100 µL), containing enzyme (4.65 nM-186 µM), 1 mM substrate, 42 mM sodium phosphate buffer (pH 7.0), and 0.02 mg/mL BSA, was incubated at 37°C for 10 min. In the reaction with *p*NPG, the reaction was terminated by adding 200 µL of 1 M Na<sub>2</sub>CO<sub>3</sub>. Concentration of *p*NP was measured using  $\epsilon_{1 \text{ mM}, 400 \text{ nm}} = 5.56$  (Saburi *et al.*, 2006). In the reaction with other substrates, 50 µL of 4 M Tris-HCl buffer (pH 7.0) was added to stop the reaction, and liberated D-glucose was measured as described above (section II.2.8).

Kinetic parameters for *p*NPG and G2 were determined using following equations as described previously (Kobayashi *et al.*, 2011; Saburi *et al.*, 2013)

$$\text{Eq. 1: } v_{\text{ag}} = (k_{\text{cat}2}[\text{S}]^2 + k_{\text{cat}1}K_{\text{m}2}[\text{S}]) / ([\text{S}]^2 + K_{\text{m}2}[\text{S}] + K_{\text{m}1}K_{\text{m}2})$$

$$\text{Eq. 2: } v_{\text{h}} = k_{\text{cat}1}K_{\text{m}2}[\text{S}] / ([\text{S}]^2 + K_{\text{m}2}[\text{S}] + K_{\text{m}1}K_{\text{m}2})$$

$$\text{Eq. 3: } v_{\text{tg}} = k_{\text{cat}2}[\text{S}]^2 / ([\text{S}]^2 + K_{\text{m}2}[\text{S}] + K_{\text{m}1}K_{\text{m}2})$$

$$\text{Eq. 4: } v_{\text{glc}} = (k_{\text{cat}2}[\text{S}]^2 + 2k_{\text{cat}1}K_{\text{m}2}[\text{S}]) / ([\text{S}]^2 + K_{\text{m}2}[\text{S}] + K_{\text{m}1}K_{\text{m}2})$$

Kinetic parameters for G3–G7 were determined by fitting the Michaelis-Menten equation to the D-glucose-releasing velocities at 1–25 mM. Grafit version 7.0.2 (Erithacus Software, East Grinstead, UK) was used for non-linear regression.

### II.2.13 Transglucosylation with maltooligosaccharides

Transglucosylation ratio ( $r_{TG}$ ) for the reaction with 10 mM maltooligosaccharides (G2 to G6) was determined from velocity from transglucosylation ( $v_{tg}$ ) and velocity from hydrolysis ( $v_h$ ),  $r_{TG} = v_{tg}/v_{ag} \times 100$ . A reaction mixture (1 mL), containing enzyme (1.37-13.7 nM), 10 mM substrate, 42 mM sodium phosphate buffer (pH 7.0), and 0.02 mg/mL BSA, was incubated at 35°C. An aliquot (0.2 mL) was taken every 3 min, and the reaction was stopped by heating the sample at 100°C for 5 min. The reaction products were analyzed by high performance anion-exchange chromatography with pulsed amperometric detection (HPAEC-PAD; Dionex™ ICS-5000<sup>+</sup>, Thermo Fisher Scientific, Waltham, MA, USA). The analytical conditions were as follows: sample injection volume, 10  $\mu$ L; column, CarboPac PA1 column (4 mm i.d.  $\times$  250 mm; Thermo Fischer Scientific); eluent, 640 mM NaOH; flow rate, 0.8 mL/min. Authentic maltooligosaccharides (10–100  $\mu$ M) was used as standard.

### II.2.14 Structural analysis of transglucosylation product from *p*NPG

A reaction mixture (10 mL), containing 0.44  $\mu$ M *Bsp*AG13\_31A, 16 mM *p*NPG, and 13 mM MES-NaOH buffer (pH 6.0), was incubated at 37 °C for 1 h. After heating at 100°C for 5 min, the sample was concentrated to 5 mL under a reduced pressure, and separated by a Bio-Gel P-2 column chromatography ( $\phi$ 1.7 $\times$ 100 cm; Bio-Rad) equilibrated with water, and freeze-dried. Molecular mass of the product was analyzed by electrospray ionization mass spectrometry (ESI-MS) using an Exactive Mass Spectrometer (Thermo Scientific, San Jose, CA, USA). The sample was introduced by flow injection using methanol as a mobile phase solvent. Negative ion was detected at 80V of tube lens and 30V of skimmer voltage. Nuclear magnetic resonance (NMR) spectra were recorded in D<sub>2</sub>O (99.9%, Sigma, St. Louis, MO, USA) using Bruker AMX500 (500 MHz, Bruker, Billerica, MA, USA). A series of two-dimensional homo- and heteronuclear correlated spectra [correlated spectroscopy, heteronuclear single quantum coherence (HSQC), HSQC-total correlation spectroscopy, and heteronuclear multiple bond correlation (HMBC)] were obtained.

### II.2.15 Crystallization and data Collection

The initial crystallization screening was performed using a series of crystallization kits from Qiagen (Hilden, Germany) by the sitting-drop vapor-diffusion method, in which 0.75  $\mu$ L of protein solution (16.1 mg/mL) in 10 mM Tris-HCl buffer (pH 7.0) was mixed with an equal volume of reservoir



solution. The appropriate crystals of *BspAG13\_31A* wild type were obtained within two weeks at 20°C with reservoir solution containing 0.2 M CaCl<sub>2</sub> and 20% (w/v) polyethylene glycol (PEG) 3350.

To obtain the substrate-bound complex, an inactive mutant E256Q enzyme was used. The crystals of E256Q complex with substrates, E256Q-G2, E256Q-G3 and E256Q-G4, were obtained by co-crystallization with 10 mM substrates in drops under the same condition as for the wild type. For X-ray diffraction experiments the crystals of *BspAG13\_31A* and each complex were directly picked up from crystallization solution and flash cooled.

Diffraction data of *BspAG13\_31A* and each complex were collected on beamline BL-41XU at SPring-8 (Hyogo, Japan) and beamline BL-1A at Photon Factory (Tsukuba, Japan), respectively. The data sets were indexing, integrating, scaling and merged using the *XDS* program suite (Kabsch, 2010). The asymmetric unit of *BspAG13\_31A* contained one molecule corresponding to a Matthews coefficient (Matthews, 1986) of 2.31 Å<sup>3</sup> Da<sup>-1</sup> and an estimated solvent content of 46.7%. All data collection statistics are summarized in Table II.1.

## II.2.16 Structure solution and refinement

The structures of *BspAG13\_31A* apo-form and substrate-bound enzymes were determined by the molecular replacement (MR) method with the program *AutoMR* in the *Phenix* program package (Adam *et al.*, 2010; McCoy *et al.*, 2007). The structure of apo-form was solved using the structure of *GsjAG* (PDB: 2ZE0) as the search model. Subsequently, the structures of each complex were determined using the structure of apo-form as the search model. Several rounds of refinement were performed using the program *Phenix.refine* in the *Phenix* program suite, alternating with manual fitting and rebuilding based on  $2F_o - F_c$  and  $F_o - F_c$  electron density using *COOT* (McCoy *et al.*, 2007; Emsley and Cowtan, 2004). Then, water molecules, calcium ions and substrates were built based on  $2F_o - F_c$  and  $F_o - F_c$  electron densities. The final refinement statistics and geometry defined by MolProbity (Chen *et al.*, 2010) are shown in Table II.1. All structure figures were generated by PyMol.

## II.3 Results

### II.3.1 Identification of AGase in *Bacillus* sp. AHU2216

Cell-free extract of *Bacillus* sp. AHU2216 isolated from soil near a hot spring in Hiratanai, Hokkaido, Japan showed transglucosylation activity producing G3 from G2 even at a low G2 concentration (15 mM) (Figure II.1A), while other AGases catalyze predominantly hydrolysis at a similar substrate concentration (20 mM) (Hung *et al.*, 2005; Saburi *et al.*, 2013). The length of the partial 16S rDNA sequence, 1,276 bp amplified by PCR was 99.6% identical to the corresponding region of *B. megaterium* WSH\_002. The genome sequence of *B. megaterium* WSH\_002 contains the

gene *BMWSH\_3792*, which encodes a putative AGase belonging to GH13\_31 (Figure II.2). Although its product is recorded as oligo-1,6-glucosidase in GenBank, its deduced amino acid sequence possesses an Ala next to the catalytic nucleophile as frequently observed in  $\alpha$ -(1 $\rightarrow$ 4)-glucoside-acting AGase without carrying three residues essential for  $\alpha$ -(1 $\rightarrow$ 6)-linkage specificity (Yammamoto *et al.*, 2004; Tsujimoto *et al.*, 2007; Saburi *et al.*, 2015). Thus, the protein was predicted to be  $\alpha$ -(1 $\rightarrow$ 4)-specific AGase, and the corresponding gene in *Bacillus* sp. AHU2216 was cloned. The gene product *BspAG13\_31A* was composed of 555 amino acid residues and 98.0% identical with *BMWSH\_3792*.

### **II.3.2 Purification of the recombinant *BspAG13\_31A***

The recombinant *BspAG13\_31A* was expressed in the *E. coli* BL21 (DE3) transformant in 1 L-scale. The cell-free extract (70 mL, 1390 mg of protein) showed 43,100 U of activity (specific activity, glucose-releasing activity from 4 mM, G2 22.1 U/mg). Recombinant *BspAG13\_31A* was purified to homogeneity by Ni-affinity column chromatography (Figure II.3 and 4.A), and 167 mg of purified enzyme with 193 U/mg was obtained. Purified enzyme showed a single band (61.7 kDa) on SDS-PAGE (Figure II.4B). The summary of purification of *BspAG13\_31A* is shown in Table II.2.

### **II.3.3 Reaction products from maltooligosaccharides (MOS) by purified *BspAG13\_31A***

The reaction products with 15 mM and 440 mM G2 were investigated. Purified *BspAG13\_31A* produced D-glucose and G3 from 15 mM G2 as observed in the reaction of the cell-free extract of *Bacillus* sp. AHU2216 (Figure II.1B). Transglucosylation products, G4 and G5, were synthesized in the reactions with G3 and G4, respectively (Figure II.1C and 1D). G5 was slightly detected in the reaction with G4, indicating that *BspAG13\_31A* mainly catalyzed hydrolysis toward G4.

### **II.3.4 Effects of pH and temperature on enzyme activity and stability**

Recombinant *BspAG13\_31A* showed the highest activity to 4 mM G2 at pH 7.3 and at 35°C. The enzyme retained the activity in a pH ranges of 6.8–8.7 at 37°C for 20 min and 5.9–10.5 at 4°C for 24 h. *BspAG13\_31A* showed more than 95% of residual activity after 20 min incubation below 37°C (Figure II.5 and 6).

### **II.3.5 Screening of substrates**

Substrates of *BspAG13\_31A* was screened based on degrading activity to various  $\alpha$ -glucosides (1 mM; Table II.3). *BspAG13\_31A* showed high activity only towards MOS (9.21–94.3 s<sup>-1</sup>

<sup>1</sup>) and *p*NPG (5.36 s<sup>-1</sup>). This enzyme showed very low activity to oligosaccharides linked by other linkages, and it had high specificity to  $\alpha$ -(1 $\rightarrow$ 4)-glucosidic linkage. The activity to G2 was the highest among the MOS.

### II.3.6 Structural analysis of transglucosylation product from *p*NPG

In the reaction of *Bsp*AG13\_31A with 16 mM *p*NPG, transglucosylation product was detected on TLC after 15 min reaction (Figure II.7). The reaction was continued up to 1 h, and product was purified by gel-filtration column chromatography. The chemical structure of the product was determined by ESI-MS and NMR. In the ESI-MS analysis, signals of at 486.12 *m/z* [M + Na]<sup>+</sup> and 462.13 *m/z* [M - H]<sup>-</sup> were observed as positive and negative ions, respectively (Figure II.8). The mass was in a good agreement with theoretical mass, 463.39 Da, of *p*-nitrophenyl  $\alpha$ -maltoside. In the two-dimensional NMR analysis, HMBC, correlation peaks between 4-C of the internal D-glucosyl residue (Glc-A) and 1-H of the non-reducing end D-glucosyl residue (Glc-B), and between 4-H of Glc-A and 1-C of Glc B were observed (Figure II.9). The  $J_{(H-H)1}$  of Glc B was determined to be 3.8 Hz. These results indicate that Glc-B linked Glc-A through  $\alpha$ -(1 $\rightarrow$ 4)-glucosidic linkage. The chemical shifts of the product are summarized in Table II.4.

### II.3.7 Kinetic analysis of reactions with *p*NPG and G2

Velocities for *p*NP and D-glucose liberations from *p*NPG were measured at various *p*NPG concentrations. Velocities of *p*NP release ( $v_{ag}$ ),  $v_h$ , and  $v_{ig}$  at various *p*NPG concentrations followed to the rate equations Eq.1–Eq. 3 (Figure II.10A). The kinetic parameters determined from  $v_{ag}$  are shown in Table II.5. The  $r_{TG}$  followed a saturation curve, and  $K_{TG}$  value was determined to be 2.48 mM (Figure II.10B).

In the reaction with G2, Eq. 4 for the reaction in which both hydrolysis and transglucosylation simultaneously occurred was fitted to velocities of D-glucose liberation ( $v_{glc}$ ) from G2 (Figure II.10C). The  $K_{TG}$  value (21.6 mM) was 8.7-fold higher than that of *p*NPG.

### II.3.8 Substrate chain-length specificity

Initial reaction velocities of *Bsp*AG13\_31A to 10 mM MOS (G2-G6) were measured, and  $r_{TG}$  values were determined (Table II.6). The  $r_{ig}$  for G2 was the highest (30.1%), and decreased to 7.0% for G5 as the chain-length of the MOS increased. Because of the low  $r_{TG}$  values,  $v_h$  for 1–25 mM G3–G7, calculated from  $v_{glc}$ , followed the Michaelis-Menten equation (Table II.7). The  $k_{cat}/K_m$  values for MOS decreased with an increasing degree of polymerization of the substrates, mainly because of

increase in the  $K_m$  value. The  $k_{cat}/K_{m1}$  for G2, which is comparable to the  $k_{cat}/K_m$  from the Michaelis-Menten equation, was 3.8-fold higher than  $k_{cat}/K_m$  for G3.

### II.3.9 Overall structure of *BspAG13\_31A*

Crystal structures of *BspAG13\_31A* wild type in apo-form and E256Q in complex with G2, G3, and G4 were determined at 2.5 Å, 1.7 Å, 1.7 Å and 1.6 Å resolutions, respectively (Table II.1). E256Q showed typical behavior of mutant enzymes of general acid/base catalyst: reaction rate of E256Q to 1 mM *p*NPG with good leaving group was 0.3% of that of wild type, but its activity to G2 with poor leaving group was less than  $1.6 \times 10^{-3}$ % of that of wild type. All complex-structures were highly similar to that of apo-form with root-mean-square deviation (RMSD) of 0.18–0.21 Å for the 555 *Cas*. Overall structure of *BspAG13\_31A* (Figure II.11A) consists of the catalytic domain A (residues 1–104, 172–362 and 455–476), a loop-rich domain B (residues 105–171), domain B' (residues 363–454) and domain C (residues 477–555). Domain A is a (c/α)<sub>8</sub>-barrel, and domain B and B' were protruding loops connecting third β-strand and third α-helix (β→α loop 3) of the (β/α)<sub>8</sub>-barrel and β→α loop 8, respectively. Domain C is formed by two antiparallel β-sheets. A deep active-site pocket was composed of domains A, B, and B'. The β→α loop 6 (Phe282–Pro295) included a disordered part (Gly291–Lys294 of the apo-form and Asp289–Glu293 of the complexes) because of poor electron density and took different conformations between the apo-form and the complexes. In the apo-form of *BspAG13\_31A*, Trp288 on this loop was placed to prevent substrates from binding at subsites +1 and +2, while in the substrate complexes, this loop showed a different conformation suitable for binding substrates (Figure II.11C). These results showed flexible structural movement of β→α loop 6.

An electron-density blob, which appeared to be an ion and was coordinated by oxygen atoms of Asp21 OD1, Asn23 OD1, Asp25 OD1, Asp29 OD1, Ile27, and a water molecule, was found in all the structures. Considering the crystallization condition, the coordination bonds, and refinement results, this blob was assigned as Ca<sup>2+</sup> (Figure II.12). This position is the β→α loop 1 calcium-binding site, which is observed in some GH13 enzymes (Kobayashi *et al.*, 2011) in addition to other GH13\_31 enzymes (Hondoh *et al.*, 2008; Shirai *et al.*, 2008; Møller *et al.*, 2012).

### II.3.10 Orientation of MOS bound to *BspAG13\_31A* and interactions with the enzyme

The  $F_o-F_c$  map clearly revealed the existence of a substrate molecule, although the electron density for part of the D-glucose ring at subsite +3 was poor in the complex with G4 (Figure II.13A–C). The ligands were accommodated in subsite -1 to subsite +3. In all three complexes, the substrates spanned from subsite -1, which was located at the bottom of the active site pocket. In all three

complexes, equivalent D-glucosyl residues in each subsite showed similar orientations. The torsion angles,  $\Phi$  (5-O, 1-C, 4'-O, and 4'-C) and  $\Psi$  (1-C, 4'-O, 4'-C, and 5'-C), of bound MOS were as follows:  $(\Phi, \Psi) = (40^\circ\text{--}43^\circ, -150^\circ\text{--}155^\circ)$  for residues in subsites -1 and +1,  $(57^\circ\text{--}65^\circ, -164^\circ\text{--}168^\circ)$  for residues in subsites +1 and +2, and  $(105^\circ, -113^\circ)$  for residues in subsites +2 and +3. Only the torsion angles of residues at subsites +2 and +3 were similar to the D-glucosyl residues in  $\alpha$ -(1 $\rightarrow$ 4)-glucan:  $(\Phi, \Psi) = (102^\circ, -120^\circ)$  (Gessler *et al.*, 1999). The torsion angles of the residues between -1 and +1 of *BspAG13\_31A* were similar to those of the MOS-complexes of other GH13 enzymes: G2 bound to *HaG*,  $(\Phi, \Psi) = (35^\circ, -148^\circ)$  (Shen *et al.*, 2015); G4 bound to neopullulanase,  $(\Phi, \Psi) = (34^\circ, -144^\circ)$  (Hondoh *et al.*, 2003); and G7 bound to amylosucrase,  $(\Phi, \Psi) = (34^\circ, -155^\circ)$  (Skov *et al.*, 2002). At subsites +1 and +2, however, the glucosyl residues of the complexes were accommodated to form a hydrogen bond between the two 6-OH groups, while  $\alpha$ -(1 $\rightarrow$ 4)-glucan forms the hydrogen bonds between 2-OH and 3-OH of the adjacent D-glucosyl residues (Gessler *et al.*, 1999). The torsion angles of the residues between +1 and +2 subsites of *BspAG13\_31A* were similar to those of G7 bound to amylosucrase,  $(\Phi, \Psi) = (67^\circ, -148^\circ)$ , while those of G4 bound to neopullulanase [ $(\Phi, \Psi) = (92^\circ, -112^\circ)$ ] were similar to the D-glucosyl residues in  $\alpha$ -(1 $\rightarrow$ 4)-glucan.

The subsite -1 of *BspAG13\_31A* consists of the catalytic nucleophile Asp199, general acid/base catalyst Glu256, transition state stabilizer Asp327, and residues for substrate binding Asp60, Tyr63, His103, Arg197, His326, and Arg411. These residues in subsite -1 were well-conserved in GH13 AGases, and amylosucrase, and other un-modified glucosidic-acting enzymes. At subsite +1, the side-chains of His203, Gln256 (Glu256 in wild type), and Asn258 were in suitable locations for hydrogen bonds with 2-O, 3-O, and 2-O of the D-glucosyl residue, respectively. The D-glucosyl residue in subsite +2 has only two water-mediated hydrogen bonds except possible hydrogen bond between 4-O and Asn258 side chain. At subsite +3 is fixed by three direct (Phe282, Met285, and Gln328) and one water-mediated hydrogen bonds (Figure II.14).

## II.4 Discussions

*BspAG13\_31A* with high transglucosylation activity was biochemically and structurally characterized in this chapter. *BspAG13\_31A* showed high regioselectivity to  $\alpha$ -(1 $\rightarrow$ 4)-glucosidic linkage in both hydrolysis and transglucosylation to G2. From the structures of the enzyme-substrate complexes, Ala200 contributes to formation of the substrate-binding site to accommodate  $\alpha$ -(1 $\rightarrow$ 4)-linked substrates in *BspAG13\_31A*.  $\alpha$ -(1 $\rightarrow$ 4)-Linkage-specific GH13 AGases have Ala or Thr at this position (Figure II.15), and this Ala/Thr is thought to be important for linkage specificity as demonstrated in *SmDG* (Saburi *et al.*, 2015). His203 and Asn258, located on the  $\beta$  $\rightarrow$  $\alpha$  loops 4 and 5, respectively, were regarded to be involved in forming subsite +1 through hydrogen bonding with 2-O of the D-glucosyl residue (Figure II.13).  $\alpha$ -(1 $\rightarrow$ 4)-Linkage specific GH13\_31 AGases from *GsaAG*

and *GsjAG* also have His and Asn at equivalent positions (Takii *et al.*, 1996; Hung *et al.*, 2005). The His residue corresponding to His203 of *BspAG13\_31A* is frequently found in  $\alpha$ -(1 $\rightarrow$ 4)-linkage specific GH13 enzymes including  $\alpha$ -amylases and cyclodextrin glucoamylases (MacGregor *et al.*, 2001).

*BspAG13\_31A* showed high disaccharide specificity (Tables II.3, 6 and 7), while most AGases prefer trisaccharides to disaccharides (Okuyama *et al.*, 2016). In *HaG* showing disaccharide preference, steric hindrance caused by long  $\beta\rightarrow\alpha$  loop 4 (Leu201-Arg246), which situated in subsite +1 above the above D-glucose residue of G2, is responsible for disaccharide specificity (Shen *et al.*, 2015). The overall structure of *BspAG13\_31A* displayed high similarity to *HaG* with an RMSD of 1.8 Å for the 546 C $\alpha$  atom. However,  $\beta\rightarrow\alpha$  loop 4 of *BspAG13\_31A* is shorter than that of *HaG* by 12 residues, and as short as those of typical GH13\_31 enzymes (Figure II.11B, and II.15). The  $k_{cat}/K_m$  for G3 was lower than  $k_{cat1}/K_{m1}$  of G2, indicating that substrate binding beyond subsite +1 is less favorable. The torsion angles of D-glucosyl residues in subsites +1 and +2 were different from those of the stable  $\alpha$ -(1 $\rightarrow$ 4)-glucan presumably because of steric hindrance by Asn258. According to the molecular mechanics study published by Dowd *et al.*, 1992, these torsion angles are similar to those of  $\alpha$ -maltose in the orientation with slightly higher relaxed energy [( $\Phi$ ,  $\Psi$ ) = (65°, -168°); 96.6 kJ/mol] than the global minimum [( $\Phi$ ,  $\Psi$ ) = (97°, -142°); 95.3 kJ/mol], torsion angles of which are similar to those of stable  $\alpha$ -glucan. This energy difference (1.3 kJ/mol) might account for part of negative affinity at subsite +2. As only a few possible indirect hydrogen bonds were observed in subsite +2, *BspAG13\_31A* presumably had low activity towards G3.

High transglucosylation in G2 might have arisen from the different orientation of  $\beta\rightarrow\alpha$  loop 6. Possible steric hindrance caused by Trp288 on this loop in the substrate-free form was avoided in the substrate complexes (Figure II.11C).  $\beta\rightarrow\alpha$  Loop 6 may take an orientation similar to that of the apo-form after the aglycone part departs. The conformational change of this loop along with the reaction process may be important for transglucosylation by stabilizing the glucosyl enzyme intermediate and preventing water molecules from binding and acting as substrate.

**Table II.1 Summary of crystallization conditions, data collection and refinement statistics.**

	Apo-form	E256Q-G2	E256Q-G3	E256Q-G4
PDB ID	5ZCB	5ZCC	5ZCD	5ZCE
<b>Data collection</b>				
Beamline	SPring-8 BL41XU	PF BL-1A	PF BL-1A	PF BL-1A
Space group	P2 <sub>1</sub> 2 <sub>1</sub> 2 <sub>1</sub>	P2 <sub>1</sub> 2 <sub>1</sub> 2 <sub>1</sub>	P2 <sub>1</sub> 2 <sub>1</sub> 2 <sub>1</sub>	P2 <sub>1</sub> 2 <sub>1</sub> 2 <sub>1</sub>
Unit cell parameters a, b, c, (Å)	54.9, 84.9, 128.4	55.0, 84.8, 128.8	55.6, 84.7, 128.5	55.0, 84.5, 128.7
Wavelength (Å)	0.9795	1.1	1.1	1.1
Resolution range (Å)	50.0-2.5 (2.65-2.5)	50.0-1.7 (1.81-1.7)	50.0-1.7 (1.81-1.7)	50.0-1.56 (1.65-1.56)
R <sub>meas</sub> (%)	7.3 (22.6)	9.5 (65.6)	11.7 (74.3)	11.7 (77.3)
<I/σ(I)>	22.2 (8.3)	13.9 (2.4)	11.1 (2.0)	11.7 (2.4)
Completeness (%)	96.8 (85.1)	99.5 (97.0)	99.6 (97.8)	97.4 (94.7)
Redundancy	7.1 (6.5)	6.6 (5.8)	6.6 (5.8)	6.9 (6.8)
<b>Refinement</b>				
No. reflection	20,783	66,318	66,627	84,636
R <sub>work</sub> /R <sub>free</sub> (%)	18.0/21.5	16.4/18.9	17.8/20.6	17.2/19.1
No. of atoms				
Macromolecules	4,502	4,494	4,494	4,494
Ligand/ion	3	26	37	48
Water	203	820	702	817
B-factors (Å <sup>2</sup> )				
Macromolecules	26.5	21.0	20.8	17.9
Ligand/ion	38.9	18.1	21.1	21.8
Water	30.2	32.3	31.3	30.7
Estimated coordinate error	0.26	0.15	0.17	0.14
RMSD from ideal				
Bond lengths (Å)	0.002	0.007	0.006	0.007
Bond angles (°)	0.64	1.07	1.04	1.19
Ramachandran				
Favored (%)	95.2	96.9	96.7	96.1
Allowed (%)	4.63	3.15	3.34	3.90
Outliers (%)	0.19	0	0	0

Values in parentheses are for the highest resolution shell.

\*  $R_{meas} = \sum_{hkl} \{N(hkl) / [N(hkl) - 1]\}^{1/2} \sum_i |I_i(hkl) - \langle I(hkl) \rangle| / \sum_{hkl} \sum_i I_i(hkl)$ , where  $\langle I(hkl) \rangle$  and  $N(hkl)$  are the mean intensity of a set of equivalent reflections and the multiplicity, respectively.

\*\*  $R_{work} = \sum_{hkl} ||F_{obs}| - |F_{calc}|| / \sum_{hkl} |F_{obs}|$ ,  $R_{free}$  was calculated for 5% randomly selected test sets that were not used in the refinement.

**Table II.2 Summary of purification of recombinant *BspAG13\_31A*.**

<b>Purification step</b>	<b>Total protein (mg)</b>	<b>Volume (mL)</b>	<b>Total activity (U)</b>	<b>Specific activity (U/mg)</b>	<b>Recovery (%)</b>	<b>Purification (-fold)</b>
• Cell-free extract	1390*	70.0	43,100	31.0	100	1
• Nickel affinity column chromatography	167**	4.70	32,300	193	74.9	6.23

\* Protein concentration was measured by Bradford method.

\*\* Protein concentration was measured by amino acid analysis.



**Table II.3**      **Glucose-releasing velocities to various substrates.**

<b>Substrate</b>	<b><math>v</math> (<math>s^{-1}</math>)</b>	<b>Relative <math>v</math> (%)</b>
G2	$94.3 \pm 2.8$	100
G3	$33.2 \pm 0.5$	35.2
G4	$27.2 \pm 0.2$	28.8
G5	$18.7 \pm 0.4$	19.9
G6	$11.7 \pm 0.4$	12.4
G7	$9.21 \pm 0.1$	9.78
<i>p</i> NPG	$5.36 \pm 0.23$	5.69
Sucrose	$0.179 \pm 0.004$	0.190
IG2	$(4.43 \pm 0.04) \times 10^{-3}$	$4.70 \times 10^{-3}$
Trehalose	$(1.02 \pm 0.01) \times 10^{-3}$	$1.08 \times 10^{-3}$
Kojibiose	$(9.48 \pm 0.09) \times 10^{-3}$	$1.01 \times 10^{-2}$
Nigerose	$0.131 \pm 0.004$	0.139

Reaction velocity of glucose to 1 mM of each substrates is shown. Velocity on G2 was given as 100% calculating relative  $v$ . The values are average  $\pm$  standard deviation of values from three independent experiments. IG2; isomaltose.

**Table II.4** Chemical shifts of *p*NP  $\alpha$ -maltoside in the  $^1\text{H}$ - and  $^{13}\text{C}$ -NMR spectra.

		$\delta_{\text{C}}$ (ppm)	$\delta_{\text{H}}$ (ppm)		$J$ (H, H)
Glc-A	1	97.2	5.78 <sup>*c</sup>	d	3.45
	2	71.6	3.79	m	
	3	74.1	4.20	m	
	4	77.3 <sup>*a</sup>	3.75 <sup>*b</sup>	m	
	5	72.2	3.76	m	
	6	61.0	3.74	m	
Glc-B	1	100.6 <sup>*b</sup>	5.41 <sup>*a</sup>	d	3.80 3.83, 9.33
	2	72.6	3.57	dd	
	3	73.7	3.67	m	
	4	70.1	3.40	t	
	5	73.5	3.59	m	
	6	61.3	3.81	m	
<i>p</i> NP	1	178.0			
	ArH	135.0	6.50	d	9.25
	ArH	144.0	7.25	d	9.20
	4	162.0 <sup>*c</sup>			

Asterisks indicate correlation peaks observed. Glc-B is at the non-reducing end.

**Table II.5 Kinetic parameters for G2 and *p*NPG.**

<b>Substrate</b>	$k_{\text{cat1}}$ (s <sup>-1</sup> )	$k_{\text{cat2}}$ (s <sup>-1</sup> )	$K_{\text{m1}}$ (mM)	$K_{\text{m2}}$ (mM)	$k_{\text{cat1}}/K_{\text{m1}}$ (s <sup>-1</sup> mM <sup>-1</sup> )	$K_{\text{TG}}$ (mM)
G2	205 ± 12	1890 ± 126	1.52 ± 0.19	201 ± 53	135	21.6
<i>p</i> NPG	4.72 ± 2.62	13.9 ± 1.00	2.05 ± 1.03	4.71 ± 0.82	2.30	2.48

The values are average ± standard deviation of values from three independent experiments.

**Table II.6 Hydrolysis and transglucosylation velocities for the reaction with 10 mM MOS.**

<b>Substrate</b>	<b><math>v_h</math> (<math>s^{-1}</math>)</b>	<b><math>v_{tg}</math> (<math>s^{-1}</math>)</b>	<b><math>r_{TG}</math></b>
G2	$193 \pm 5$	$82.9 \pm 13.8$	30.1
G3	$103 \pm 8$	$26.6 \pm 3.39$	20.5
G4	$83.4 \pm 4.6$	$7.90 \pm 4.2$	8.65
G5	$65.1 \pm 2.1$	$4.92 \pm 1.03$	7.03
G6	$66.4 \pm 2.5$	$6.34 \pm 1.2$	8.71

The values are average  $\pm$  standard deviation of values from three independent experiments.

In reaction on MOS under in the standard assay conditions,  $v_h$  and  $v_{tg}$  were examined.  $v_{tg}$  was calculated from ( $v_{ag} - v_h$ ).

**Table II.7** Kinetic parameters for maltooligosaccharides.

<b>Substrate</b>	$k_{\text{cat}}$ ( $\text{s}^{-1}$ )	$K_{\text{m}}$ ( $\text{mM}$ )	$k_{\text{cat}}/K_{\text{m}}$ ( $\text{s}^{-1}\text{mM}$ )	<b>Relative <math>k_{\text{cat}}/K_{\text{m}}</math></b> (%)
G3	148 ± 1	4.22 ± 0.15	35.1	26.0
G4	145 ± 16	5.75 ± 1.10	25.3	18.7
G5	143 ± 5	7.55 ± 0.62	19.0	14.1
G6	133 ± 4	15.3 ± 0.8	8.64	6.40
G7	155 ± 6	19.0 ± 1.2	8.19	6.07

The values are average ± standard deviation of values from three independent experiments.

Relative  $k_{\text{cat}}/K_{\text{m}}$  is the value relative to  $k_{\text{cat1}}/K_{\text{m1}}$  shown in Table II.5.

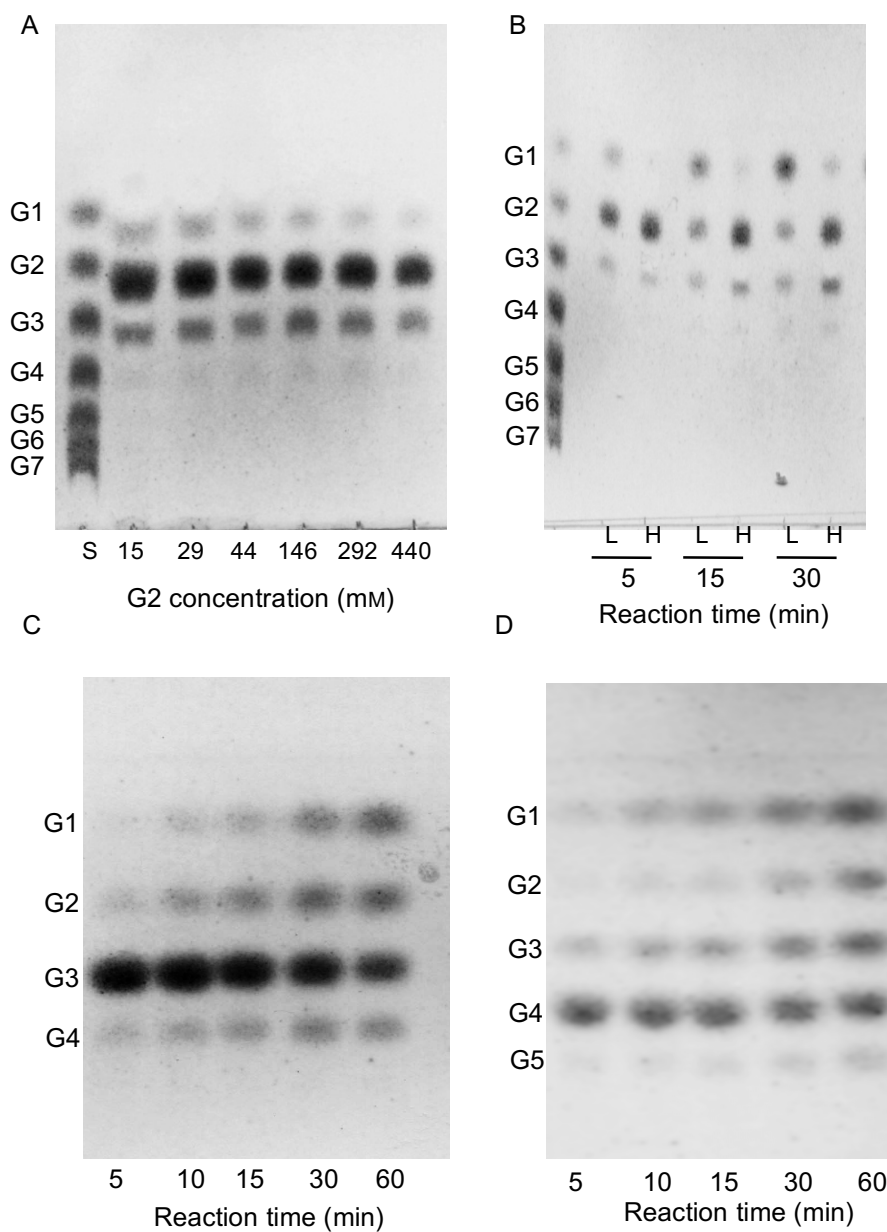


**Figure II.1. TLC analysis of reaction products by *BspAG13\_31A*.**

Lane S, standard MOS. G1, G2, G3, G4, and G5 are indicated. A, Reaction of the cell-free extract of *Bacillus* sp. AHU2216. G2 concentrations are indicated below, and the reaction was carried out at 37°C for 18 h. B, Time course of the reactions of recombinant *BspAG13\_31A* with G2. Lanes L and H are the reactions with 15 mM and 440 mM G2, respectively. C, Time courses of reactions with 15 mM G3. D, Time courses of reactions with 15 mM G4.

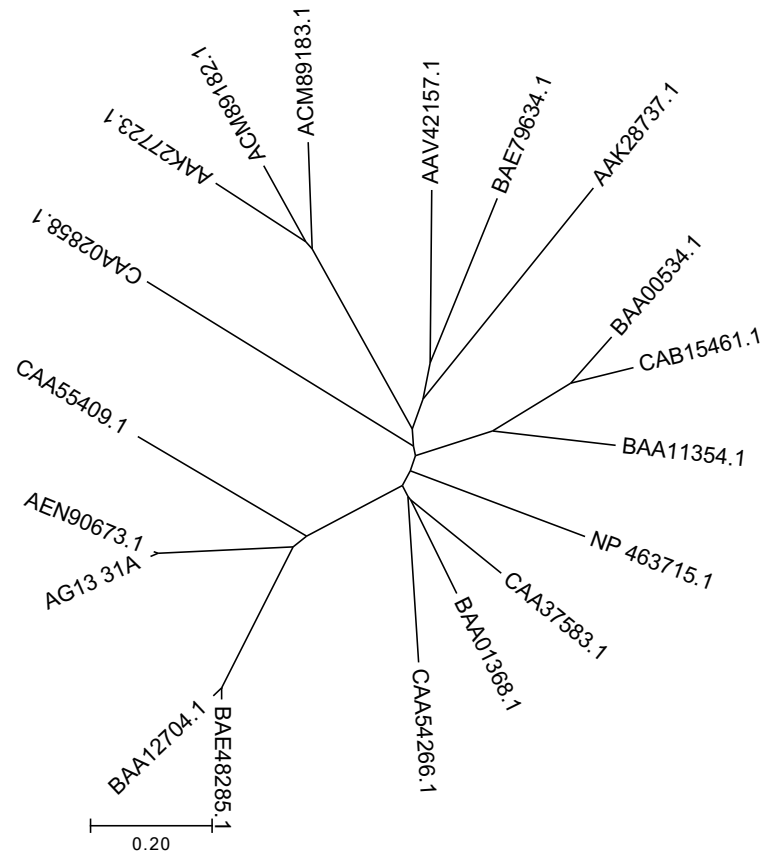


**Figure II.2 Phylogenetic tree of GH13\_31 AGases and related glycosidases.**

Phylogenetic tree of GH13\_31 AGases, oligo-1,6-glucosidases (O16Gases), and dextran glucosidases (DGases) was constructed by the neighbor joining method using the ClustalW program (Thompson *et al.*, 1994). GenBank IDs are shown.

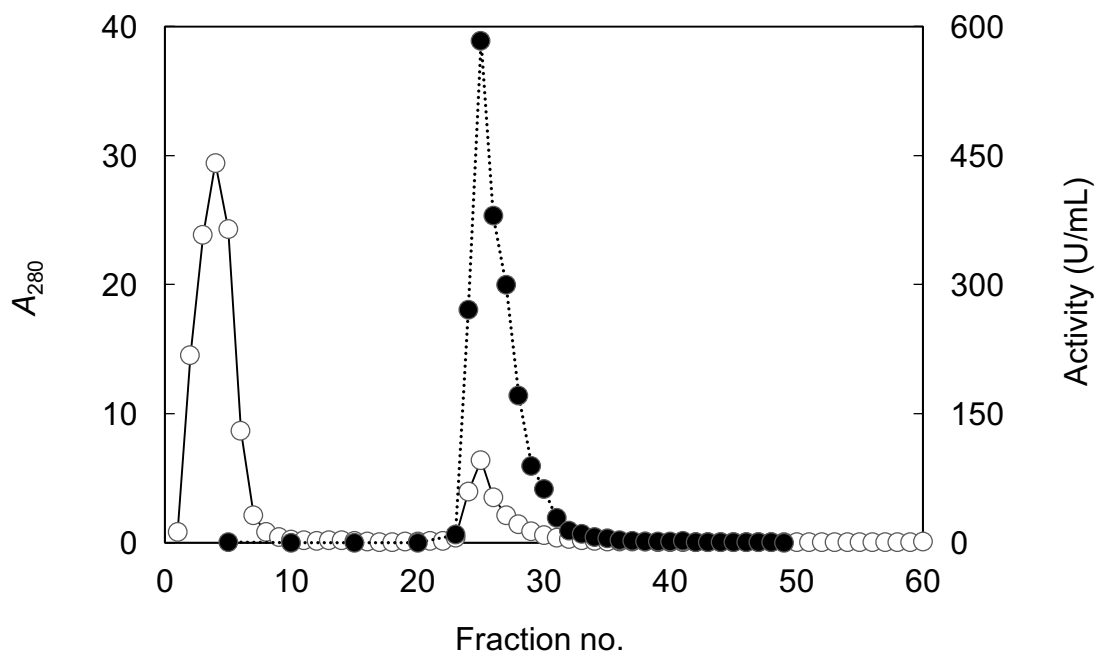


**Figure II.3 Nickel-immobilized Chelating Sepharose Fast Flow column chromatography of *BspAG13\_31A*.**

Absorbance at 280 nm (-○-) and enzyme activity (-●-) are shown. Nickel-immobilized Chelating Sepharose Fast Flow column ( $\phi 2.7 \times 2.5$  cm) was equilibrated with 10 mM sodium phosphate buffer (pH 7.0) containing 0.5 M NaCl. The adsorbed proteins were eluted by 0.3 M imidazole in the same buffer. The fraction numbers 24–32 (45 mL in total) were pooled.



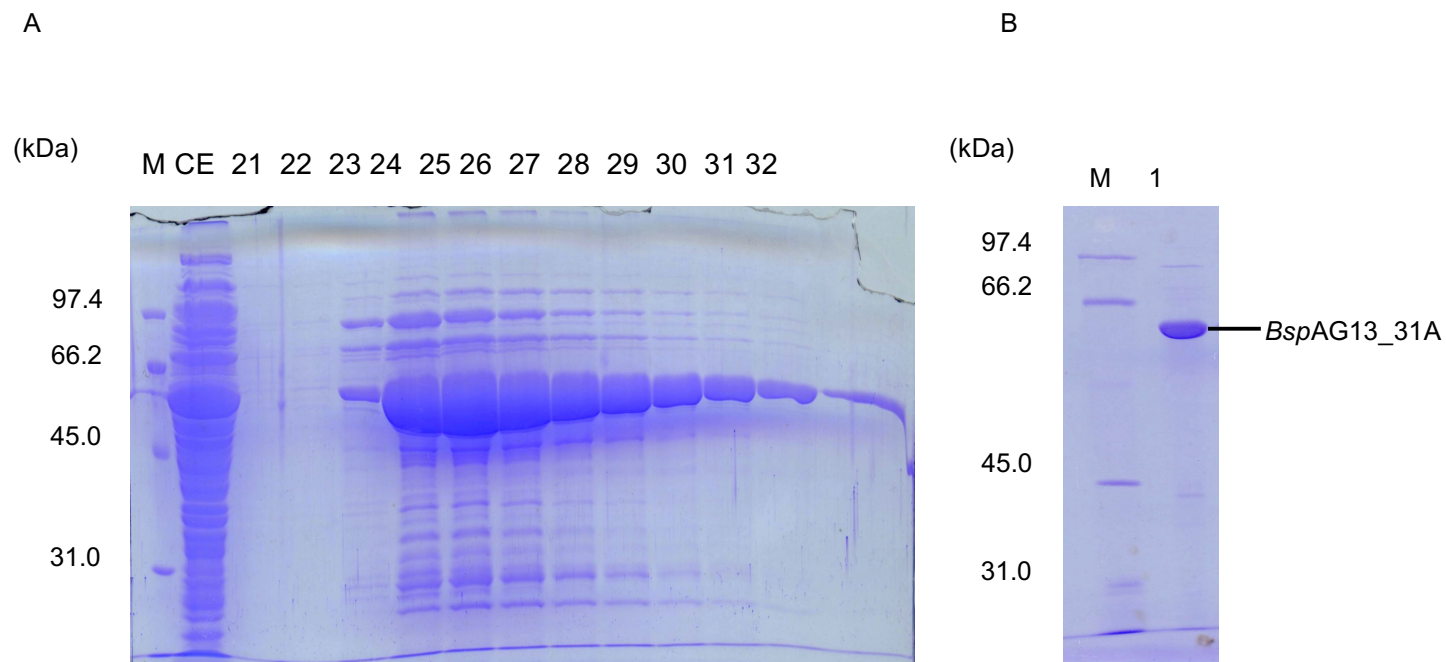


**Figure II.4 SDS-PAGE analysis of adsorbed proteins containing *BspAG13\_31A* in Nickel-immobilized Chelating Sepharose Fast Flow column chromatography.**

A, adsorbed proteins were eluted with 0.3 M imidazole containing 0.5 M NaCl in 10 mM sodium phosphate buffer (pH 7.0). Active fractions (23–32) containing *BspAG13\_31A* were investigated by SDS-PAGE. Ten  $\mu\text{L}$  of protein samples were loaded. Number above the figure indicates the fraction numbers. B, the concentrated purified *BspAG13\_31A*. Lane 1, sample (2  $\mu\text{g}$ ). Lane M, low molecular size protein marker.

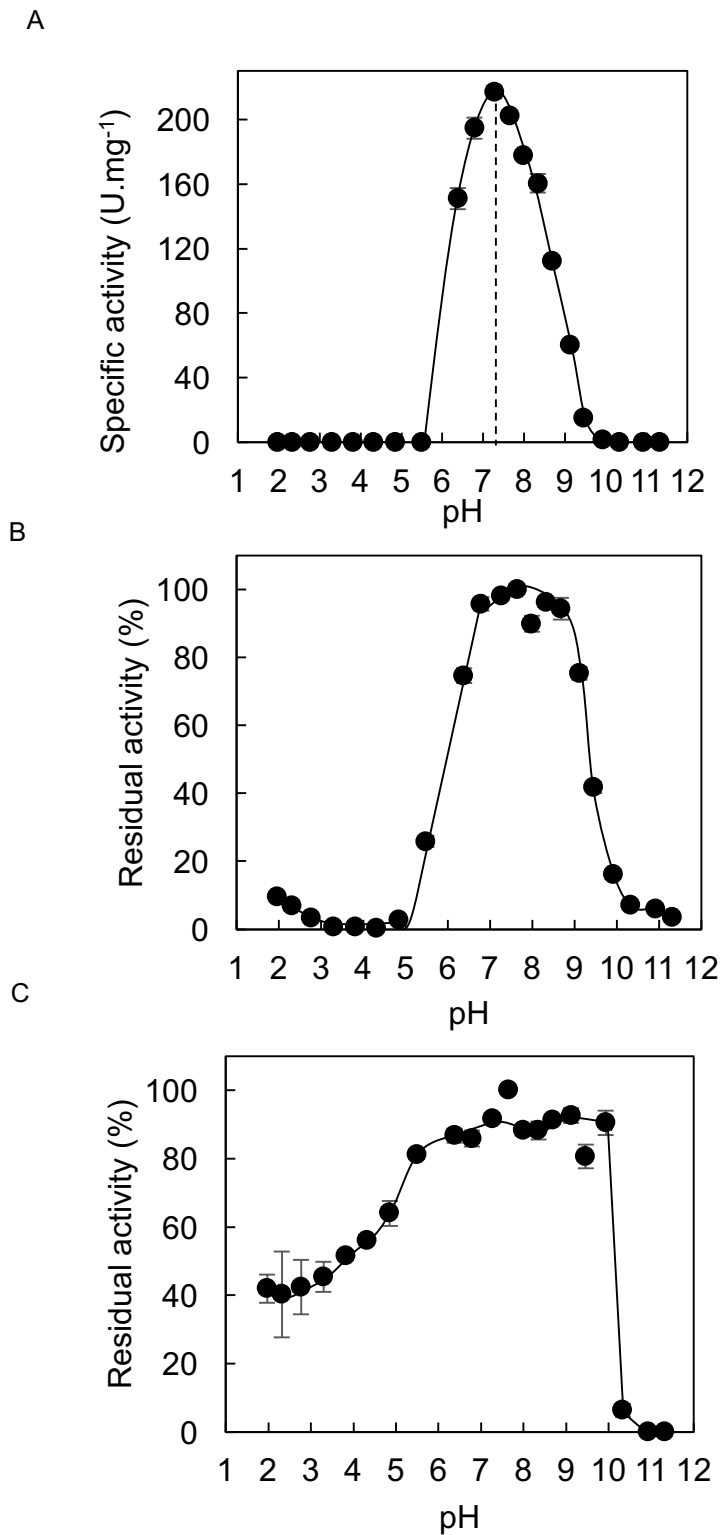


**Figure II.5** Effects of pH on enzyme activity and stability.

A, The *BspAG13\_31A* activity was measured at various pH values (1.97-11.3). The pH stability was investigated with the remaining activity after pH treatment. B, and C, The stability at 37°C for 20 min and 4°C for 24 h.

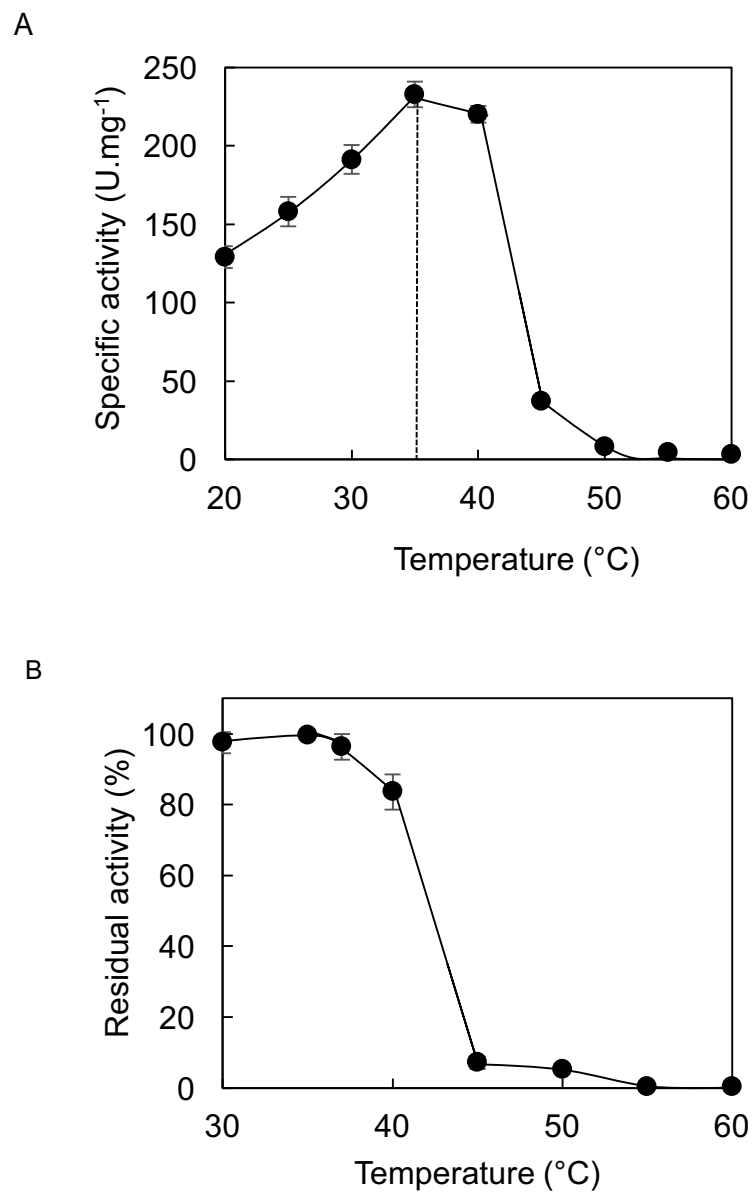


**Figure II.6 Effects of temperature on enzyme activity and stability.**

A, The *BspAG13\_31A* activity (••) was measured at various temperatures (20–60°C). B, The temperature stability after heat treatment (30–60°C).

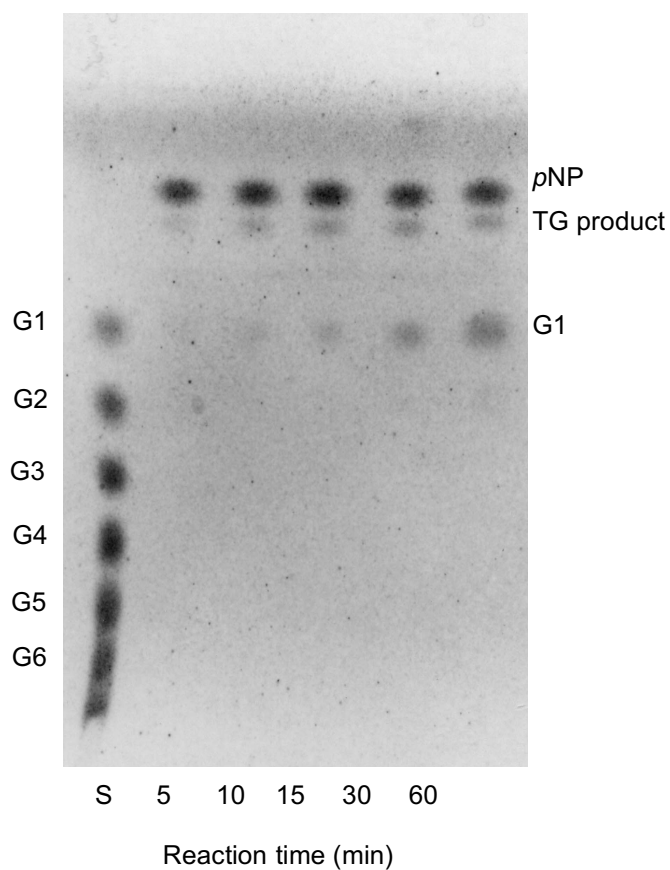


**Figure II.7 Time course of the reactions of purified recombinant *BspAG13\_31A* towards *pNPG* substrate.**

Purified recombinant *BspAG13\_31A* was reacted with 16 mM *pNPG* in 13 mM MES-NaOH buffer (pH6.0) at 37°C. Ten µg of *pNPG* equivalent was analyzed on TLC. Lane S, MOS standard.

Sample No. : C:\xcalibur\...1213\171265\_pNPG2\_pn  
Operator name : yamada miho  
Date : 12/13/2017 10:42:41 AM  
Instrumental method : C:\xcalibur\methods\HESI\_100ul\pn\_H80\_S30.meth  
Instrumental Analysis Division, Global Facility Center, Creative Research Institution, Hokkaido University

Mobile phase solvent : MeOH  
Sample solvent : submitting solution

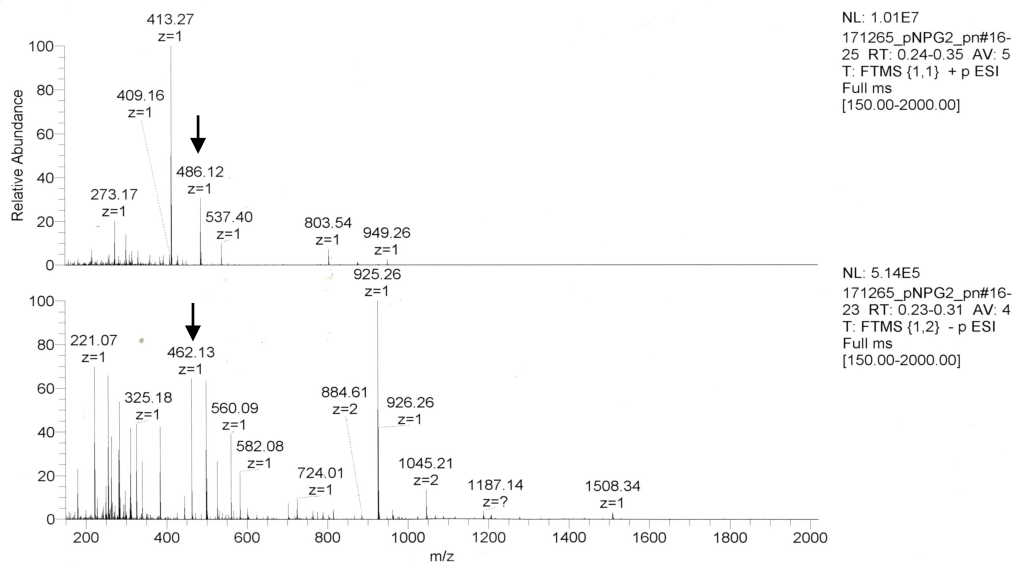


**Figure II.8 ESI-MS spectra of the transglucosylation product from *p*NPG of *Bsp*AG13\_31A.**  
ESI-MS spectra of the transglucosylation product in 16 mM *p*NPG. The 482.12  $[M + Na]^+$  m/z and 462.13  $[M - H]^-$  of signal ions were positive and negative ions, respectively.

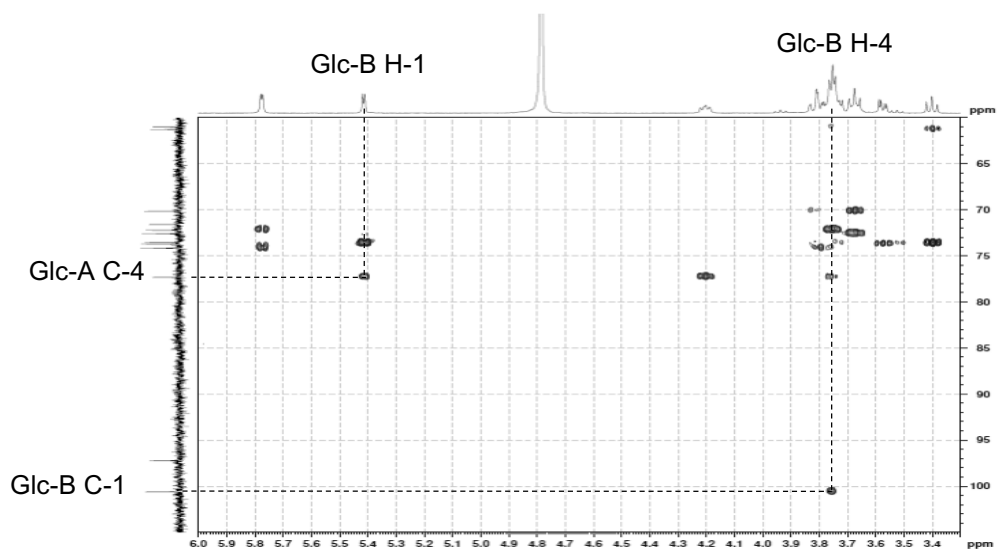


**Figure II.9** Structural analysis of transglucosylation product from *p*NPG by HMBC.

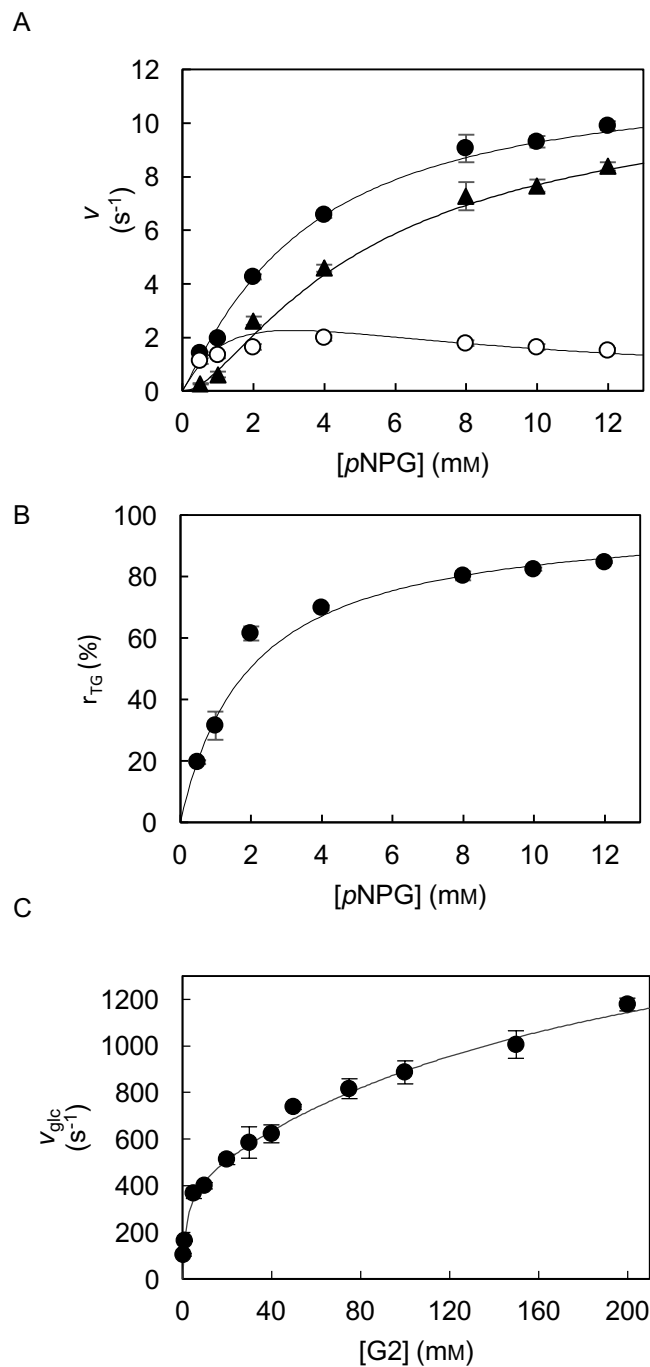


**Figure II.10 Kinetic analysis of reaction of *BspAG13\_31A* with *pNPG* and *G2*.**

Values are the mean  $\pm$  standard deviation for independent three experiments. A, s-v plot for the reaction with *pNPG*. Initial velocities for aglycone releasing ( $\bullet$ ), hydrolysis ( $\circ$ ), and transglucosylation ( $\blacktriangle$ ) are shown. The lines are theoretically obtained from Eq. 1-3, respectively. Parameters are summarized in Table II.5. B, Plot of transglucosylation ratio versus the *pNPG* concentration. C, s-v plot for the reaction with *G2*.  $v_{glc}$  are plotted. The line is from Eq. 4 with parameters shown in Table II.5.

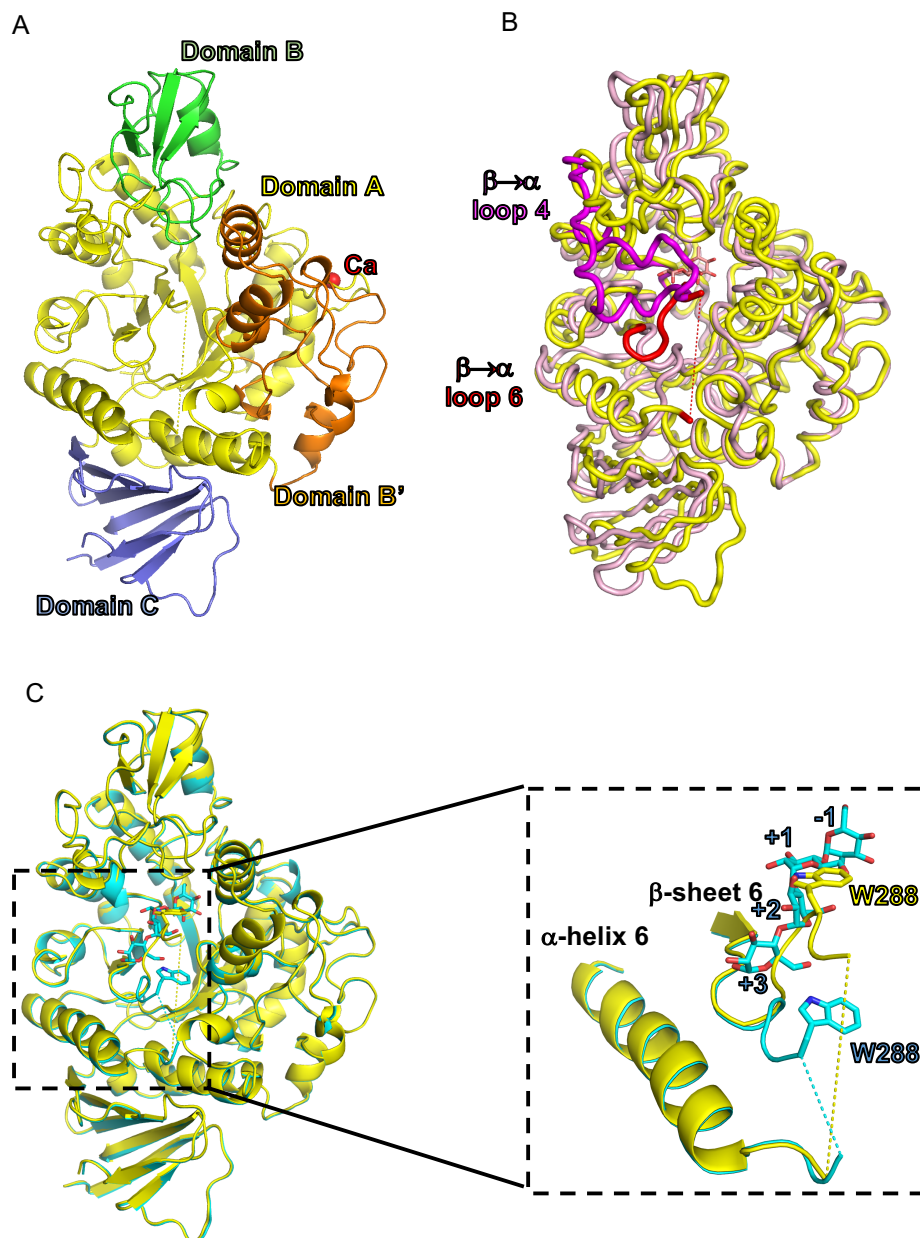


**Figure II.11 Structure of *BspAG13\_31A*.**

A, the cartoon model of *BspAG13\_31A* apo-form. A calcium ion is shown as red sphere. B, superimposition of structures of apo-form (yellow) and *HaG* (pink). The flexible  $\beta \rightarrow \alpha$  loop 6 of *BspAG13\_31A* is shown in red. The long  $\beta \rightarrow \alpha$  loop 4 of *HaG* is shown in magenta. G2 in *HaG* is represented as stick model. C, superimposition of structures of *BspAG13\_31A* apo-form (yellow) and E256Q-G4 complex (cyan). G4 and Trp288 are represented as stick model. A magnified drawing of the  $\beta \rightarrow \alpha$  loop 6 is shown in dotted box.



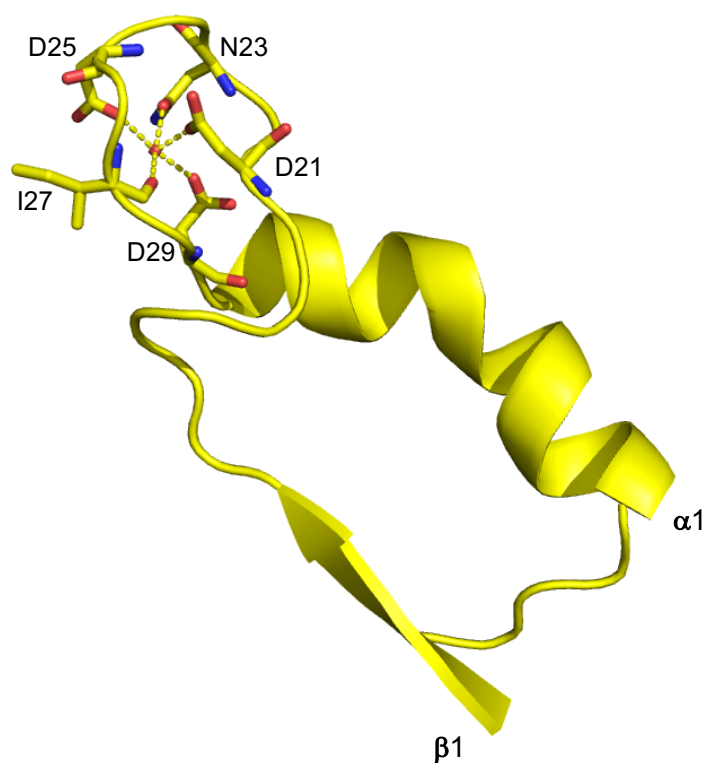


**Figure II.12** A calcium ion located in  $\beta \rightarrow \alpha$  loop1 in the  $(\beta/\alpha)_8$  barrel structure of *BspAG13\_31A*.

A calcium ion interacts with the five atoms of side chains (D21, N23, D25, D29), one carbonyl oxygen of the I27, and a water molecule (not shown). The strand of  $\beta \rightarrow \alpha$  loop1 are indicated. A calcium ion with the red sphere was shown.

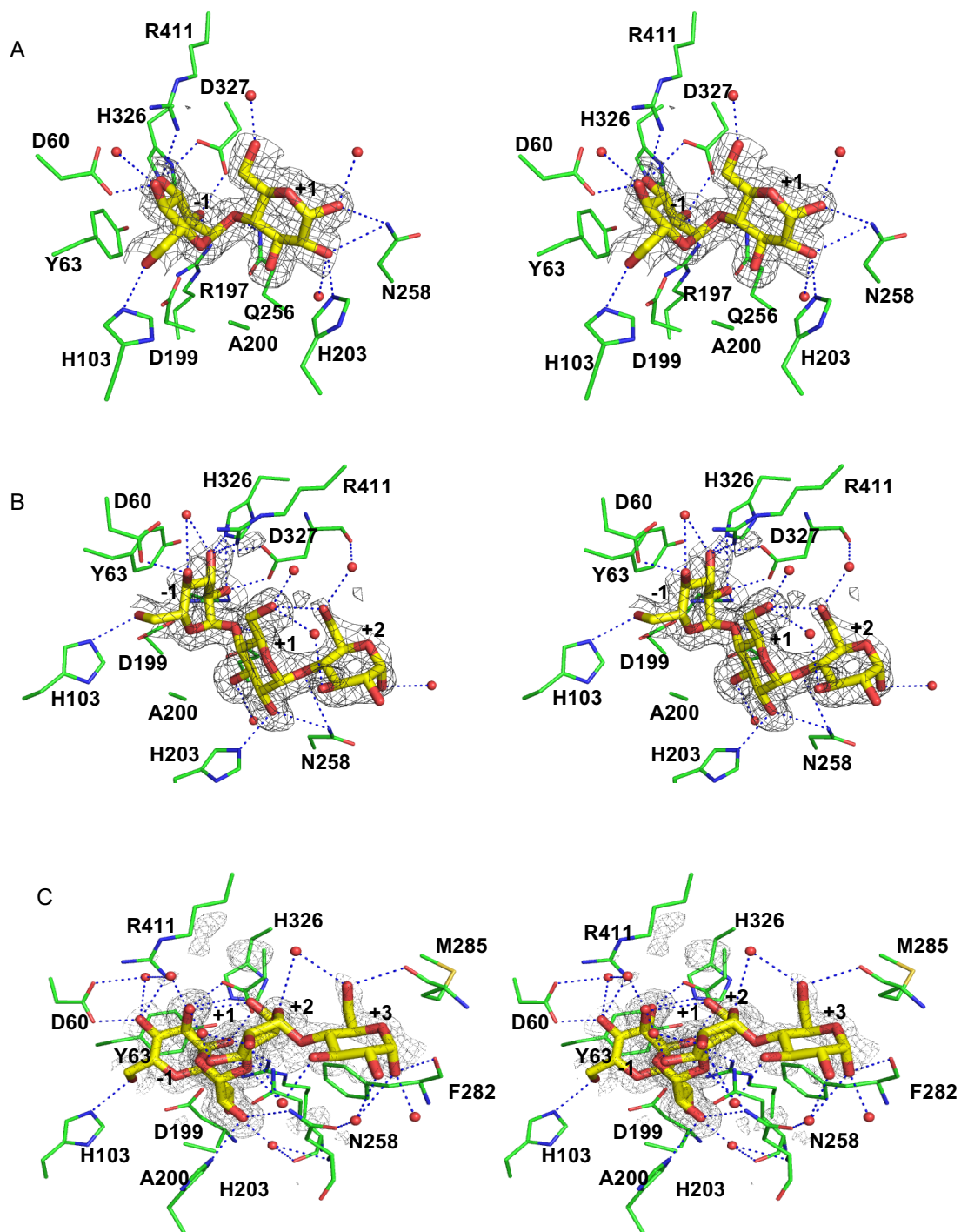


**Figure II.13** Close-up of the active site of the E256Q-substrate complexes.

The  $F_o - F_c$  OMIT maps of G2 (A), G3 (B), and G4 (C) (contoured at  $2.5 \sigma$ ) are shown in stereo view. Water molecules bound to the ligands are indicated by red balls. Ligands are shown in yellow stick representation. Putative hydrogen bonds are indicated by dotted lines. The numbers denote subsite numbering.

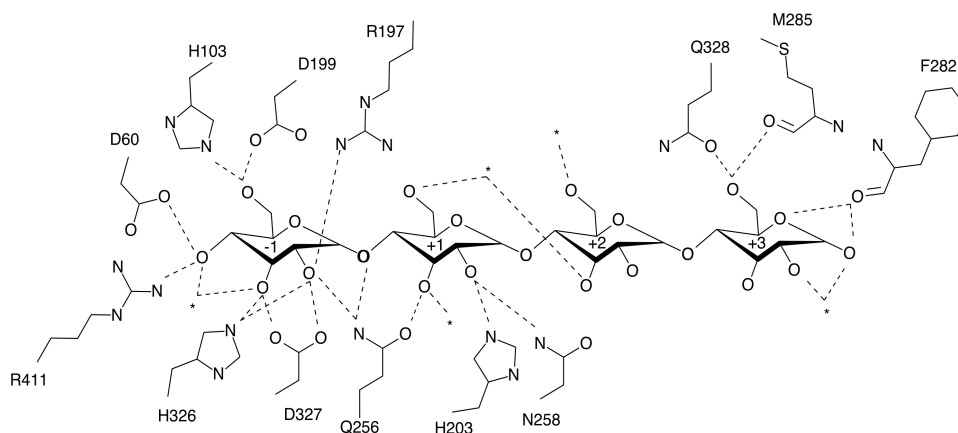


**Figure II.14 Schematic drawing of the E256Q-G4 complex.**

A, B and C, the  $F_o-F_c$  omit map of G2, G3 and G4, respectively (contoured at  $2.5 \sigma$ ). D, schematic drawing of G4 binding. Hydrogen bonds are indicated by dotted lines. The numbers in the D-glucose units denote subsite numbering. Water molecules are indicated by asterisks.

	β-strand 4		α-helix 4	β-strand 5	
α-(1→4)-specific	■		▬	■	
<i>BspAG13A</i>	195:	GFRVDAISHIKK	VAGFPDLPNPEKLDYVPSFEGHMN	-----RPGIQEHLKELKEKTF	AKYDIMTVGEANG
<i>GsjAG</i>	195:	GFRIDAISHIKKK	PGLPDLPNPKGLKYVPSFAGHMN	-----QPGIMEYLR	RELKEQTFARYDIMTVGEANG
<i>GsaAG</i>	195:	GFRIDAISHIKKK	PGLPDLPNPKGLKYVPSFAAHMN	-----QPGIMEYLR	RELKEQTFARYDIMTVGEANG
<i>HaG</i>	198:	GFRLDTVNFYFHDAEL	RDNPPVPGGEAKTLGAPEANPYTWQRHVYDLSR	PENLDFLKDLRALMDEYPGTTTVGE	IIGD
α-(1→6)-specific					
<i>SmDG</i>	190:	GFRMDVIDMIGKIP	-----AQHIVSN	-----GPKLHAYLKEMNAASFGQH	DLLTVGETWG
<i>LaDG</i>	194:	GFRMDVIELIGKDP	-----DKNIREN	-----GPMLHPYLQEMNKATFGKRD	VMTVGETWN
<i>BcO16G</i>	195:	GFRMDVINFISKEEGLPTVETEE	-EGYVSGHKHFMN	-----GPNIHKYLHEMNEEVLSHYD	IMTVGEMPG
<i>BsMall</i>	195:	GWRMDVIGSISKYTDFPDYETDH	-SRSYIVGRYHSN	-----GURLHEFIQEMNREVL	SHYDCMTVGEANG
<i>BSAMAG</i>	195:	GFRMDVINAIAKAEGLPDAPARPGERYAWGGQYFLN	-----QPKVHEYLREMYDKVLSHYD	IMTVGETGG	

**Figure II.15 Comparison of amino acid sequences of *BspAG13\_31A* and related enzymes.**

Multiple-sequence alignment was constructed with the Clustal W program (Thompson *et al.*, 1994). Black balls on the sequence represent amino acid residues important for α-1,4-glucosidic linkage specificity. The amino acid sequences of *GsjAG*, *GsaAG*, *HaG*, *SmDG*, *LaDG*, *BcO16G*, *BsO16G*, and *BSAMAG* were aligned.

## **CHAPTER III. Alternation of substrate specificity and transglucosylation activity of *BspAG13\_31A* through site-directed mutagenesis at Asn258**

### **III.1 Introduction**

In the previous chapter, the biochemical properties and enzyme structure of *BspAG13\_31A* were investigated. *BspAG13\_31A* showed high disaccharide specificity, and exhibited high  $\alpha$ -(1 $\rightarrow$ 4)-regioselectivity. From the structural analysis, a steric hindrance upon substrate binding in subsite +2 by Asn258 was predicted. Asn258 is situated two residues after general acid/base residue (Glu256). The  $\alpha$ -(1 $\rightarrow$ 4)-linkage-specific enzymes such as *BspAG13\_31A* and *Geobacillus* sp. AGases have Asn in the position (Figure III.1, Cihan *et al.*, 2009). The residue at this position is diverse in GH13 enzymes and important for substrate specificity (MacGregor *et al.*, 2001).  $\alpha$ -(1 $\rightarrow$ 6)-linkage-specific GH13\_31 AGases mostly have a large hydrophobic or aromatic residue at this position. For example, Trp238 of *SmDG* at equivalent position to Asn258 of *BspAG13\_31A*, provides aromatic stacking interaction with substrate in subsite +2, and is important for transglucosylation activity (Saburi *et al.*, 2006; Kobayashi *et al.*, 2011). The substitution of Gly273 to Pro at this position in *BSAMAG* is essential for activity to trehalose. The activity to trehalose was severely reduced which higher 12-fold of  $K_m$  than wild type (Inohara-Ochiai *et al.*, 1997). To understand the structural basis for substrate specificity of *BspAG13\_31A*, site-directed mutagenesis at Asn258 was conducted. Biochemical properties of substrate preference, kinetic parameters, and three-dimensional structures of double-mutation enzymes are analyzed in this chapter.

### **III.2 Materials and methods**

#### **III.2.1 Preparation of Asn258 mutated *BspAG13\_31A***

*BspAG13\_31A* Asn258 mutants were prepared in the same manner as the inactive mutant enzyme E256Q in II.2.4. The primers for the mutants were as follows: 5'-GAGGCAXXXGGTGTAACATCGGACAGG -3' (sense; XXX: GGT, CCG, TGG, CTG, TAT, and GAT for N258G, N258P, N258W, N258L, N258Y, and N258D, respectively) and 5'-TACACCXXXTGCCTCTCCAACCGTCAT -3' (antisense; XXX: ACC, CGG, CCA, CAG, ATA, and ATC for N258G, N258P, N258W, N258L, N258Y, and N258D, respectively). The expression plasmid for wild-type *BspAG13\_31A* (II.2.3) was used as a template. The sequence encoding each mutant enzyme was confirmed.

### III.2.2 Preparation of the double-mutation enzymes of E256Q/N258G and E256Q/N258P

Expression plasmids for E256Q/N258G and E256Q/N258P, were prepared through site-directed mutagenesis of the E256Q plasmid the expression plasmid (II.2.4). E256Q *BspAG13\_31A* was used as the template. Primers used were 5'- GTTGGACAGGCAXXXGGTGTAAACATCGGAC -3' (sense; XXX: GGT and CCG for E256Q/N258G and E256Q/N258P, respectively) and 5'- GCTGTCCGATGTTACACCXXXTGCCTGTCC-3' (antisense; XXX: ACC and CGG for E256Q/N258G and E256Q/N258P, respectively).

### III.2.3 Production and purification of *BspAG13\_31A* mutants

The *E. coli* BL21(DE3) transformant carrying the expression plasmid was grown in 1 L of LB medium containing 100 µg/mL ampicillin at 37°C. The induction and purification were carried out as described in Chapter II.2.5.

Two double mutant, E256Q/N258G and E256Q/N258P, were further purified by a Ni-immobilized column chromatography, and anion-exchange chromatography using a diethylaminoethyl (DEAE) sepharose Fast Flow column (ϕ2.7×36 cm, GE Healthcare, Uppsala, Sweden), equilibrated in buffer A. The non-adsorbed proteins were eluted by buffer A. Then, the adsorbed protein was eluted by a linear gradient of 0-0.5 M NaCl in buffer A. The fractions containing highly purified protein were collected, and dialyzed against 10 mM Tris-HCl buffer (pH 7.0). The sample was concentrated to 29 mg/mL by ultrafiltration.

### III.2.4 Measurement of protein concentration

The determination of protein concentrations of the cell-free extract and column chromatography fractions were carried out as described in Chapter II.2.6. The concentration of purified enzyme was calculated from the amino acid concentrations. From the concentration of purified enzyme, the extinction coefficients ( $A_{280}$  for 1 mg/mL solution) were determined to be 2.16, 2.48, 2.04, 1.97, 1.40, and 3.61 for N258G, N258P, N258W, N258L, N258Y, and N258D, respectively.

### III.2.5 Kinetic analysis of reactions with various substrates

Activities of the Asn258 mutant enzymes were examined based on reaction velocities to 1 mM various substrates as described in chapter II.2.12.

Kinetic parameters for *pNPG* and *G2* (N258G and N258P) in which hydrolysis and transglucosylation simultaneously occurred, were determined as described in II.2.12. Kinetic

parameters for G2 (Asn258 *Bsp*AG13\_31A variants other than N258G and N258P), G3–G7, and sucrose were determined by fitting the Michaelis-Menten equation to the hydrolytic velocities at 0.1–50 mM.

### III.2.6 Analysis of the reaction products from sucrose by TLC

A reaction mixture (1 mL) containing the purified wild-type *Bsp*AG13\_31A (9.8  $\mu$ M), N258P (0.8  $\mu$ M) or N258L (12  $\mu$ M), 100 mM sucrose, and 10 mM MES-NaOH buffer (pH 6.0), was incubated at 37°C. An aliquot (0.14 mL) was taken from the reaction mixtures, and heated at 100°C for 5 min. Five  $\mu$ g of carbohydrates was spotted on silica gel TLC plate. A developing solvent chloroform/acetic acid/water (6/7/1; v/v/v) was used, and the carbohydrates were visualized by spraying with the detection reagent, 85% orthophosphoric acid/ 0.1 g/L aniline in acetone (10/1; v/v) (Farang, 1979), and heating the TLC plate.

### III.2.7 Determination of transglucosylation products from G2 and sucrose

Transglucosylation ratio ( $r_{TG}$ ) for the reaction with 10 mM G2 was determined as described in Chapter II.2.13. Transglucosylation product from sucrose by N258P was analyzed by HPAEC-PAD. A reaction mixture (0.5 mL), containing 0.49  $\mu$ M enzyme, 100 mM sucrose, and 10 mM MES-NaOH buffer (pH 6.0), was incubated at 37°C for 30 min. The reaction was stopped by heating for 5 min. The reaction products were analyzed by HPAEC-PAD as described in II.2.13. The eluent, 480 mM NaOH was used. Glucose, fructose (Nacalai Tesque, Kyoto, Japan), sucrose, and erlose ( $\alpha$ -maltosyl  $\beta$ -fructoside; Seikagaku, Tokyo, Japan; 200  $\mu$ M) were used as standards.

### III.2.8 Crystallization and data collection

Crystals of *Bsp*AG13\_31A E256Q/N258G and E256Q/N258P in complex with maltooligosaccharides were obtained by hanging drop vapor diffusion method, in which 1  $\mu$ L of protein solution (29 mg/mL) was mixed with the same volume of a mixture containing 10 mM G3 or G4, 0.2 M CaCl<sub>2</sub>, and 20% (w/v) PEG 3350 and incubated for 1 week at 20°C. For X-ray diffraction experiments, the crystals were directly picked up from crystallization solution and flash-cooled. Diffraction data of the *Bsp*AG13\_31A mutants were collected on beamline BL-41XU at SPring-8. The data sets were indexed, integrated, scaled, and merged using the *XDS* program suite (Kabsch, 2010). All data collection statistics are summarized in Table III.1.

### III.2.9 Structure solution and refinement

The structures of *BspAG13\_31A* mutants were determined by the molecular replacement method with the program AutoMR in the Phenix program package (McCoy *et al.*, 2004; Adams *et al.*, 2010). Structural comparison using SuprePose version 1.0 (Maiti *et al.*, 2004). The structure of *BspAG13\_31A* E256Q in complex with G3 was used as the search model. Several rounds of refinement were carried out using the program *Phenix.refine* in the *Phenix* program suite, alternating with manual fitting and rebuilding based on  $2F_o-F_c$  and  $F_o-F_c$  electron densities using *COOT* (Emsley and Cowtan, 2004; Adams *et al.*, 2010). Water molecules,  $Ca^{2+}$ , and substrates were built based on  $2F_o-F_c$  and  $F_o-F_c$  electron densities. The final refinement statistics and geometry defined by MolProbity (Chen *et al.*, 2010) are shown in Table III.1.

## III.3 Results

### III.3.1 Production and purification of *BspAG13\_31A* mutants

Six *BspAG13\_31A* mutants were produced in *E. coli* transformants in 1 L-scale and purified to homogeneity. The yields and specific activities are as follows: N258D, 81.8 mg (7.97 U/mg); N258G, 88.9 mg (8.18 U/mg); N258L, 106 mg (1.26 U/mg); N258P, 114 mg (10.9 U/mg); N258W, 68.9 mg (0.302 U/mg); and N258Y, 113 mg (0.533 U/mg). All the mutant enzymes prepared showed a single band on SDS-PAGE (Figure III.2).

### III.3.2 Kinetic analysis of reactions with *p*NPG and G2

To evaluate transglucosylation activity of *BspAG13\_31A* Asn258 mutants, kinetic analysis of the reaction with *p*NPG was carried out. The velocities of aglycone release (*p*NP), transglucosylation, and hydrolysis at various *p*NPG concentrations fit well to the rate equations Eq.1–Eq. 3, respectively, and  $r_{TG}$  followed a saturation curve (Figure III.3 to III.8). The kinetic parameters determined from  $v_{ag}$  are shown in Table III.2. N258G and N258Y showed 3.1- and 2.5-fold lower  $K_{TG}$  than that of the wild type, while the other mutant enzymes showed 1.8–6.7-fold higher  $K_{TG}$ . This indicates the former two mutant enzymes showed higher preference for transglucosylation in this reaction than the wild type. The  $k_{cat1}/K_{m1}$  values of all the mutant enzymes were 1.6–52-fold higher than that of the wild type. N258P showed the highest  $k_{cat1}/K_{m1}$  among these *BspAG13\_31A* variants.

The  $r_{TG}$  values for Asn258 mutant enzymes in the reaction with 10 mM G2 were measured (Table III.3). N258G exhibited 3.0-fold higher  $r_{TG}$  (89.6%) than the wild type (30.1%), and  $r_{TG}$  of N258P (37.8%) was similar to that of the wild type. The other mutant enzymes showed 3.61–4.60% of  $r_{TG}$ , indicating that they predominantly catalyzed hydrolysis unlike the wild type. In the reaction



of N258G and N258P with G2, Eq. 4 was fitted to velocities of D-glucose liberation ( $v_{\text{glc}}$ ) from G2 (Figure III.3 to 8). The  $k_{\text{cat1}}/K_{\text{m1}}$  values of N258G and N258P were 23- and 30-fold lower than that of the wild type.  $K_{\text{TG}}$  of N258G was 19.1-fold lower than that of wild type, while N258P showed similar  $K_{\text{TG}}$  to that of wild type (Table III.2). Kinetic parameters of the other mutant enzymes for the reaction with G2 were described later.

### III.3.3 Substrate specificities for *BspAG13\_31A* mutants

Substrate specificity of the mutant enzymes was evaluated based on reaction rates to 1 mM substrates. All the mutant enzymes analyzed showed high specificity to  $\alpha$ -(1 $\rightarrow$ 4)-glucosidic as the wild type (Table III.4). N258D, N258L, and N258Y showed the highest activity to G2 as the wild type, but N258G, N258P, and N258W had higher activity to G3 than G2. The  $k_{\text{cat}}/K_{\text{m}}$  values of N258G and N258P for G3 were 11- and 27-fold higher than their  $k_{\text{cat1}}/K_{\text{m1}}$  values for G2, respectively, while  $k_{\text{cat}}/K_{\text{m}}$  value of the wild type for G3 was only 26% of  $k_{\text{cat1}}/K_{\text{m1}}$  for G2 (Table III.5). These mutant enzymes showed 1.8–3.5-fold higher  $k_{\text{cat}}/K_{\text{m}}$  for G3 than wild type, although their  $k_{\text{cat1}}/K_{\text{m1}}$  values for G2 were only 3.3–4.4% of that of the wild type as described above. The  $k_{\text{cat}}/K_{\text{m}}$  values of N258G and N258P for maltooligosaccharides longer than G2 decreased with degree of polymerization, but  $k_{\text{cat}}/K_{\text{m}}$  values for G7 were also higher than  $k_{\text{cat1}}/K_{\text{m1}}$  for G2 unlike the wild type. N258D, N258L, N258W, and N258Y carrying bulkier residue than Gly and Pro at the Asn258 position showed much lower  $k_{\text{cat}}/K_{\text{m}}$  for all maltooligosaccharides tested.

Wild-type *BspAG13\_31A* prefers G2 as substrate to *p*NPG in terms of  $k_{\text{cat1}}/K_{\text{m1}}$  values, but all Asn258 mutated enzymes had higher activity to *p*NPG than to G2 (Table III.4 and 5). The  $k_{\text{cat1}}/K_{\text{m1}}$  values of the mutant enzymes for *p*NPG were 3.8–91-fold higher than  $k_{\text{cat}}/K_{\text{m}}$  for G2 ( $k_{\text{cat1}}/K_{\text{m1}}$  in N258G and N258P). Especially, N258W and N258Y, in which aromatic amino acid residues are introduced to the Asn258 position, showed high preference for *p*NPG.

Sucrose was not a good substrate for wild type, but N258L and N258P showed higher preference for sucrose than the wild type (Table III.4 and 5). The  $k_{\text{cat}}/K_{\text{m}}$  values of N258L and N258P for sucrose were 28.8% and 87.4% of  $k_{\text{cat}}/K_{\text{m}}$  ( $k_{\text{cat1}}/K_{\text{m1}}$ ) for G2, respectively, while  $k_{\text{cat}}/K_{\text{m}}$  of the wild type for sucrose was only 0.0993% of  $k_{\text{cat1}}/K_{\text{m1}}$  for G2.

### III.3.4 Reaction products from sucrose

The reaction with 100 mM sucrose of wild type, and N258L, and N258P were investigated (Figure III.9.A). Only hydrolytic products, fructose and glucose, were detected in the reaction of the wild type and N258L. However, in the reaction of N258P, production of a transglucosylation product was observed in the early stage of the reaction. This product showed the same retention time as

authentic erlose (Glc $\alpha$ 1-4Glc $\alpha$ 1-2 $\beta$ Fru) in the HPAEC-PAD analysis (Figure III.9.B). This suggested that N258P catalyzed  $\alpha$ -(1 $\rightarrow$ 4)-glucosyl transfer from sucrose to produce erlose.

### III.3.5 Protein structures of *BspAG13\_31A* E256Q/N258G and E256Q/N258P

*BspAG13\_31A* N258G and N258P mutants showed high trisaccharide specificity unlike the wild type and the other tested mutant enzymes. To understand the molecular basis of the specificity, crystal structures of inactive double mutant enzymes E256Q/N258G and E256Q/N258P in complex with G3 were solved at 1.69 and 1.50 Å resolution, respectively. The structural comparison using SuprePose showed that the structures of two double-mutation enzymes were highly similar to the structure of E256Q-G3 complex with a RMSD of 0.36 Å for 545 C $\alpha$ s for E256Q/N258G and 542 C $\alpha$ s for E256Q/N258P. Similar to E256Q-G3 complex, the  $\beta$  $\rightarrow$  $\alpha$  loop 6 (Phe282–Pro295) of catalytic domain A included a disordered part with poor electron density, Lys290–Glu293 in N256Q/N258G and Leu287–Lys294 in N256Q/N258P.

The  $F_o$ - $F_c$  maps of E256Q/N258G and E256Q/N258P clearly revealed the existence of a substrate molecule (Figure III.10). In E256Q/N258P, the electron density for the glucose at subsite +3 was disordered and this glucose residue could not be modeled, although G4 was used as the ligand in the co-crystallization. Electron density of a non-sugar compound was observed in the crystal structure of E256Q/N256P with G3, and G3 binding structure could not be solved by co-crystallization with G3 (data not shown). Structures of G3 bound to E256Q/N258G and E256Q/N258P were similar to each other. The conformation of glucose residue in subsite +2 of the double-mutant enzymes was different from that in the E256Q, whereas orientations of the glucosyl residues in subsite -1 and +1 were similar in the three mutant enzymes (Figure III.10C). Torsion angles of glucose residues in subsite +1 and +2 of E256Q/N258G and E256Q/N258P were close to the torsion angles of glucosyl residues in  $\alpha$ -glucan (Gessler *et al.*, 1999), which is in the global minimum (Dowd *et al.*, 1996) (Table III.6). In E256Q/N258G, SD of Met229 located on C-terminal of  $\beta$  $\rightarrow$  $\alpha$  loop 4 formed hydrogen bond with 3-O of glucose residue in subsite +2. This hydrogen bonding interaction was not observed in the complexes of E256Q and E256Q/N258P. In E256Q/N258P, Phe282 did not form water-mediated hydrogen bond with glucose residue in subsite +2 unlike in E256Q and E256Q/N258G.

### III.4 Discussions

Asn258 is located at  $\beta$  $\rightarrow$  $\alpha$  loop 5 of the catalytic domain and forms hydrogen bond with 2-O of glucosyl residue in subsite +1. Elimination of this hydrogen bond by substitution of Asn258 with Leu, which has similar size of side-chain to Asn resulted in large loss of activity to G2 (Table

III.5), indicating that the hydrogen bond by Asn258 is important for activity to G2. Transglucosylation activity towards 10 mM G2 was also lower than the wild type (Table III.3). As activity to G2 and transglucosylation activity largely decreased by N258D mutation, Asp introduced did not replace the function of Asn258. Thus, negative charge at Asn258 position is not suitable for the substrate binding in *BspAG13\_31A*. Introduction of bulky amino acid residues, Tyr and Trp, than Asn significantly decreased activity to G2. Severe steric hindrance upon binding to G2 presumably occurred. However, N258W and N258Y showed 3.2–3.3-fold higher  $k_{cat}/K_m$  for *p*NPG than that of the wild type. Aromatic residue introduced might give favorable interactions with *p*NP group at subsite +1, and enhance the activity to *p*NPG. Low transglucosylation activity of N258W and N258Y is presumably because of steric hindrance, caused by introduced bulky residues, upon acceptor binding. N258G and N258P, carrying smaller amino acid at Asn258 position, showed lower activity to G2 presumably because of lacking the hydrogen bonding interaction with substrate at subsite +1. But these mutant enzymes showed very high preference for G3 over G2 (Table III.5). The affinity at subsite +2 ( $A_{+2}$ ) of N258G and N258P were 6.1 and 8.5 kJ/mol, respectively, while  $A_{+2}$  of the wild type was -3.5 kJ/mol.

Structural analysis of E256Q/N258G and E256Q/N258P in complex with G3 revealed that the conformation of glucose residue in subsite +2 of the double-mutant enzymes was different from that in E256Q. Torsion angles of the glucosyl residues in subsite +1 and +2 of these mutant enzymes were close to those of glucosyl residues in stable  $\alpha$ -glucan (Table III.6). This conformational difference of G3 is predicted to be arisen from the elimination of steric hindrance by Asn258 (Figure III.10C). Molecular mechanics study of maltose suggested that torsion angles of glucosyl residues at subsite +1 and +2 in E256Q-G3 complex are less stable than the global minimum (Dowd *et al.*, 1992). Thus, the conformation of G3 observed in E256Q/N258G and E256Q/N258P is predicted to be more stable than that in E256Q. In E256Q/N258P-G3 complex, any additional interactions through N258P mutation were not found in subsite +2, and a water-mediated hydrogen bond between Phe282 and glucose residue in subsite +2 was not formed unlike E256Q-G3 complex (Figure III.10C). Therefore, stabilizing conformation of G3 is a possible reason for enhancing the trisaccharide specificity. In E256Q/N258G-G3 complex, an additional hydrogen bond between Met229 and 3-O of glucose residue in subsite +2 was observed (Figure III.10A). This hydrogen bond might stabilize the Michaelis-complex, and resulted in stabilization of the transition state, because N258G showed 25-fold lower  $K_m$  for G3 than the wild type. This interaction also could be favorable for acceptor binding in transglucosylation, and N258G showed higher transglucosylation activity than the wild type (Tables III.2 and 3). Asn258 is not preferable for the sucrase activity, only hydrolysis in the reaction with 100 mM sucrose in wild type and N258L. N258P showed 29-fold higher  $k_{cat}/K_m$  for sucrose than the wild type (Table III.5). From the superimposition of sucrose bound to amylosucrase (Mirza *et al.*, 2001), Pro258 of E256QN258P is predicted to have hydrophobic contact with 1-C of the

fructosyl residue in subsite +1 (Figure III.11). As N258L also showed high preference for sucrose, hydrophobic interaction is thought to be favorable for the reaction with sucrose. Asn258 is not preferable for the sucrase activity although this residue is predicted to form a hydrogen bond with 4-O of the fructosyl residue. In contrast to the wild type and N258L, which catalyzed only hydrolysis in the reaction with 100 mM sucrose, N258P produced erlose by transglucosylation.  $\alpha$ -(1→4)-Glucosidic linkage was specifically formed even in the reaction with sucrose. This mutation might be useful to create biocatalyst to produce oligosaccharides from sucrose.

**Table III.1 Summary of crystallization conditions, data collection, and refinement statistics.**

	E256QN258G-G3	E256QN258P-G3
<b>Data collection</b>		
Beamline	SPring-8 BL41XU	SPring-8 BL41XU
Space group	P2 <sub>1</sub> 2 <sub>1</sub> 2 <sub>1</sub>	P2 <sub>1</sub> 2 <sub>1</sub> 2 <sub>1</sub>
Unit cell parameters a, b, c, (Å)	57.1, 89.2, 128.6	56.5, 89.2, 128.3
Wavelength (Å)	1.00	1.00
Resolution range (Å)	50.0-1.69 (1.80-1.69)	50.0-1.50 (1.59-1.50)
R <sub>meas</sub> (%)	10.1 (88.4)	8.8 (83.5)
<I/σ(I)>	16.9 (2.09)	19.7 (2.76)
Completeness (%)	99.6 (98.3)	99.9 (99.6)
Redundancy	11.8 (11.8)	13.1 (13.3)
<b>Refinement</b>		
No. reflection	72,861	104,554
R <sub>work</sub> /R <sub>free</sub> (%)	17.4/20.2	16.6/18.2
No. of atoms		
Macromolecules	4515	4,488
Ligand/ion	35	35
Water	718	773
B-factors (Å <sup>2</sup> )		
Macromolecules	23.8	18.6
Ligand/ion	26.4	25.3
Water	33.8	30.0
RMSD from ideal		
Bond lengths (Å)	0.006	0.005
Bond angles (°)	0.79	0.81
Ramachandran		
Favored (%)	97.2	97.0
Allowed (%)	2.77	2.97
Outliers (%)	0	0

Values in parentheses are for the highest resolution shell.

\*  $R_{\text{meas}} = \sum_{hkl} \{N(hkl) / [N(hkl) - 1]\}^{1/2} \sum_i |I_i(hkl) - \langle I(hkl) \rangle| / \sum_{hkl} \sum_i I_i(hkl)$ , where  $\langle I(hkl) \rangle$  and  $N(hkl)$  are the mean intensity of a set of equivalent reflections and the multiplicity, respectively.

\*\*  $R_{\text{work}} = \sum_{hkl} ||F_{\text{obs}}| - |F_{\text{calc}}|| / \sum_{hkl} |F_{\text{obs}}|$ ,  $R_{\text{free}}$  was calculated for 5% randomly selected test sets that were not used in the refinement.

**Table III.2 Kinetic parameters of *Bsp*AG13\_31A Asn258 variants for G2 and *p*NPG.**

Enzyme	<i>p</i> NPG						G2					
	$k_{cat1}$ (s <sup>-1</sup> )	$k_{cat2}$ (s <sup>-1</sup> )	$K_{m1}$ (mM)	$K_{m2}$ (mM)	$k_{cat1}/K_{m1}$ (s <sup>-1</sup> mM <sup>-1</sup> )	$K_{TG}$ (mM)	$k_{cat1}$ (s <sup>-1</sup> )	$k_{cat2}$ (s <sup>-1</sup> )	$K_{m1}$ (mM)	$K_{m2}$ (mM)	$k_{cat1}/K_{m1}$ (s <sup>-1</sup> mM <sup>-1</sup> )	$K_{TG}$ (mM)
Wild type	4.72±2.62	13.9±1.0	2.05±1.03	4.71±0.82	2.30	2.48	205±12	1,890±130	1.52±0.19	201±53	135	21.6
N258D	21.3±1.2	32.2±2.5	2.02±0.18	25.1±0.8	10.5	16.6	N.D.	N.D.	N.D.	N.D.	N.D.	N.D.
N258G	1.95±0.28	2.29±0.09	0.194±0.060	0.971±0.211	10.0	0.792	3.20±0.20	190±7	0.534±0.089	66.9±3.3	5.99	1.13
N258L	5.61±0.30	8.77±0.15	1.51±0.15	7.66±0.71	3.71	4.90	N.D.	N.D.	N.D.	N.D.	N.D.	N.D.
N258P	81.3±7.0	125±18	0.674±0.108	10.5±2.8	120	6.81	46.8±3.9	379±86	10.5±1.5	219±89	4.46	27.0
N258W	1.48±0.05	2.39±0.22	0.193±0.019	12.2±1.4	7.67	7.58	N.D.	N.D.	N.D.	N.D.	N.D.	N.D.
N258Y	1.79±0.47	6.36±0.96	0.243±0.102	6.94±3.71	7.37	0.988	N.D.	N.D.	N.D.	N.D.	N.D.	N.D.

The values are average ± standard deviation of values from three independent experiments. N.D., not determined

**Table III.3 Transglucosylation ratio of *BspAG13\_31A* Asn258 variants for 10 mM G2.**

Enzyme	$v_h$ ( $s^{-1}$ )	$v_{tg}$ ( $s^{-1}$ )	$r_{TG}$ (%)
Wild type	193 ± 5	82.9 ± 13.9	30.1
N258D	13.7 ± 1.5	0.600 ± 0.022	4.18
N258G	2.03 ± 0.76	17.4 ± 2.3	89.6
N258L	2.02 ± 0.40	0.0975 ± 0.0289	4.60
N258P	11.3 ± 2.4	6.86 ± 1.26	37.8
N258W	0.367 ± 0.028	0.0137 ± 0.0030	3.61
N258Y	0.725 ± 0.038	0.0292 ± 0.0090	3.87

The values are average ± standard deviation of values from three independent experiments.

**Table III.4 Reaction velocities of *Bsp*AG13\_31A Asn258 variants for various substrates.**

Substrate	Wild type	N258D	N258G	N258L	N258P	N258W	N258Y
G2	94.3±2.8 (100)	2.28±0.06 (100)	2.92±0.042 (100)	0.367±0.008 (100)	3.87 ± 0.15 (100)	0.0766±0.0008 (100)	0.297±0.016 (100)
G3	33.2±0.5 (35.2)	0.884±0.015 (38.8)	9.66±0.078 (331)	0.202±0.005 (55.1)	79.1 ± 1.5 (2,050)	0.0973±0.0018 (127)	0.244±0.003 (82.2)
G4	27.2±0.2 (28.8)	0.372±0.006 (16.3)	7.51±0.29 (257)	0.234±0.003 (63.8)	57.6 ± 0.9 (1,490)	0.0386±0.0041 (50.4)	0.147±0.002 (49.5)
G5	18.7±0.4 (19.9)	0.436±0.004 (19.1)	6.52±0.14 (223)	0.716±0.008 (195)	20.7 ± 0.2 (535)	(6.71±0.09)×10 <sup>-3</sup> (8.76)	0.0567±0.0012 (19.1)
G6	11.7±0.4 (12.4)	0.283±0.006 (12.4)	5.11±0.25 (175)	0.374±0.006 (102)	10.1 ± 0.1 (262)	(5.36±0.10)×10 <sup>-3</sup> (7.00)	0.0448±0.0023 (15.1)
G7	9.21±0.1 (9.78)	0.222±0.006 (9.74)	3.84±0.06 (132)	0.405±0.005 (110)	6.75 ± 0.03 (175)	(2.26±1.17)×10 <sup>-3</sup> (2.95)	0.0347±0.0007 (11.7)
<i>p</i> NPG	5.36±0.23 (5.69)	6.12±0.11 (269)	2.41±0.03 (82.7)	2.55±0.06 (694)	64.5 ± 0.615 (1,670)	1.24±0.02 (1,620)	1.75±0.02 (591)
Sucrose	0.179±0.0004 (0.190)	0.0650±0.0181 (2.85)	0.0746±0.0029 (2.56)	0.120±0.002 (32.6)	3.39 ± 0.09 (87.7)	0.0182±0.0002 (23.7)	0.0211±0.0003 (7.11)
Trehalose	(1.02±0.01)×10 <sup>-3</sup> (1.08×10 <sup>-3</sup> )	(3.20±0.73)×10 <sup>-4</sup> (0.0140)	(1.72±0.12)×10 <sup>-4</sup> (5.89×10 <sup>-3</sup> )	(3.23±1.03)×10 <sup>-4</sup> (0.0880)	(1.18±0.11)×10 <sup>-3</sup> (0.0305)	(0.828±0.091)×10 <sup>-3</sup> (1.08)	(0.855±0.007)×10 <sup>-4</sup> (0.0288)
Kojibiose	(9.48±0.09)×10 <sup>-3</sup> (0.0101)	(10.4±0.4)×10 <sup>-3</sup> (0.454)	(9.02±0.01)×10 <sup>-3</sup> (0.0309)	(4.34±0.46)×10 <sup>-4</sup> (0.118)	0.253±0.009 (6.55)	(0.386±0.114)×10 <sup>-3</sup> (0.504)	(1.41±0.06)×10 <sup>-3</sup> (0.474)
Nigerose	0.131±0.004 (0.139)	(7.00±0.96)×10 <sup>-4</sup> (0.307)	0.0102±0.0009 (0.349)	(4.08±2.11)×10 <sup>-4</sup> (0.111)	0.0440±0.0016 (1.14)	(0.536±0.176)×10 <sup>-3</sup> (0.700)	(1.45±0.04)×10 <sup>-3</sup> (0.409)
IG2	(4.43±0.04)×10 <sup>-3</sup> (4.70×10 <sup>-3</sup> )	(5.56±0.54)×10 <sup>-3</sup> (0.244)	(1.85±0.07)×10 <sup>-3</sup> (0.0633)	(7.66±1.28)×10 <sup>-5</sup> (0.0208)	0.0125±0.0003 (0.324)	0.0766±0.0008 (1.63)	(0.384±0.014)×10 <sup>-3</sup> (0.129)

Reaction velocities for 1 mM substrates are shown. Velocity relative to that to G2 is shown in parenthesis. Values are average ± standard deviation from three independent experiments.



**Table III.5 Kinetic parameters of *BspAG13\_31A Asn258* variants for maltooligosaccharides and sucrose.**

Substrate	Wild type	N258D	N258G	N258L	N258P	N258W	N258Y
G2	$k_{\text{cat}}$ ( $\text{s}^{-1}$ )	N.D.	$28.2 \pm 0.5$	N.D.	$4.27 \pm 0.09$	N.D.	$1.54 \pm 0.07$
	$K_{\text{m}}$ (mM)	N.D.	$10.2 \pm 0.6$	N.D.	$11.5 \pm 1.4$	N.D.	$6.37 \pm 0.55$
	$k_{\text{cat}}/K_{\text{m}}$ ( $\text{s}^{-1}\text{mM}^{-1}$ )	N.D.	2.76 (100)	N.D.	0.372 (100)	N.D.	0.0847 (100)
G3	$k_{\text{cat}}$ ( $\text{s}^{-1}$ )	$148 \pm 1$	$17.9 \pm 1.0$	$10.8 \pm 0.4$	$2.83 \pm 0.14$	$234 \pm 6$	$0.824 \pm 0.063$
	$K_{\text{m}}$ (mM)	$4.22 \pm 0.15$	$22.2 \pm 2.1$	$0.170 \pm 0.018$	$14.3 \pm 1.3$	$1.92 \pm 0.08$	$7.47 \pm 1.27$
	$k_{\text{cat}}/K_{\text{m}}$ ( $\text{s}^{-1}\text{mM}^{-1}$ )	35.1 (26.0)	0.806 (29.2)	63.7 (1,060)	0.197 (53.0)	122 (2,740)	0.110 (130)
G4	$k_{\text{cat}}$ ( $\text{s}^{-1}$ )	$145 \pm 16$	$11.9 \pm 0.8$	$13.3 \pm 0.1$	$2.99 \pm 0.25$	$270 \pm 3$	$1.22 \pm 0.03$
	$K_{\text{m}}$ (mM)	$5.75 \pm 1.10$	$44.5 \pm 5.1$	$0.367 \pm 0.019$	$17.8 \pm 2.5$	$3.91 \pm 0.15$	$12.4 \pm 0.5$
	$k_{\text{cat}}/K_{\text{m}}$ ( $\text{s}^{-1}\text{mM}^{-1}$ )	25.3 (18.7)	0.267 (9.67)	36.1 (603)	0.168 (45.2)	69.1 (1,550)	0.0278 (32.8)
G5	$k_{\text{cat}}$ ( $\text{s}^{-1}$ )	$143 \pm 5$	N.D.	$10.2 \pm 0.4$	$4.64 \pm 0.09$	$192 \pm 2$	$0.969 \pm 0.08$
	$K_{\text{m}}$ (mM)	$7.55 \pm 0.62$	N.D.	$0.465 \pm 0.054$	$6.11 \pm 0.36$	$9.64 \pm 0.11$	$30.4 \pm 4.3$
	$k_{\text{cat}}/K_{\text{m}}$ ( $\text{s}^{-1}\text{mM}^{-1}$ )	19.0 (14.1)	N.D.	22.0 (367)	0.759 (204)	19.9 (446)	0.0319 (13.2)
G6	$k_{\text{cat}}$ ( $\text{s}^{-1}$ )	$133 \pm 4$	N.D.	$12.1 \pm 0.4$	$4.22 \pm 0.23$	$299 \pm 11$	N.D.
	$K_{\text{m}}$ (mM)	$15.3 \pm 0.8$	N.D.	$0.768 \pm 0.035$	$7.05 \pm 0.69$	$35.7 \pm 1.9$	N.D.
	$k_{\text{cat}}/K_{\text{m}}$ ( $\text{s}^{-1}\text{mM}^{-1}$ )	8.64 (6.40)	N.D.	15.7 (262)	0.599 (161)	8.39 (188)	N.D.
G7	$k_{\text{cat}}$ ( $\text{s}^{-1}$ )	$155 \pm 6$	N.D.	$8.73 \pm 0.61$	$4.87 \pm 0.15$	$179 \pm 7$	N.D.
	$K_{\text{m}}$ (mM)	$19.0 \pm 1.2$	N.D.	$1.16 \pm 0.16$	$8.65 \pm 0.66$	$26.1 \pm 1.6$	N.D.
	$k_{\text{cat}}/K_{\text{m}}$ ( $\text{s}^{-1}\text{mM}^{-1}$ )	8.19 (6.07)	N.D.	7.50 (125)	0.562 (151)	6.86 (154)	N.D.
Sucrose	$k_{\text{cat}}$ ( $\text{s}^{-1}$ )	$4.58 \pm 0.1$	N.D.	N.D.	$1.94 \pm 0.07$	$39.2 \pm 0.6$	N.D.
	$K_{\text{m}}$ (mM)	$34.2 \pm 2.6$	N.D.	N.D.	$18.1 \pm 0.5$	$10.1 \pm 0.4$	N.D.
	$k_{\text{cat}}/K_{\text{m}}$ ( $\text{s}^{-1}\text{mM}^{-1}$ )	0.134 (0.0993)	N.D.	N.D.	0.107 (28.8)	3.90 (87.4)	N.D.

Values are average  $\pm$  standard deviation from three independent experiments. Relative  $k_{\text{cat}}/K_{\text{m}}$  to G2 is shown in parenthesis (values of wild type, N258G, and N258P are relative to  $k_{\text{cat1}}/K_{\text{m1}}$  to G2). N.D., not determined.

**Table III.6 Comparison of torsion angles of G3 bound to *Bsp*AG13\_31A variants.**

Enzyme	Origin	Ligand	Residues in subsite -1 and +1		Residues in subsite +1 and +2		Reference
			$\Phi$	$\Psi$	$\Phi$	$\Psi$	
<i>Bsp</i> AG13_31A	<i>Bacillus</i> sp. AHU2216						
E256Q		G3	42.8°	-151°	64.6°	-168°	9
E256Q/N258G		G3	31.6°	-153°	105°	-113°	This study
E256Q/N258P		G3	43.9°	-156°	106°	-109°	This study
$\alpha$ -Amylase	<i>Bacillus subtilis</i>	G5	28.6°	-148°	109°	-125°	35
$\alpha$ -Amylase	<i>Homo sapiens</i> (pancreatic)	G6	34.6°	-148°	112°	-117°	36
CGTase	<i>Bacillus circulans</i>	G4	25.2°	-154°	110°	-125°	37
Neopullulanase	<i>Geobacillus stearothermophilus</i>	G4	33.8°	-144°	92°	-112°	38
Amylosucrase	<i>Neisseria polysaccharea</i>	G7	33.8°	-155°	67.1°	-148°	39

$\Phi$  (5-O, 1-C, 4'-O, 4'C),  $\Psi$  (1-C, 4'O, 4'-C, 5'-C). CGTase, cyclodextrin glucanotransferase.

$\alpha$ -(1→4)-linkage  
specific

<i>Bsp</i> AG13_31A	252: MTVGEANGVT
BAE48285.1	252: MTVGEANGVT
BAA12704.1	252: MTVGEANGVT
AEN90673.1	252: MTVGEANGVT
CAA55409.1	253: MTVGEANGVN

References

In this study  
Hung *et al.*, 2005  
Takii *et al.*, 1996  
Liu *et al.*, 2011  
Egeter and Brucker, 1995

$\alpha$ -(1→6)-linkage  
specific

CAB15461.1	251: MTVGEANGSD
CAA37583.1	251: MTVGEMPGVT
BAA01368.1	252: MTVGETPGVT
NP_463715.1	250: MTVGEMPGAS
AAK27723.1	286: MNVGEAPGIT
ACM89182.1	289: LTVGEAPGIT
ACM89183.1	288: LTVGEAPGIT
CAA54266.1	268: MTVGETGGVT
BAA00534.1	250: MTVGEAGGSD
CAA02858.1	260: MTVGEAFGVT
BAA11354.1	252: MTVGEAIGSD
AAV42157.1	236: MTVGETWNAT
BAE79634.1	232: LTVGETWGAT
AAK28737.1	239: VTVGETWSAT

Belda *et al.*, 2013  
Watanabe *et al.*, 1990  
Watanabe *et al.*, 1991  
Toledo-Arana *et al.*, 2009  
Van den Broek *et al.*, 2003  
Pokusaeva *et al.*, (unpublished)  
Pokusaeva *et al.*, (unpublished)  
Nakao *et al.*, 1994  
Yamamoto and Horikoshi, 1990  
unidentified  
Watanabe *et al.*, 1996  
Altermann *et al.*, 2005  
Saburi *et al.*, 2006  
Bornke *et al.*, 2001

**Figure III.1** Sequence comparison of amino acid residues of *exo*- $\alpha$ -glucosidases around Asn258 *Bsp*AG13\_31A.

Multiple sequence alignment was constructed using a MAFFTash program (Standley *et al.*, 2007). Amino acid residues corresponding to Asn258 of *Bsp*AG13\_31A are shaded. Black ball above the sequences indicates general acid/base catalyst. GenBank IDs are provided as protein names.

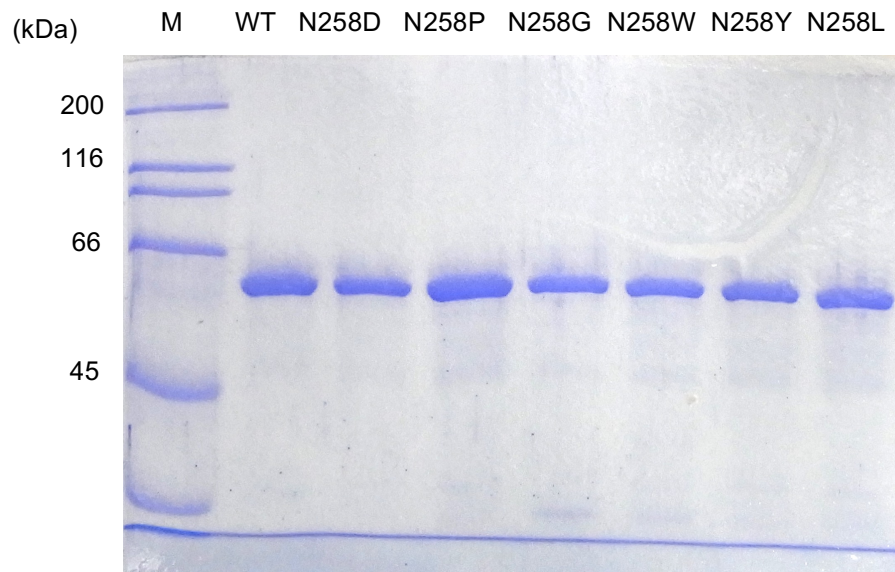


**Figure III.2** SDS-PAGE analysis of Asn258 *BspAG13A* mutants.

The protein samples (2  $\mu$ g) were loaded. Lane M, molecular size protein marker.

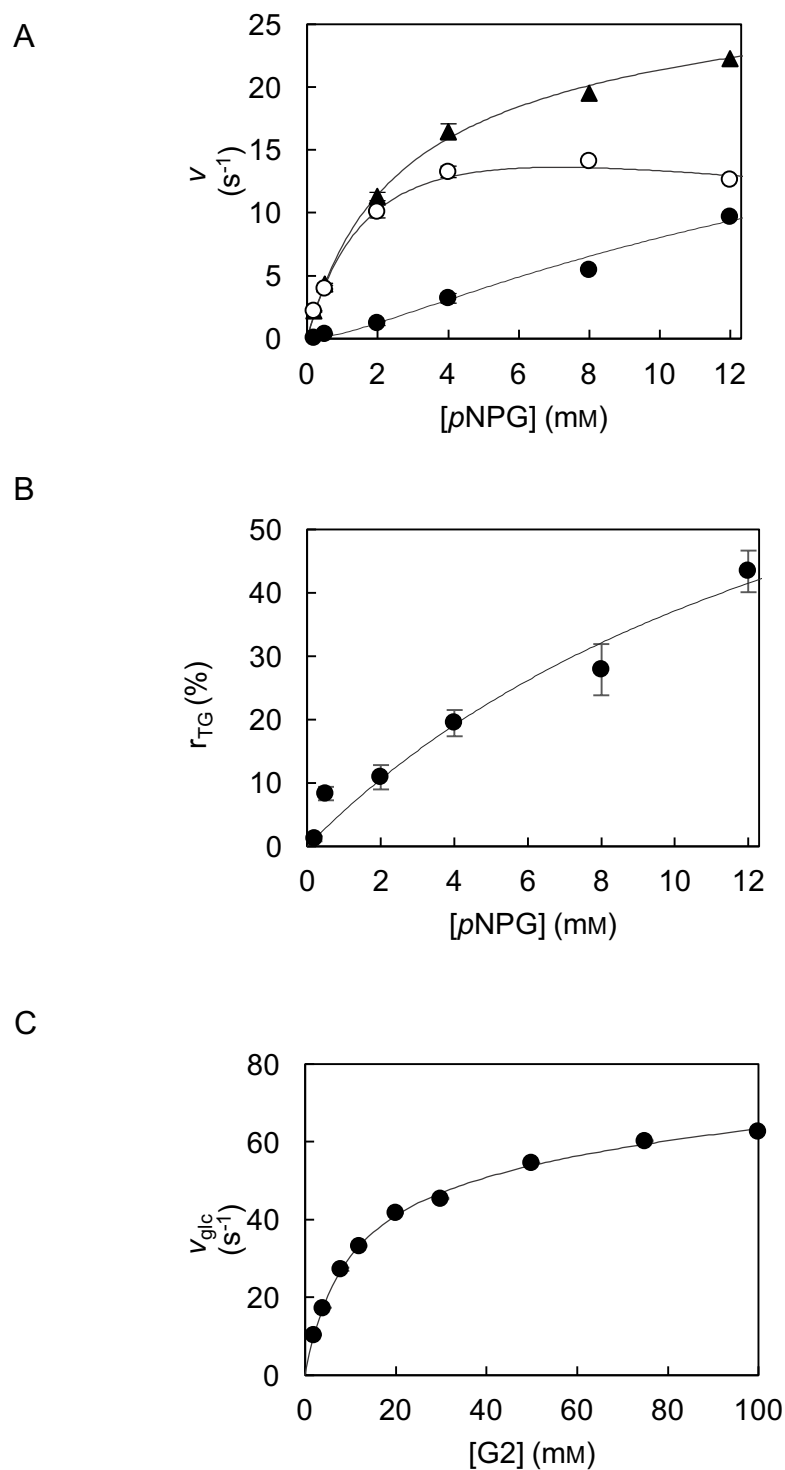
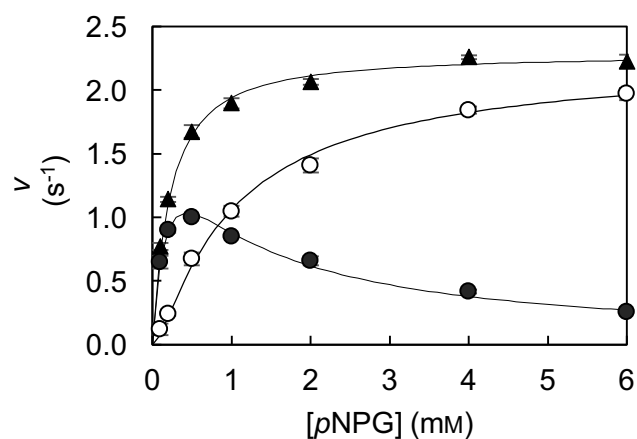


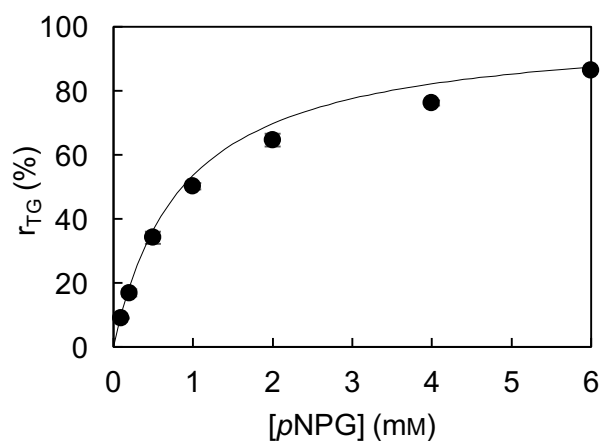
**Figure III.3 Kinetic analysis of reaction of N258D with pNPG and G2.**

Values are the mean  $\pm$  standard deviation for independent three experiments. A, s-v plot for the reaction with pNPG. Initial velocities for aglycone releasing ( $\blacktriangle$ ), hydrolysis ( $\bullet$ ), and transglucosylation ( $\circ$ ) are shown. The lines are theoretically obtained from Eq. 1-3, respectively (II.2.12), and parameters are summarized in Table III.2. B, Plot of transglucosylation ratio versus the pNPG concentration. C, s-v plot for the reaction with G2. D-Glucose-releasing velocity ( $v_{glc}$ ) are plotted. The line is from Eq. 4 with parameters shown in Table III.2.

A



B



C

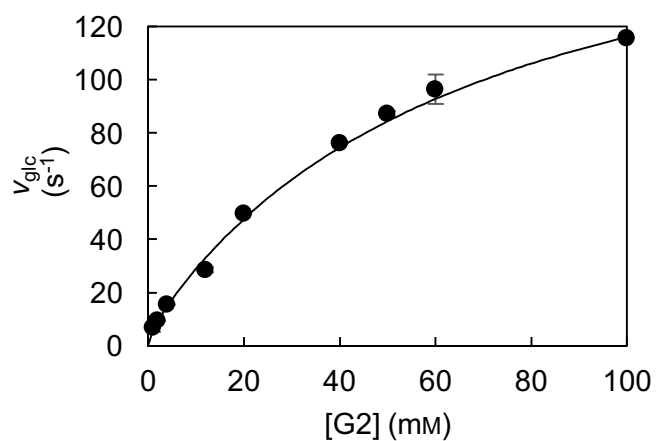


**Figure III.4 Kinetic analysis of reaction of N258G with  $p\text{NPG}$  and G2.**

Values are the mean  $\pm$  standard deviation for independent three experiments. A,  $s$ - $v$  plot for the reaction with  $p\text{NPG}$ . Initial velocities for aglycone releasing ( $\blacktriangle$ ), hydrolysis ( $\bullet$ ), and transglucosylation ( $\circ$ ) are shown. The lines are theoretically obtained from Eq. 1-3, respectively (II.2.12), and parameters are summarized in Table III.2. B, Plot of transglucosylation ratio versus the  $p\text{NPG}$  concentration. C,  $s$ - $v$  plot for the reaction with G2. D-Glucose-releasing velocity ( $v_{\text{glc}}$ ) are plotted. The line is from Eq. 4 with parameters shown in Table III.2.

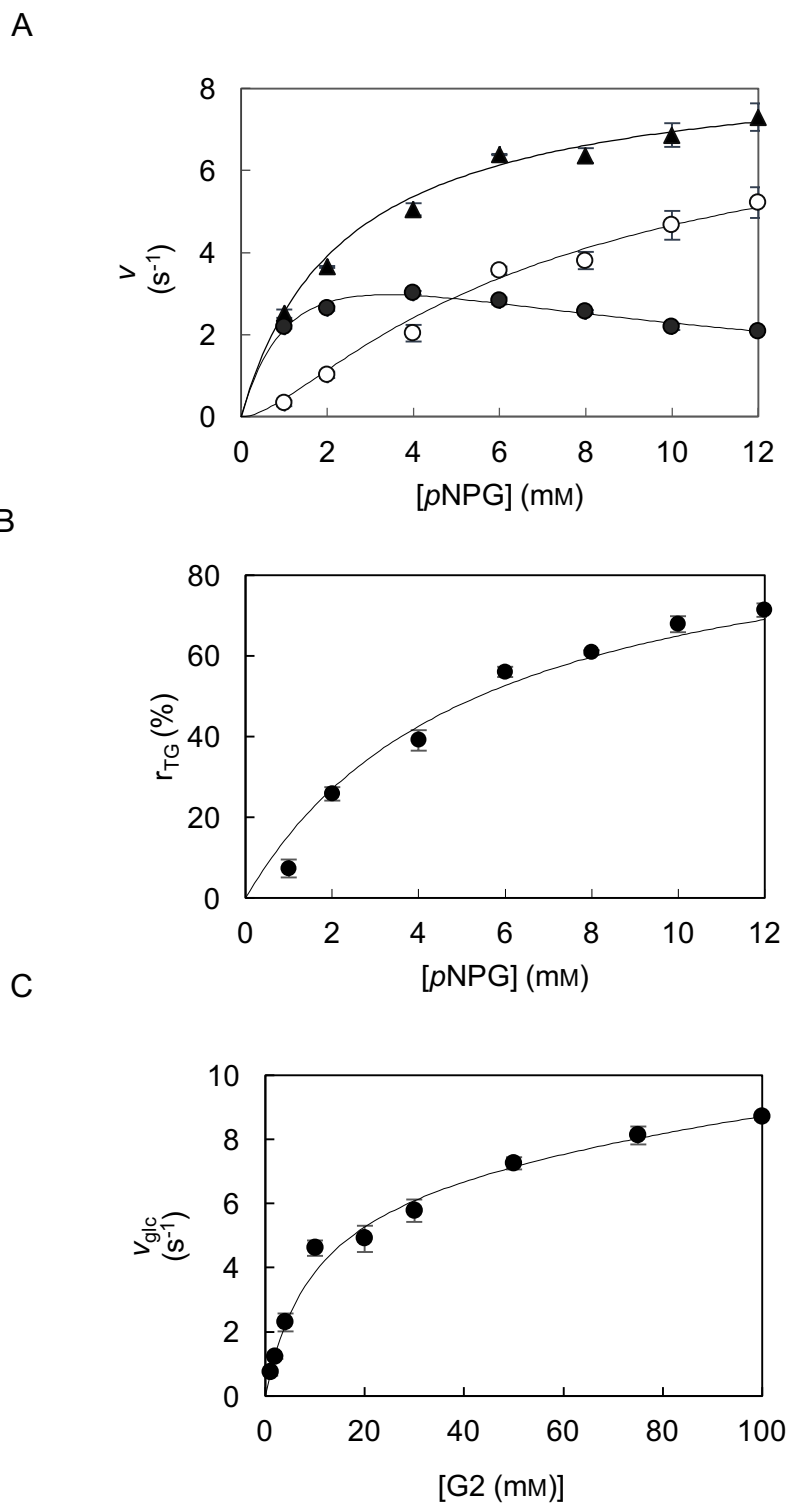


**Figure III.5 Kinetic analysis of reaction of N258L with *p*NPG and G2.**

Values are the mean  $\pm$  standard deviation for independent three experiments. A,  $s$ - $v$  plot for the reaction with *p*NPG. Initial velocities for aglycone releasing ( $\blacktriangle$ ), hydrolysis ( $\bullet$ ), and transglucosylation ( $\circ$ ) are shown. The lines are theoretically obtained from Eq. 1-3, respectively (II.2.12), and parameters are summarized in Table III.2. B, Plot of transglucosylation ratio versus the *p*NPG concentration. C,  $s$ - $v$  plot for the reaction with G2. D-Glucose-releasing velocity ( $v_{\text{glc}}$ ) are plotted. The line is from Eq. 4 with parameters shown in Table III.2.

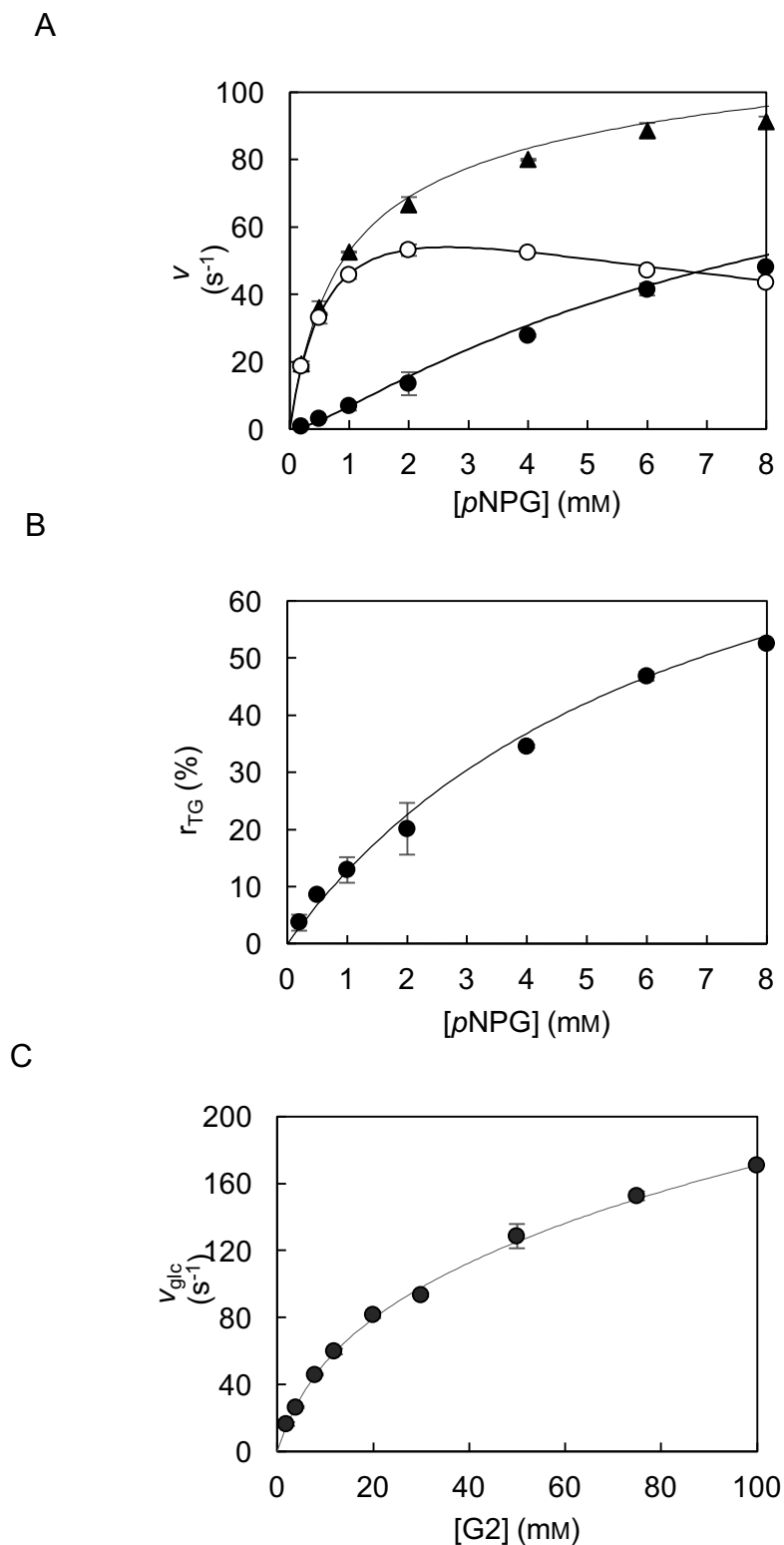


**Figure III.6 Kinetic analysis of reaction of N258P with *p*NPG and G2.**

Values are the mean  $\pm$  standard deviation for independent three experiments. A,  $s$ - $v$  plot for the reaction with *p*NPG. Initial velocities for aglycone releasing ( $\blacktriangle$ ), hydrolysis ( $\bullet$ ), and transglucosylation ( $\circ$ ) are shown. The lines are theoretically obtained from Eq. 1-3, respectively (II.2.12), and parameters are summarized in Table III.2. B, Plot of transglucosylation ratio versus the *p*NPG concentration. C,  $s$ - $v$  plot for the reaction with G2. D-Glucose-releasing velocity ( $v_{\text{glc}}$ ) are plotted. The line is from Eq. 4 with parameters shown in Table III.2.



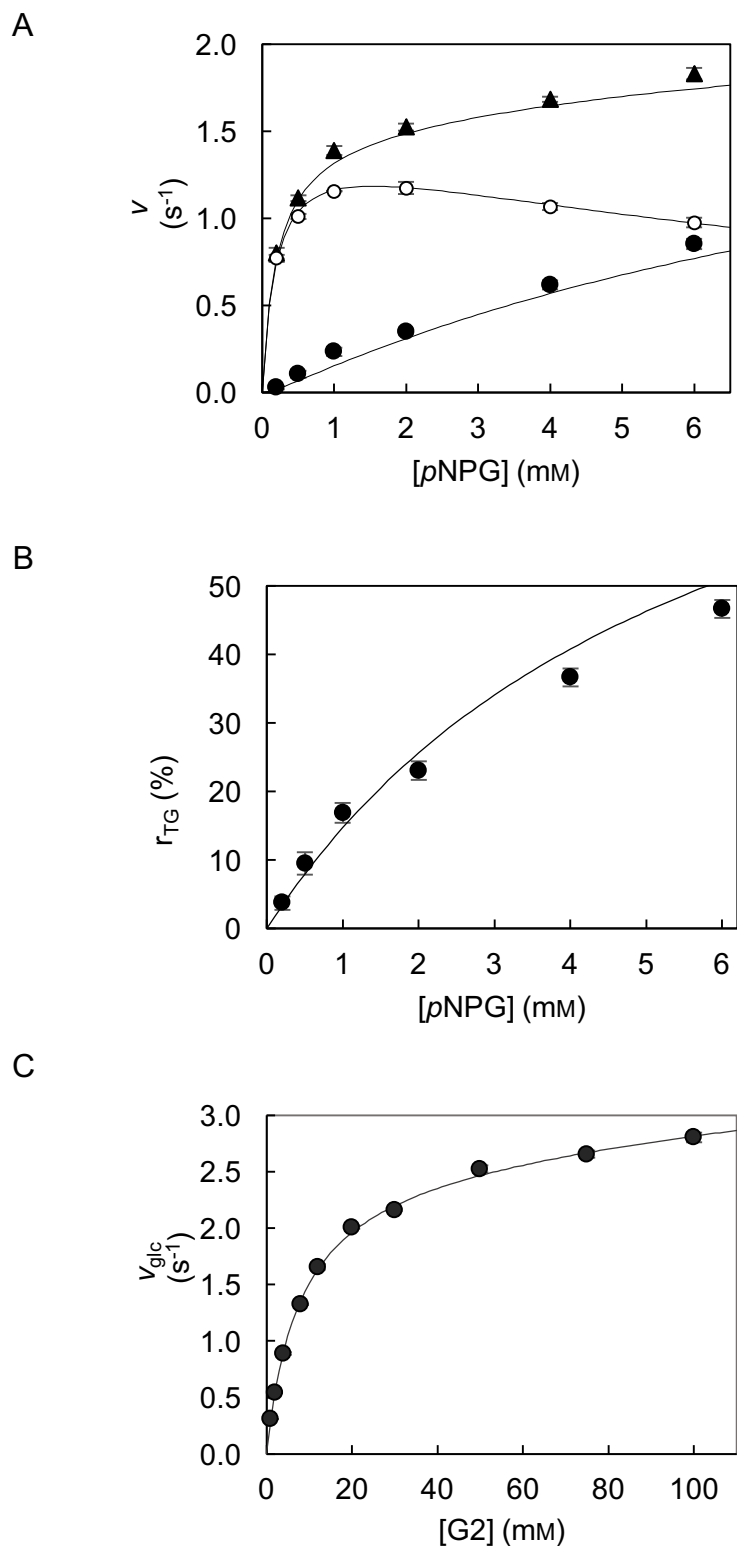


**Figure III.7 Kinetic analysis of reaction of N258W with *p*NPG and G2.**

Values are the mean  $\pm$  standard deviation for independent three experiments. A,  $s$ - $v$  plot for the reaction with *p*NPG. Initial velocities for aglycone releasing ( $\blacktriangle$ ), hydrolysis ( $\bullet$ ), and transglucosylation ( $\circ$ ) are shown. The lines are theoretically obtained from Eq. 1-3, respectively (II.2.12), and parameters are summarized in Table III.2. B, Plot of transglucosylation ratio versus the *p*NPG concentration. C,  $s$ - $v$  plot for the reaction with G2. D-Glucose-releasing velocity ( $v_{glc}$ ) are plotted. The line is from Eq. 4 with parameters shown in Table III.2.

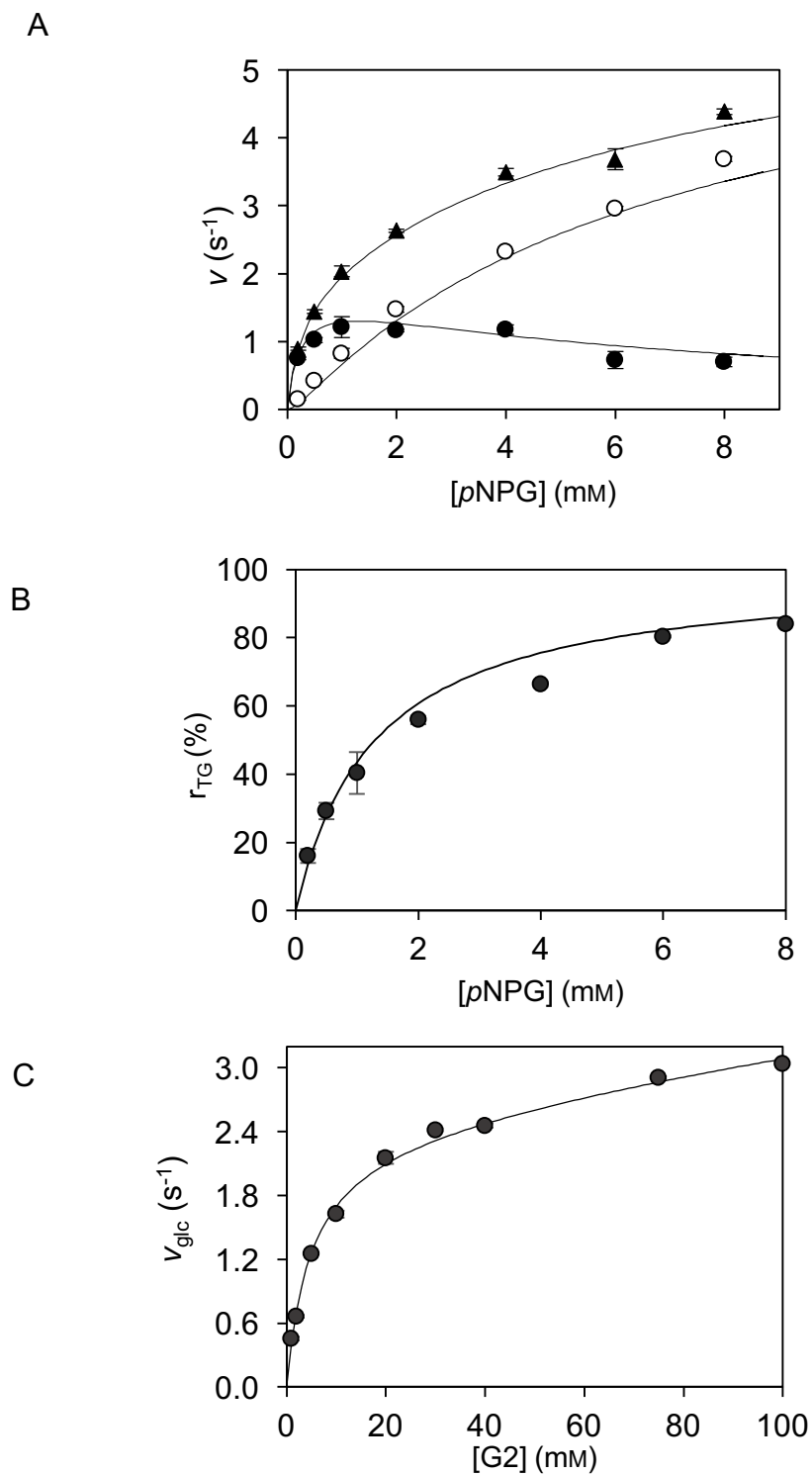


**Figure III.8 Kinetic analysis of reaction of N258Y with *p*NPG and G2.**

Values are the mean  $\pm$  standard deviation for independent three experiments. A,  $s$ - $v$  plot for the reaction with *p*NPG. Initial velocities for aglycone releasing ( $\blacktriangle$ ), hydrolysis ( $\bullet$ ), and transglucosylation ( $\circ$ ) are shown. The lines are theoretically obtained from Eq. 1-3, respectively (II.2.12), and parameters are summarized in Table III.2. B, Plot of transglucosylation ratio versus the *p*NPG concentration. C,  $s$ - $v$  plot for the reaction with G2. D-Glucose-releasing velocity ( $v_{\text{glc}}$ ) are plotted. The line is from Eq. 4 with parameters shown in Table III.2.

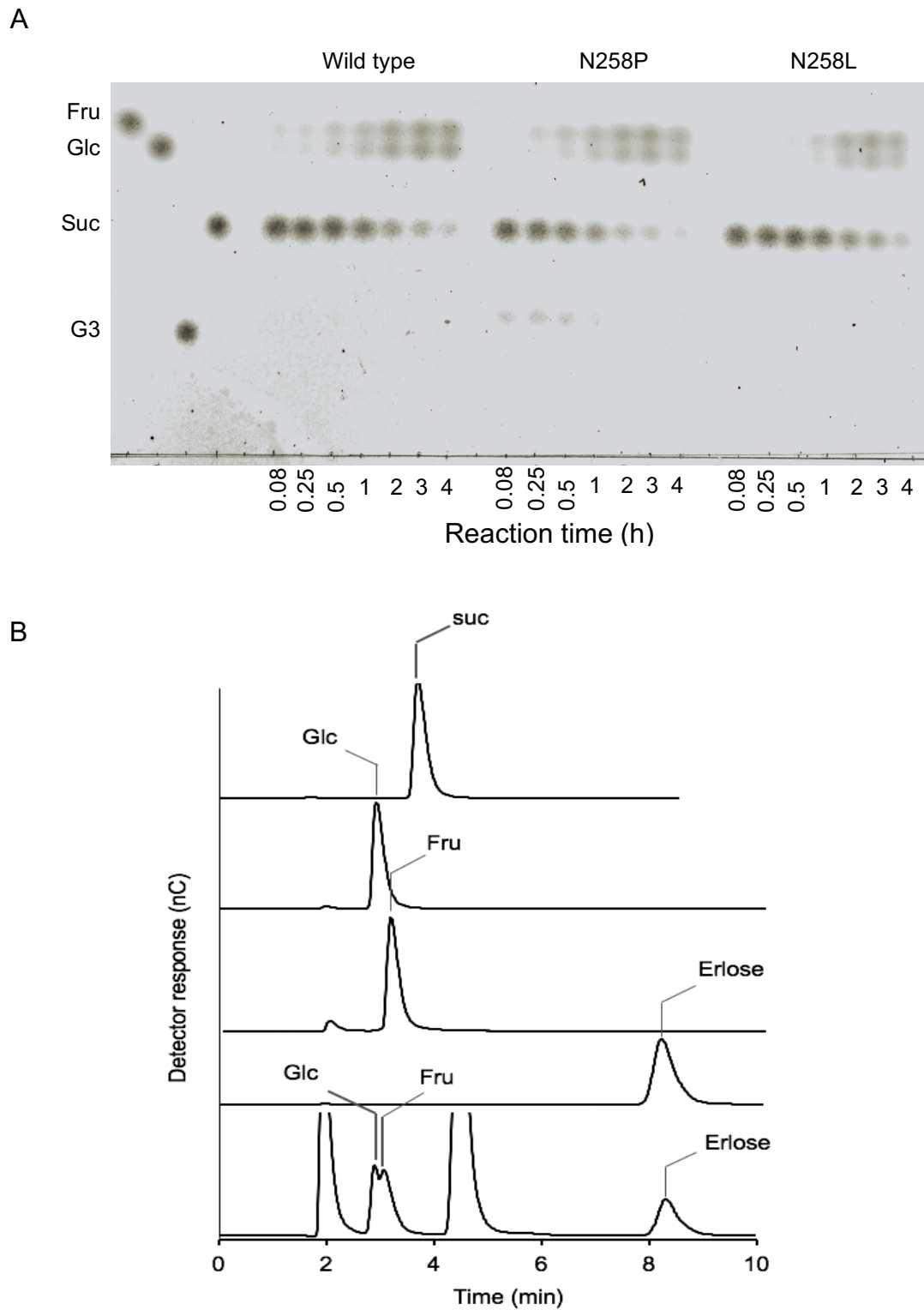


**Figure III.9 Analysis of reaction products from sucrose.**

A, TLC analysis of reaction product from 100 mM sucrose by wild type, N258P, and N258L. Reaction time is shown below the figure. Fru, fructose; Glc; Suc, sucrose; G3. Five  $\mu\text{g}$  of carbohydrate was loaded. B, HPAEC-PAD analysis of reaction products by N258P. Fru, Glc, Suc, and erlose (200  $\mu\text{M}$ ) were used as the standards.

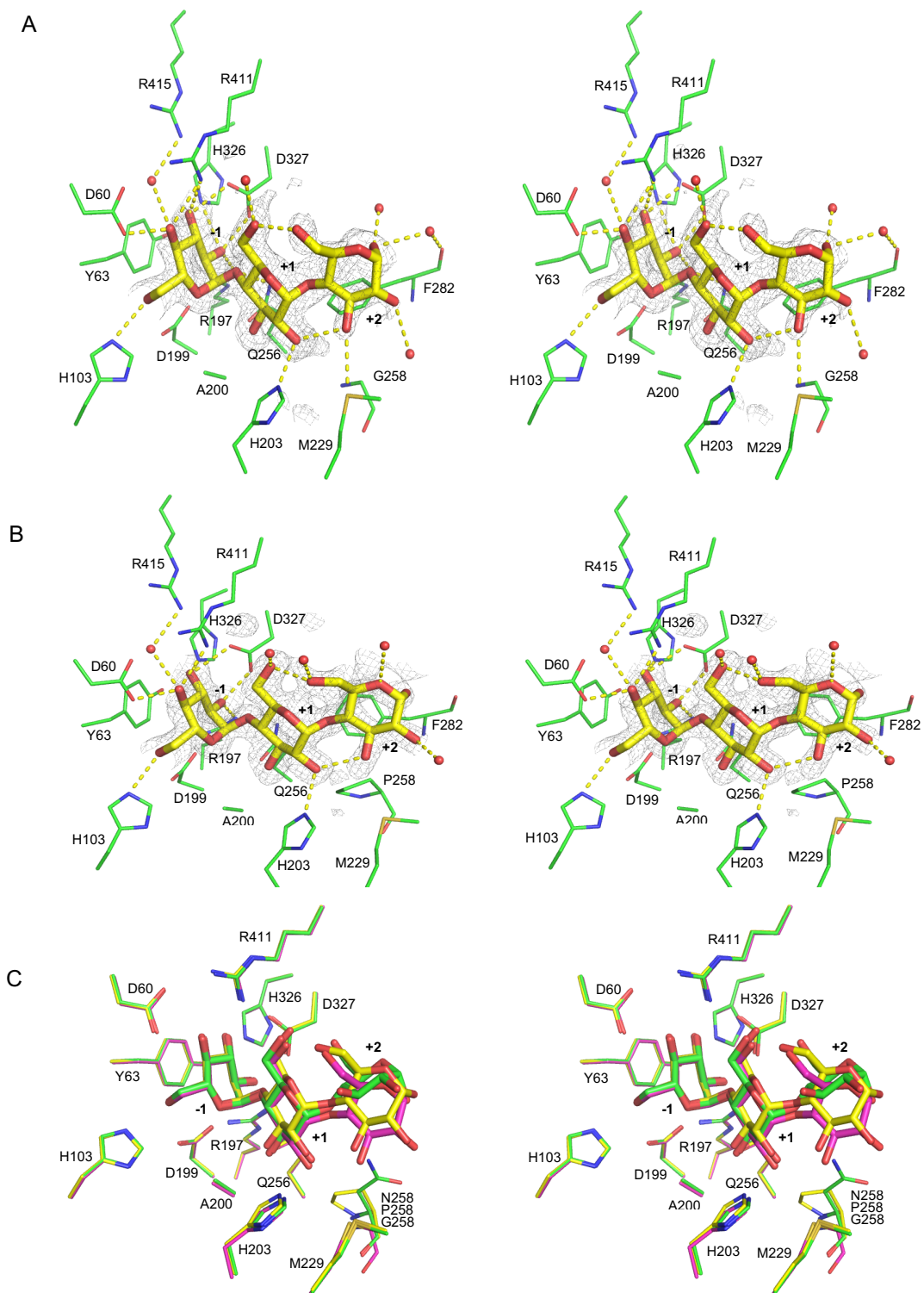


**Figure III.10 Close-up of the active sites of E256Q/N258G and E256Q/N258P in complex with G3.**

The  $F_o - F_c$  OMIT maps of E256Q/N258G (A) and E256Q/N258P (B) (contoured at  $2.5 \sigma$ ) are shown in stereo view. Water molecules bound to the ligands are indicated by red balls. Ligands are shown in yellow stick representation. Putative hydrogen bonds are indicated by dotted lines. The numbers denote subsite numbering. Superimposition of E256Q, E256Q/N258G, and E256Q/N258P is shown in panel C. E256Q, E256Q/N258G, and E256Q/N258P are shown in green, magenta, and yellow stick representations, respectively.

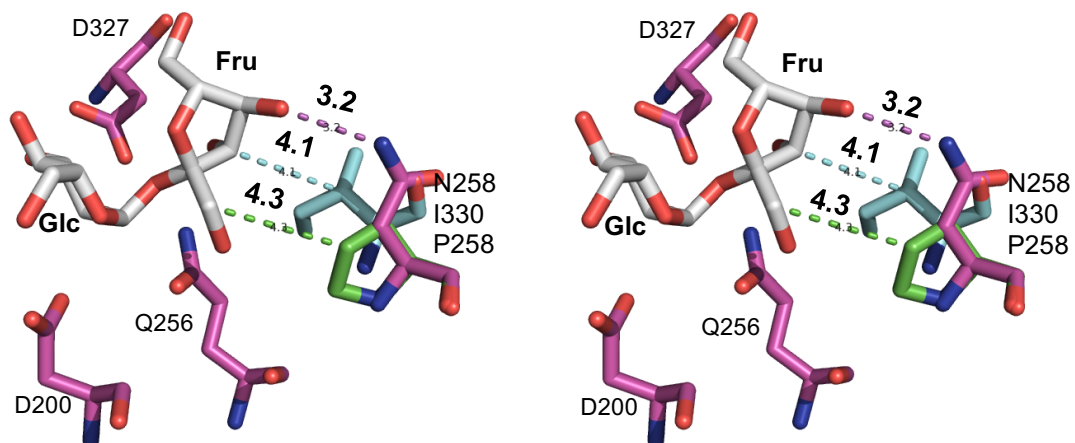


**Figure III.11 Sucrose binding model of E256Q and E256Q/N258P on E328Q amylosucrase (PDB entry, 1JGI).**

Sucrose bound to amylosucrase (white stick) is superimposed onto E256Q (magenta) and E256Q/N258P (green). A residue, I330 at the equivalent position (cyan) is shown. Numbers indicate distance (Å) between atoms connected by dashed line.

## CHAPTER IV. General discussion

AGase is an exo-type retaining glycosidase, which hydrolyzes  $\alpha$ -glucosidic linkage at the non-reducing end of substrates. This enzyme is distributed to various organisms including microorganisms, plants, and animals (Okuyama *et al.*, 2016). Substrate specificity of AGases in terms of substrate chain-length and glucosidic linkage is diverse depending on enzyme sources. In addition to hydrolysis, this enzyme catalyzes transglucosylation to the natural substrates and non-sugar molecule as the acceptor molecules under a high substrate concentration (Nakagawa *et al.*, 2000; Sato *et al.*, 2000; Kurosu *et al.*, 2002; Hung *et al.*, 2005, Ojima *et al.*, 2012). This activity has a beneficial potential for use in the productions of oligosaccharides and glucosides (Takaku 1988; Yamamoto *et al.*, 1999; Ojima *et al.*, 2012). In this study, an AGase, *BspAG13\_31A*, with high transglucosylation activity was found in a soil isolate *Bacillus* sp. AHU2216, and biochemically and structurally characterized in detail. On the basis of amino acid sequence similarity, *BspAG13\_31A* is classified into GH13\_31, which includes exo-type glucosidases specific to  $\alpha$ -(1 $\rightarrow$ 4)-glucosidic linkage (AGase) and  $\alpha$ -(1 $\rightarrow$ 6)-glucosidic linkage (oligo-1,6-glucosidase and dextran glucosidase). Amino acid sequence of *BspAG13\_31A* is 62% and 63% identical with *G. stearothermophilus* AGase and *Geobacillus* sp. HTA462 AGase, respectively. *BspAG13\_31A* is highly specific to  $\alpha$ -(1 $\rightarrow$ 4)-glucosidic linkage in both hydrolysis and transglucosylation, and G2 is the best substrate among maltooligosaccharides.

In contrast to  $\alpha$ -(1 $\rightarrow$ 6)-glucosidic linkage-specific enzymes in GH13\_31, structure-function relationship of  $\alpha$ -(1 $\rightarrow$ 4)-glucosidic linkage-specific enzyme in this subfamily was poorly understood. Thus, in this study, structural analysis of *BspAG13\_31A* in complex with substrate was conducted. The overall structure of *BspAG13\_31A* is similar to those of GH13\_31 enzymes analyzed thus far. Three residues, Ala200 and His203, located on  $\beta$  $\rightarrow$  $\alpha$  loop 4, and Asn258, located on  $\beta$  $\rightarrow$  $\alpha$  loop 5, are predicted to be important for  $\alpha$ -(1 $\rightarrow$ 4)-glucosidic linkage specificity in *BspAG13\_31A*. Ala corresponding to Ala200 of *BspAG13\_31A* is often observed in GH13 AGases specific to  $\alpha$ -(1 $\rightarrow$ 4)-glucosidic linkage (not limited in GH13\_31). His203 and Asn258 form hydrogen bond with 2-O of the D-glucosyl residue in subsite +1 (Figure II.12 and 13). The His residue is frequently found in  $\alpha$ -(1 $\rightarrow$ 4)-linkage-specific enzymes (Takii *et al.*, 1996; MacGregor *et al.*, 2001; Hung *et al.*, 2005), and the function of this His is thought to be common in these enzymes. Asn in the equivalent position of Asn258 of *BspAG13\_31A* is found in other GH13\_31 AGases specific to  $\alpha$ -(1 $\rightarrow$ 4)-glucosidic linkage. *BspAG13\_31A* is clearly distinct from AGases from *G. stearothermophilus* and *Geobacillus* sp. HTA462 in terms of substrate chain-length specificity, because the later two enzymes prefer G3 to G2. This result might have arisen from no steric hindrance at the glucosyl residue in subsite +2 by Asn258 in *Geobacillus* sp. HTA462 AGase at the equivalent position (Figure IV.1). Although in  $\alpha$ -1,6-glucosidase (Mall; accession no CAB15461.1) from *Bacillus subtilis* has Asn in this position

(Figure III.1), the structural features of the enzyme are more similarity to  $\alpha$ -(1 $\rightarrow$ 6)-glucosidic linkage-specific enzymes. The structure analysis of *BspAG13\_31A* in complex with maltooligosaccharides suggested that the conformation of glucosyl residue at subsite +2 was less stable than the global minimum. Disaccharide specificity of *BspAG13\_31A* is thought to arise from steric hindrance by Asn258 upon binding to maltooligosaccharides longer than G2. Substitution of Asn258 with amino acid residues with small side chain, Gly and Pro, enhanced G3 specificity, and orientation of bound glucosyl residue at subsite +2 changed to the relaxed form (Figure III.10). However, Asn corresponding to Asn258 of *BspAG13\_31A* is conserved in AGases with high G3 specificity. This indicates that substrate-binding mode of G3 specific GH13\_31 AGases is different from that of *BspAG13\_31A*. Structural analysis of such enzymes is required in future study.

Structural analysis of *BspAG13\_31A* implied that structural change of  $\beta$  $\rightarrow$  $\alpha$  loop 6 during the reaction process. Possible steric hindrance by Trp288 on this loop, observed in the apo-form was avoided in the substrate bound complexes. The conformational change of this loop along with the reaction process may be important for transglucosylation by stabilizing the glucosyl enzyme intermediate and preventing water molecules from binding and acting as substrate. Structural analysis of the glucosyl enzyme intermediate, trapped using  $\alpha$ -glucosyl fluoride and E256Q inactive acid/base mutant, would give fruitful information about structural insight into transglucosylation by *BspAG13\_31A*. Introduction of mutation to reduce flexibility of this loop would be interesting to analyze the functions of this loop in transglucosylation.

In this study, the biochemical functions of GH13\_31 AGase *BspAG13\_31A* including specificity to glucosidic linkage and substrate chain-length, and transglucosylation activity were analyzed, and new structural insights into these functions of the GH13\_31 enzyme were provided. The findings shown in this study would contribute to advance of understanding structure-function relationships of GH13 enzymes. Transglucosylation activity of *BspAG13A* to natural substrates is attractive for enzymatic synthesis of oligosaccharides and glucosides. Therefore, it is important to investigate chemoenzymatic production of oligosaccharides and glucoside using *BspAG13A* for application of this enzyme.

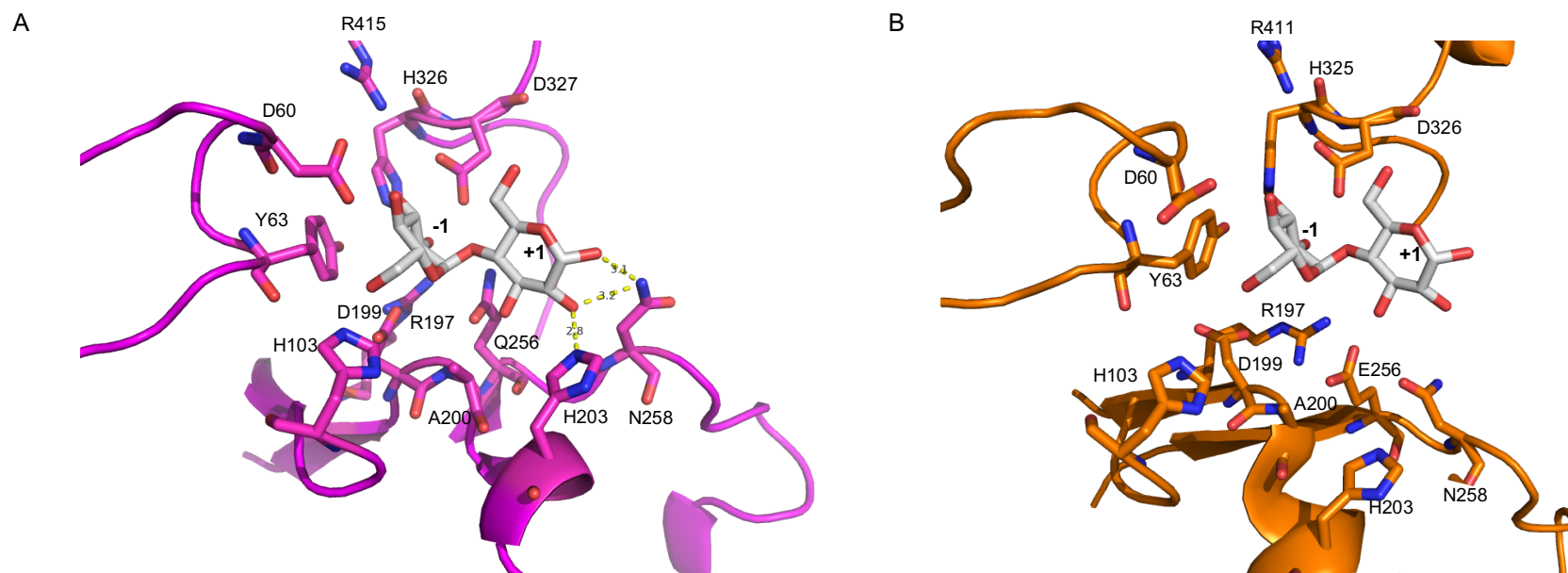


**Figure IV.1** Close-up view in active site of *BspAG13\_31A* with G2 complex and *Geobacillus* sp. HTA462 AGase.

A, *BspAG13\_31A*-bound G2; B, the superimposed structure of *Geobacillus* sp. HTA462 AGase (PDB entry, 2ZE0) onto *BspAG13\_31A*-bound G2. Numbers indicate distance (Å) between atoms connected by dashed line



## REFERENCES

- Adams PD, Afonine PV, Bunkoczi G, Chen VB, Davis IW, Echols N, Headd JJ, Hung LW, Kapral GJ, Grosse-Kunstleve RW, McCoy AJ, Moriarty NW, Oeffner R, Read RJ, Richardson DC, Richardson JS, Terwilliger TC, Zwart PH (2010) PHENIX: a comprehensive Python-based system for macromolecular structure solution. *Acta Crystallogr D66*:213-221.
- Altermann E, Russell W.M, Azcarate-Peril M.A, Barrangou R, Buck B.L, McAuliffe O, Souther N, Dobson A, Duong T, Callnan M, Lick S, Hamrick A, Cano R, Klaenhammer T.R (2005) Complete genome sequence of the probiotic lactic acid bacterium *Lactobacillus acidophilus* NCFM. *Proc natl Acad Sci U.S.A.* 1764:688-698.
- Altschul SF, Gish W, Miller W, Myers EW, Lipman DJ (1990) Basic local alignment search tool. *J Mol Biol* 215:403-410.
- Bali V, Panesar P.S, Bera M.B, Panesar R (2015). Fructo-oligosaccharides: production and potential applications. *Crit Rev Food Sci Nutr* 55:1475-1490.
- Belda E, Sekowska A, Le Fevre F, Morgat A, Mornico D, Ouzounis C, Vallenet D, Medigue C, and Danchin A (2013) An updated metabolic view of the *Bacillus subtilis* 168 genome. *Microbiology* 159:757-770.
- Bornke F, Hajirezaei M, Sonnewald U (2001) Cloning and characterization of the gene cluster for palatinose metabolism from the phytogetic bacterium *Erwinia rhapontici*. *J Bacteriol* 183: 2425-2430.
- Bourne Y, Henrissat E (2001) Glycoside hydrolases and glycosyltransferases: families and functional modules. *Curr Opin Struct Biol* 11:593-600.
- Bradford M.M (1976) A rapid and sensitive method for the quantitation of microgram quantities of protein utilizing the principle of protein-dye binding. *Anal Biochem* 72:248-254.
- Brayer G.D, Luo Y, Withers S.G (1995) The structure of human pancreatic  $\alpha$ -amylase at 1.8 Å resolution and comparisons with related enzymes. *Protein Sci* 4:1730-1742.
- Brzozowski A.M, Davies G.J (1997) Structure of the *Aspergillus oryzae*  $\alpha$ -amylase complexed with the inhibitor acarbose at 2.0 Å resolution. *Biochemistry* 36:10837-108845.
- Chen VB, Arendall WB, Headd JJ, Keedy DA, Immormino RM, Kapral GJ, Murray LW, Richardson JS, Richardson DC (2010) MolProbity: all-atom structure validation for macromolecular crystallography. *Acta Crystallogr. D66*:12-21.

- Chiba S (2012) A historical perspective for the catalytic reaction mechanism of glycosidases; so as to bring about breakthrough in confusing situation. *Biotechnol Biochem* 76:215-231.
- Chiba S (1998) "Handbook of amylases and Related Enzymes" ed. The amylase research society of Japan, Pergamon Press, Oxford. 104-116.
- Chiba S (1997) Molecular mechanism in  $\alpha$ -Glucosidase and Glucoamylase. *Biosci Biotechnol Biochem* 61:1233-1239.
- Chiba S, Minamiura N (1988)  $\alpha$ -Glucosidases. In: The Amylase Research Society of Japan (ed) Handbook of amylases and related enzymes. Pergamon, Oxford, United Kingdom, pp 104-116.
- Chiba S, Kimura A, Kobori T, Saitoh K (1985) Quantitative determination of disaccharides produced from soluble starch through transglucosylation of the buckwheat  $\alpha$ -glucosidase. *J Jpn Soc Starch Sci* 32:213-216.
- Chiba S, Kimura A, Kobori T, Saitoh K (1985) Quantitative determination of disaccharides produced from soluble starch through transglucosylation of the buckwheat  $\alpha$ -glucosidase. *J Jpn Soc Starch Sci.* 32. 213-216.
- Chihan A. C, Ozcan B, Cokmus C (2009) Characterization of thermostable  $\alpha$ -glucosidases from newly isolated *Geobacillus* sp. A333 and thermophilic bacterium A343. *World J Microbiol Biotechnol* 25:2205-2217.
- Coutinho P.M, Henrissat B (1999) Carbohydrate-active enzymes server at URL: <http://afmb.cnrs-mrs.fr/~cazy/CAZY/index.html>.
- Dauter Z, Dauter M, Brzozowski A.M, Christensen S, Borchert T.V, Beier L, Wilson K.S, Davies G.J (1999) X-ray structure of Novamylm, the five-domain 'maltogenic'  $\alpha$ -amylase from *Bacillus Stearothermophilus*: maltose and acarbose complexes at 1.7 Å resolution. *Biochemistry* 38:8385-8392.
- Davies G, Henrissat B (1995) Structures and mechanism of glycosyl hydrolases. *Structure* 3:853-859.
- Dayhoff M.O, Pearlman G.E, and MacInnes D.A (1952) The partial specific volumes, in aqueous solution, of three proteins. *J Am Chem Soc* 74:2515-2517.
- Dowd MK, Zeng J, French AD, Reilly PJ (1992) Conformational analysis of the anomeric forms of kojibiose, nigerose, and maltose using MM3. *Carbohydr Res* 230:223-244.
- Egeter O, Bruckner R (1995) Characterization of a genetic locus essential for maltose-maltotriose utilization in *Staphylococcus xylosus*. *J Bacteriol.* 177:2408-2415.

- Emsley P, Cowtan K (2004) Coot: model-building tools for molecular graphics. *Acta Crystallogr D* 60:2126-2132.
- Farag S (1979) Separation and analysis of some sugars by using thin layer chromatography. *J ASSBT* 20:251-254.
- Gessler K, Usón I, Takaha T, Krauss N, Smith SM, Okada S, Sheldrick GM, Saenger W (1999) V-Amylose at atomic resolution: X-ray structure of a cycloamylose with 26 glucose residues (cyclomaltohexaicosaoase). *Proc Natl Acad Sci USA* 96:4246-4251.
- Hancock SM, Vaughan MD, Withers SG (2006) Engineering of glycosidases and glycosyltransferases. *Curr Opin Chem Biol* 10:509-519.
- Henrissat B, Bairoch A (1993) New families in the classification of glycosyl hydrolases based on amino acid sequence similarities. *Biochem J.* 293:781-788.
- Henrissat B (1991) A classification of glycosyl hydrolases based on amino acid sequence similarities. *Biochem J.* 280: 309-316.
- Hers HG (1963)  $\alpha$ -Glucosidase deficiency in generalized glycogen-storage disease (Pompe's disease). *Biochem J* 86:11-16.
- Hiromi K, Nitta Y, Numata C, Ono S (1973) Subsite affinities of glucoamylase: examination of the validity of the subsite theory, *Biochim Biophys Acta* 302:362-375.
- Hondoh H, Saburi W, Mori H, Okuyama M, Nakada T, Matsuura Y, Kimura A (2008) Substrate recognition mechanism of  $\alpha$ -1,6-glucosidic linkage hydrolyzing enzyme, dextran glucosidase from *Streptococcus mutans*. *J Mol Biol* 378: 911-920.
- Hondoh H, Kuriki T, Matsuura Y (2003) Three-dimensional structure and substrate binding of *Bacillus stearothermophilus* neopullulanase. *J Mol Biol* 326: 177-188.
- Horvathova V, Janecek S, Sturdik E (2000) Amylolytic enzymes: their specificities, origins and properties. *Biologia Bratislava* 55:205-615.
- Hung VS, Hatada Y, Goda S, Lu J, Hidaka Y, Li Z, Akita M, Ohta Y, Watanabe K, Matsui H, Ito S, Horikoshi K (2005)  $\alpha$ -Glucosidase from a strain of deep-sea *Geobacillus*: a potential enzyme for the biosynthesis of complex carbohydrates. *Appl Microbiol Biotechnol* 68:757-765.
- Inohara-Ochiai M, Nakayama T, Got R, Nakao M, Ueda T, Shibano Y (1997) Altering substrate specificity of *Bacillus* sp. SAM1606  $\alpha$ -glucosidase by comparative site-specific mutagenesis. *J Biol Chem* 272:1601-1607.
- Janecek S, Svensson B, Ann MacGregor E (2014)  $\alpha$ -amylase: an enzyme specificity found in various families of glycoside hydrolases. *Cell Mol Life Sci* 71:1149-1170.

- Janecek S (2002) How many conserved sequence regions are there in the  $\alpha$ -amylase family? *Biologia Bratislava*. 57 (suppl. 11):29-41.
- Janecek S (1997)  $\alpha$ -Amylase family: molecular biology and evolution. *Prog Biophys Mol Biol* 67:67-97.
- Janecek S (1994) Sequence similarities and evolutionary relationships of microbial, plant and animal  $\alpha$ -amylases. *Eur J Biochem* 224:519-524.
- Kabsch W (2010) Xds. *Acta Crystallogr D*66:125-132.
- Kadziola A, Abe J, Svensson B, Haser R (1994) Crystal and molecular structure of barley  $\alpha$ -amylase. *J Mol Biol* 239:104-121.
- Kato N, Suyama S, Shirokane M, Kato M, Kobayashi T, Tsukagoshi N (2002) Novel  $\alpha$ -glucosidase from *Aspergillus nidurans* with strong transglycosylation activity. *Appl Environ Microbiol* 68:1250-1256.
- Kimura A, Takata M, Sakai O, Matsui H, Takai N, Takayanagi T, Nishimura I, Uozumi T, Chiba S (1992) Complete amino acid sequence of crystalline  $\alpha$ -glucosidase from *Aspergillus niger*. *Biosci Biotechnol Biochem* 56:1368-1370.
- Kimura A (2000) Molecular anatomy of  $\alpha$ -glucosidase. *Trends Glycosci Glycotechnol* 12:373-380.
- Knai R, Haga K, Yamane K, Harata K (2001) Crystal structure of cyclodextrin glucanotransferase from alkalophilic *Bacillus* sp. 1011 complexed with 1-deoxynojirimycin at 2.0 Å resolution. *J Biochem* 129:593-598.
- Kobayashi M, Hondoh H, Mori H, Saburi W, Okuyama M, Kimura A (2011) Calcium ion-dependent increase in thermostability of dextran glucosidase from *Streptococcus mutans*. *Biosci Biotechnol Biochem* 75:1557-1563.
- Kohmoto T, Fukui F, Takaku H, Machida Y, Arai M, Mitsuoka T (1988) Effect of isomaltoligosaccharides on human fecal flora. *Bifidobacteria Microflora* 7:61-69.
- Kohmoto T, Fukui F, Takaku H, Mitsuoka T (1991) Dose-response test of isomaltoligosaccharides for increasing fecal bifidobacteria. *Agric Biol Chem* 55:2157-2159.
- Konishi Y, Shindo k (1997). Production of nigerose, nigerosyl glucose, and nigerosyl maltose by *Acremonium* sp. S4g13. *Biosci Biotech Biochem* 61:439-442.
- Konishi Y, Okamoto A, Takahashi J, Aitani M, Nakatani N (1994) Effect of Bay m 1099, an  $\alpha$ -glucosidase inhibitor, on starch metabolism in germinating wheat seeds. *Biosci Biotechnol Biochem* 58:135-139.

- Kunst A, Draeger B, and Ziegenhorn J (1984) Colorimetric methods with glucose oxidase and peroxidase. In methods of enzymatic analysis, Ed. Hu Bergmeyer, Weinheim: Verlag Chemie 3:178-185.
- Kurosu J, Sato T, Yoshida K, Tsugane T, Shimura S, Kirimura K, Kino K, Usami S (2002) Enzymatic synthesis of  $\alpha$ -arbutin by  $\alpha$ -anomer-selective glucosylation of hydroquinone using lyophilized cells of *Xanthomonas campestris* WU-9701. J Biosci Bioengin. 93: 328-330.
- Laemmli U.K (1970) Cleavage of structural proteins during the assembly of the head of bacteriophage T4. Nature 277:680-685.
- Lawson C.L, van Montfort R, Strokopytov B, Rozeboom H.J, Kalk K.H, de vries G.E, Penninga D, Dijkhuizen L, Dijkstra B.W (1994) Nucleotide sequence and X-ray structure of cyclodextrin glycosyltransferase from *Bacillus circulans* strain 251 in a maltose –dependent crystal form. J Mol Biol. 236:590-600.
- Liu L, Li Y, Zhang J, Zhou Z, Liu J, Li X, Du G, Wang L, Chan J (2011) Complete genome sequence of the industrial strain *Bacillus megaterium* WSH-002. J Bacteriol 193:6389-6390.
- Lombard V, Golaconda Ramulu H, Drula E, Coutinho P.M, Henrissat B (2014) The carbohydrate-active enzymes database (CaZy) in 2013. Nucleic Acids Res 42:490-495.
- MacGregor E.A, Janecek S, Svensson B (2001) Relationship of sequence and structure to specificity in the  $\alpha$ -amylase family enzymes. Biochim Biophys Acta 1546:1-20.
- Maiti R, Van Domselaar G.H, Zhang H, Wishart D.S (2004) SuperPose: a simple server for sophisticated structural superposition, Nucleic Acids Res. 32:W590-W594.
- Matsuura Y, Kusunoki M, Harada W, Kakudo M (1984) Structure and possible catalytic residues of Taka-amylase A. J Biochem 95:697-702.
- Matthews BW (1986) solvent content of protein crystals. J Mol Biol 33:491-497.
- McCleary B.V, Gibson L T.S (1989) Purification, properties, and industrial significance of transglucosidase from *Aspergillus niger*. Carbohydr Res 185:147-162.
- McCoy AJ, Grosse-Kunstleve RW, Adams PD, Winn MD, Storoni LC, Read RJ (2007) Phaser crystallographic software. J Appl Cryst 40:658–674.
- Mirza O, Skov L.K, Remaud-Simeon M, Montalk G.P, Albenne C, Monsan P, Gajhede M (2001) Crystal structures of amylosecrase from *Neisseria polysaccharea* in complex with glucose and the active site mutant Glu328Gln in complex with the natural substrate sucrose. Biochemistry 40:9032-9039.
- Miwa I, Okuda J, Maeda K., and Okuda G (1972) Mutarotase effect on colorimetric determination of blood glucose with  $\beta$ -D-glucose oxidase. Clin Chim Acta 37:538-540.

- Møller M.S, Fredslund F, Majumber A, Nakai H, Poulsen J.C, LoLeggio L, Svensson B, Abou Hachem M (2012) Enzymology and structure of the GH13\_31 glucan 1,6- $\alpha$ -glucosidase that confers isomaltooligosaccharide utilization in the probiotic *Lactobacillus acidophilus* NCFM. *J Bacteriol* 194:4249-4259.
- Moore S, and Stein W.H (1948) Photometric ninhydrin method for use in the chromatography of amino acids. *J Biol Chem* 176:367-388.
- Nakagawa H, Dobashi Y, Sato T, Yoshida K, Tsugane T, Shimura S, Kirimura K, Kino K, Usami S (2000)  $\alpha$ -Anomeraselective glucosylation of menthol with high yield through a crystal accumulation reaction using lyophilized cells of *Xanthomonas campestris* WU-9701. *J Biosci Bioengin* 89:138-144.
- Nakagawa K, Kawasaki H (2001) DNA sequence analysis. In: Society for Actinomycetes Japan (ed) Identification manual of Actinomycetes. Business Center for Academic Societies Japan, Tokyo, Japan, pp 83-117.
- Nakajima R, Imanaka T, Aiba S (1986) Comparison of amino acid sequences of eleven different  $\alpha$ -amylases. *Appl Microbiol Biotechnol* 23:355-360.
- Nakao M, Nakayama T, Harada M, Kakudo A, Ikemoto H, Kobayashi A, Shibano Y (1994) Purification and characterization of a *Bacillus* sp. SAM1606 thermostable  $\alpha$ -glucosidase with transglycosylation activity. *Appl Microbiol Biotechnol* 41:337-343.
- Nishimoto M, Kubota M, Tsuji M, Mori H, Kimura A, Matsui H, Chiba S (2001) Purification and substrate specificity of honeybee, *Apis mellifera* L.,  $\alpha$ -glucosidase III. *Biosci Biotechnol Biochem* 65:1610-1616.
- Ojima T, Saburi W, Yamamoto T, Kudo T (2012) Characterization of *Halomonas* sp. strain H11  $\alpha$ -glucosidase activated by monovalent cations and its application for efficient synthesis of  $\alpha$ -D-glucosylglycerol. *Appl Environ Microbiol* 78:1836-1845.
- Ojima T, Saburi W, Sato H, Yamamoto T, Mori H, Matsui H (2011) Biochemical characterization of a thermophilic cellobiose 2-epimerase from a thermohalophilic bacterium, *Rhodothermus marinus* JCM9785. *Biosci Biotechnol Biochem* 75:2162-2168.
- Okuyama M, Saburi W, Mori H, Kimura A (2016)  $\alpha$ -Glucosidases and  $\alpha$ -1,4-glucan lyases: structures, functions, and physiological actions. *Cell Mol Life Sci* 73:2727-2751.
- Patel S, Goyal A (2011) Functional oligosaccharides: production, properties and applications. *World J Microbiol Biotechnol* 27:1119-1128.

- Pokusaeva K, O'Connell-Montherway M, Zomer A, Fitzgerald G.F, van Sinderen D (2008) Characterization of two novel  $\alpha$ -glucosidases encoded by *Bifidobacterium breve* UCC2003 (unpublished manuscript). University College Cork, Ireland.
- Qian M, Haser R, Payan F (1995) Carbohydrate binding sites in a pancreatic  $\alpha$ -amylase-substrate complex, derived from X-ray structure analysis at 2.1 Å resolution. *Protein Sci* 4:747-755.
- Ramasubbu N, Paloth V, Luo Y, Brayer G.D, Levine M.J (1996) Structure of human salivary  $\alpha$ -amylase at 1.6 Å resolution: implications for its role in the oval cavity. *Acta Crystallogr. D Biol. Crystallogr* 52:435-446.
- Saburi W, Rachi-Otsuka H, Hondoh H, Okuyama M, Mori H, Kimura A (2015) Structural elements responsible for the glucosidic linkage-selectivity of a glycoside hydrolase family 13 exo-glucosidase. *FEBS Lett* 589:865-869.
- Saburi W, Kobayashi M, Mori H, Okuyama M, Kimura A (2013) Replacement of the catalytic nucleophile aspartyl residue of dextran glucosidase by cysteine sulfonate enhances transglycosylation activity. *J Bio Chem* 288:31670-31677.
- Saburi W, Mori H, Saito S, Okuyama M, Kimura A (2006) Structural elements in dextran glucosidase responsible for high specificity to long chain substrate. *Biochim Biophys Acta* 1764:688-698.
- Sato T, Nakagawa H, Kurosu J, Yoshida K, Tsugane T, Shimura S, Kirimura K, Kino K, Usami S (2000)  $\alpha$ -Anomer-selective glucosylation of (+)-catechin by the crude enzyme, showing glucosyl transfer activity, of *Xanthomonas campestris* WU-9701. *J Biosci Bioengin* 90:625-630.
- Schönert S, Buder T, Dahl MK (1998) Identification and enzymatic characterization of the maltose-inducible  $\alpha$ -glucosidase MalL (sucrase-isomaltase-maltase) of *Bacillus subtilis*. *J Bacteriol* 180:2574-2578.
- Shen X, Saburi W, Gai Z, Kato K, Ojima-Kato T, Yu J, Komoda K, Kido Y, Matsui H, Mori H, Yao M (2015) Structural analysis of the  $\alpha$ -glucosidase HaG provides new insights into substrate specificity and catalytic mechanism. *Acta Crystallogr* 71:1382-1391.
- Shirai T, Hung VS, Morinaka K, Kobayashi T, Ito S (2008) Crystal structure of GH13  $\alpha$ -glucosidase GSJ from one of the deepest sea bacteria. *Proteins* 73:126-133.
- Skov LK, Mirza O, Sprogøe D, Dar I, Remaud-Simeon M, Albenne C, Monsan P, Gajhede M (2002) Oligosaccharide and sucrose complexes of amylosucrase. Structural implication for the polymerase activity. *J Biol Chem* 277:47741-47747.

- Stam M.R, Danchin E.G, Rancurel C, Coutinho P.M, Henrissat B (2006) Dividing the large glycoside hydrolases family into subfamilies: towards improved function annotations of  $\alpha$ -amylase-related proteins. *Protein Engin Des Sel* 19 555-562.
- Standley D.M, Toh H, Nakamura H. (2007) ASH structure alignment package: sensitivity and selectivity in domain classification, *BMC Bioinforma* 8:116.
- Suzuki Y, Aoki R, Hayashi H (1982) Assignment of a p-nitrophenyl-  $\alpha$ -D-glucopyranoside – hydrolyzing  $\alpha$ -glucosidase of *Bacillus cereus* ATCC 7064 to an exo-oligo-1,6-glucosidase. *Biochim Biophys Acta* 704:476-483.
- Suzuki Y, Shinji M, Eto N (1984) Assignment of a p-nitrophenyl-  $\alpha$ -D-glucopyranosidase of *Bacillus stearothermophilus* ATCC 12016 to a novel exo-  $\alpha$ -1,4-glucosidase active for oligosaccharides and glucans. *Biochim Biophys Acta* 787:281-289.
- Takaku H (1988) Manufacture of oligosaccharides. In: The Amylase Research Society of Japan (ed) *Handbook of amylases and related enzymes*. Pergamon, Oxford, United Kingdom, pp 212-222.
- Takii Y, Takahashi K, Yamamoto K, Sogabe Y, Suzuki Y (1996) *Bacillus stearothermophilus* ATCC12016  $\alpha$ -glucosidase specific for  $\alpha$ -1,4 bonds of maltosaccharides and  $\alpha$ -glucans shows high amino acid sequence similarities to seven  $\alpha$ -D-glucohydrolases with different substrate specificity. *Appl Microbiol Biotechnol* 44:629-634.
- Thompson JD, Higgins DG, Gibson TJ (1994) CLUSTAL W: improving the sensitivity of progressive multiple sequence alignment through sequence weighting, position-specific gap penalties and weight matrix choice. *Nucleic Acids Res* 22:4673-4680.
- Toledo-Arana A, Dussurgey O, Nikitas G, Sesto N, Guet-Revillet H, Balestrino D, Loh E, Gripenland J, Tiensuu T, Vaitkeicius K, Barthelemy M, Vergassola M, Nahoru M, A Soubigou G, Regnault B, Coppee J.Y, Lecuit M, Johansson J, Cossart P (2009) The *Listeria* transcriptional landscape from saprophytism to virulence. *Nature* 459:950-956.
- Tsujimoto Y, Tanaka H, Takemura R, Yokogawa T, Shimonaka A, Matsui H, Kashiwabara S, Watanabe K, Suzuki Y (2007) Molecular determinants of substrate recognition in thermostable  $\alpha$ -glucosidase belonging to glycoside hydrolase family 13. *J Biochem* 142:87-93.
- Uitdehaag J.C, Mosi R, Kalk K.H, van der Veen B.A, Dijkhuizen L, Withers S.G, Dijkstra B.W (1999) x-ray structures along the reaction pathway of cyclodextrin glycosyltransferase elucidate catalysis in the  $\alpha$ -amylase family. *Nat Struct Biol* 6:432-436.



- Van den Broek L.A, Struijs K, Verdoes J.C, Beldman G, Voragen A.G (2003) Cloning and characterization of two novel  $\alpha$ -glucosidases encoded by *Bifidobacterium adolescentis* DSM20083. *Appl Microbiol Biotechnol* 61:55-60.
- Wang L.X, Hung W (2009) Enzymatic transglycosylation for glycoconjugate synthesis. *Curr Opin Chem Biol* 13:592-600.
- Watanabe K, Kitamura K, Suzuki Y (1996) Analysis of the Critical sites for protein thermostabilization by prolines substitution in oligo-1,6-glucosidases from *Bacillus coagulans* ATCC 7050 and evolutionary consideration of proline residue. *Appl Environ Microbiol* 62:2066-2073.
- Watanabe K, Chishiro K, Kitamura K, Suzuki Y (1991) Proline residues responsible for thermostability occur with high frequency in the loop regions of an extremely thermostable oligo-1,6-glucosidase from *Bacillus thermoglucosidasius* KP1006. *J Biol Chem* 266:24287-24294.
- Watanabe K, Kitanura K, Iha H, Suzuki Y (1990) Primary structure of the oligo-1,6-glucosidase of *Bacillus cereus* ATCC7064 deduced from the nucleotide sequence of the cloned gene. *Eur J Biochem* 192:609-620.
- Yamamoto K, Nakayama A, Yamamoto Y, Tabata S (2004) Val216 decides the substrate specificity of  $\alpha$ -glucosidase in *Saccharomyces cerevisiae*. *Eur J Biochem* 271:3414-3420.
- Yamamoto T, Unno T, Sugawara M, Goda T (1999) Properties of a nigerose and nigerosylmaltooligosaccharides-supplemented syrup. *J Appl Glycosci* 46:475-482.
- Yamamoto M, Hoarikoshi K (1990) Nucleotide and expression of a gene coding for thermostable  $\alpha$ -glucosidase gene and the properties of the gene product by *Escherichia coli* HB101. *Denpun Kagaku* 37:137-144.

## **ACKNOWLEDEMENTS**

I would like to express my sincere gratitude and greatest appreciation to my professor and supervisor. First, Professor. Dr. Haruhide Mori for his helpful suggestions in my studies, supervision and, encouragement. Second, Assitant Dr. Wataru Saburi who is my advisor for his kindly helps and useful advice in experiment, manuscript, and thesis. Appreciation also expressed to all the student members in the Biochemistry Laboratory for their friendships, practical help, giving the good during I stayed here. Throughout five years, I am very impressed with your warmness, and take care of me.

Next, special thanks to the Monbukagakusho (MEXT) scholarship to give me an opportunity to study in the Hokkaido University, and get good experiences in Japan, such as Japanese cultures, foods, and attractive tourist.

Finally, to my parents whom I am greatly indebted for me brought up with love, encouragement, supporting and providing the beautiful things throughout my life.

Waraporn Auiewiriyankul